

Final Report (13403)

# Evaluation and Comparison of Reservoir Simulator Performance in Waterflooding Scenarios Using MATLAB Reservoir Simulation Toolbox (MRST) and Computer Modelling Group (CMG)

Mukhammad Sholikhuddin <sup>1</sup>

<sup>1</sup> Petroleum Engineering Department, Pertamina University, South Jakarta, Indonesia; muhammadsholikhuddin1@gmail.com

**Abstract:** Reservoir simulation plays an important role in optimizing field development strategies, particularly in waterflooding scenarios. This study provides a comprehensive evaluation of reservoir simulation performance by comparing the open-source simulator MATLAB Reservoir Simulation Toolbox (MRST) and the commercial simulator Computer Modelling Group (CMG) on various sensitivity variables and computational time efficiency. Sensitivity analysis was performed by varying the grid size, applying linear, five-spot, and inverted five-spot injection patterns, and conducting tests at several injection pressures. The reservoir fluid model was built on both simulators, resulting in a 1.5% difference in Original Oil in Place (OOIP) values, indicating that the model setup was nearly identical on both simulators. The results of the study indicate that increasing grid resolution from 300 to 14,700 blocks does not always smooth the slope decline of reservoir pressure and oil production rates. The five-spot and inverted five-spot patterns improved the recovery factor compared to the linear pattern, with the inverted five-spot pattern showing more effective fluid sweeping. At low injection pressures, numerical instability was observed in MRST. The instability consisted of fluctuations in the injection rate, unstable water breakthrough, and oscillations in the oil production profile and Gas Oil Ratio (GOR) values. Part of this instability may have been caused by the solver characteristics, unadaptive time-step adjustment, and challenges in building the fluid model. In terms of computational efficiency, CMG performs significantly more efficiently, completing simulations over 77 times faster than MRST. Overall, this study demonstrates that MRST is more suitable for academic research and new method development, whereas CMG remains the preferred option for large-scale reservoir simulation applications with high time efficiency and numerical stability requirements.

**Keywords:** Reservoir Simulator, Water Injection, MRST, CMG, Numerical Stability, Runtime CPU

---

## 1. Introduction

### 1.1. Background

Reservoir simulation possesses a pivotal role in the development of oil and gas fields, particularly in the domains of planning and production optimization. The implementation of viable field development scenarios is imperative to achieve optimal planning results. Among the various development scenarios currently in use, the waterflooding method is one of the most frequently employed techniques for enhancing secondary oil and gas recovery in the industry. Waterflooding is a process of injecting water into a reservoir to maintain reservoir pressure and sweep oil toward production wells, thereby improving overall oil recovery efficiency [1]. The accuracy and efficiency of reservoir simulation processes are contingent upon the selection of an appropriate reservoir simulator.

In today's era, a variety of reservoir simulators with diverse numerical approaches are available, and these can generally be categorized as commercial simulators and open-source simulators. Commercial simulators such as Computer Modelling Group (CMG), ECLIPSE, and tNavigator are known for their advanced features and ability to handle complex reservoir model simulations, making them widely used in the oil and gas industry. On the other hand, open-source simulators such as MATLAB Reservoir Simulation Toolbox (MRST) [2], [3], Open Porous Media (OPM) Flow, Jutul Darcy from SINTEF, and UTCHEM from the University of Texas provide flexibility to users in developing reservoir models and allow users to modify solvers or simulation algorithms as needed.

Previous studies have compared reservoir simulators to evaluate the accuracy of results, numerical stability, and computational efficiency. One well-known study is the SPE Comparative Solution Project, 9th Edition, which

specifically discusses black oil simulation on a three-dimensional reservoir scale [4]. Furthermore, a study was conducted in the paper "Comparison of Solutions to a Three-Dimensional Black-Oil Reservoir Simulation Problem," which compares various simulators under similar scenarios in detail [5]. Relevant studies include recent research on the evaluation of GPU hardware and solver libraries to accelerate reservoir simulations in the OPM Flow simulator and a validation study of the OPM simulator through the Comparative Solution Project [6], [7].

Nevertheless, comprehensive studies that directly compare the performance of MRST with commercial simulators such as CMG, especially in the context of waterflooding scenarios with a wide variety of simulation parameters are still limited. However, in reservoir simulation practice, parameters such as the total number of grids, well injection pattern, and bottom hole injection pressure (BHP) have a significant influence on the accuracy of production prediction, sweeping efficiency, and numerical stability. These configuration variations can often trigger differences in model behavior due to the numerical approach and solving techniques used by each simulator.

Therefore, this study was designed to evaluate and compare the performance of MRST compared to CMG in modeling waterflooding scenarios under the influence of these key technical configurations. The evaluation is conducted not only to assess the technical accuracy of simulation results (such as recovery factor and breakthrough time), but also to understand the computational efficiency (CPU runtime) and numerical stability, in order to provide a deeper insight into the advantages and limitations of each simulator. Before the main analysis is conducted, a preliminary validation in the form of zero balance test is applied to ensure the reliability of the MRST model in this study.

## 1.2. Objective

This study focuses on evaluating the performance of reservoir simulators in waterflooding scenarios through a comparison between MRST and CMG. The evaluation is conducted by highlighting the influence of key technical configurations- the total number of grids, well injection pattern, and bottom hole injection pressure (BHP) that play a significant role on the production behavior, fluid sweep, and efficiency and stability of the numerical simulation. The objectives of this study are formulated as follows:

1. Evaluating the influence of the main technical configurations in waterflooding simulation, namely the total number of grids, well injection pattern, and bottom hole injection pressure (BHP), on reservoir model performance, to understand the sensitivity of simulation results to fluid flow in the reservoir.
2. Comparing the simulation results between MRST and CMG in terms of accuracy (oil recovery factor, breakthrough time), numerical efficiency (CPU runtime), and stability of numerical simulation in various configuration scenarios.
3. Determining the advantages and limitations of MRST over CMG, and provide recommendations for its use based on scenario characteristics, considering ease of implementation, model flexibility, and computational efficiency.

Through the accomplishment of this research, it is expected that a deeper understanding of the capabilities of the MRST simulator as an alternative in industrial and academic applications, particularly in the context of waterflooding simulation, can be obtained.

## 2. Literature Review

### 2.1. Enhanced Oil Recovery Methods

The process, which aims to enhance the recovery of hydrocarbons from reservoirs, is generally divided into three main stages: primary, secondary, and tertiary recovery methods [8], [9]. The primary method uses natural energy from the reservoir to flow oil to the surface without additional fluid injection. This method usually recovers less than 30% of the total oil contained in the reservoir. Primary recovery includes all methods of oil recovery that utilize the natural energy of the reservoir as the primary mechanism for driving hydrocarbons toward the production well. Understanding this driving mechanism is important and should be identified as early as possible in the initial stages of reservoir exploitation. An understanding of these mechanisms enables optimal reservoir management and improves efficiency and oil recovery in the mid to late production phase. The main driving mechanisms are: (i) solution gas drive, where gas dissolved in oil drives oil out as pressure decreases; (ii) gas cap drive, which utilizes pressure from gas above the oil zone; (iii) water drive, where water pressure from aquifers below or around the reservoir helps maintain reservoir pressure; (iv) gravity drainage, where gravity helps drain oil downward toward production wells; and (v) combined or mixed drivers, which involve more than one driving mechanism simultaneously. Of these five mechanisms, water drive is considered the most effective in maintaining reservoir pressure [9].

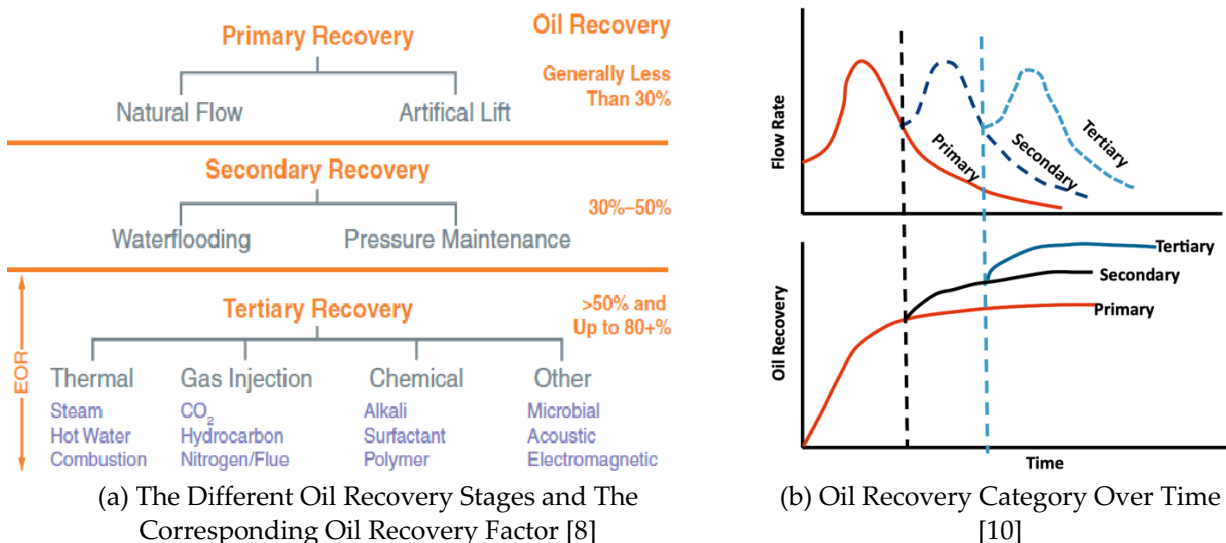


Figure 1 Different Oil Recovery Stages

Secondary methods are implemented by injecting external fluids such as water or gas to maintain reservoir pressure and increase oil recovery. One of the most commonly used secondary methods is waterflooding, which involves injecting water into the reservoir through injection wells to push oil into production wells as in Figure 2 illustrates the waterflooding process. This method can increase additional oil recovery by approximately 30-50% of the total initial oil stored in the reservoir. Tertiary methods or Enhanced Oil Recovery (EOR) were applied after the primary and secondary methods reached their economic limits. The EOR method can increase additional oil recovery by about 50% to 80%. The oil recovery stages diagram is shown in Figure 1. EOR involves more advanced techniques to reduce the residual oil saturation remaining in the reservoir after the two previous methods have been applied. EOR is generally divided into two main categories: thermal and non-thermal. Thermal techniques include steam flooding, hot water injection, and in-situ combustion, where thermal energy is used to reduce oil viscosity, thereby decreasing the mobility ratio. Increased heat reduces surface tension and facilitates oil movement toward the production well [9].

Non-thermal techniques include the injection of chemicals such as polymers, surfactants, or alkalis to improve the efficiency of oil displacement from reservoir pores. These techniques also include the injection of gas such as carbon dioxide (CO<sub>2</sub>) or nitrogen (N<sub>2</sub>), which can be used either as immiscible or miscible depending on reservoir conditions. These gases can reduce oil viscosity, increase oil volume, and reduce oil-water interfacial tension, thereby increasing the amount of oil that can be produced [8].

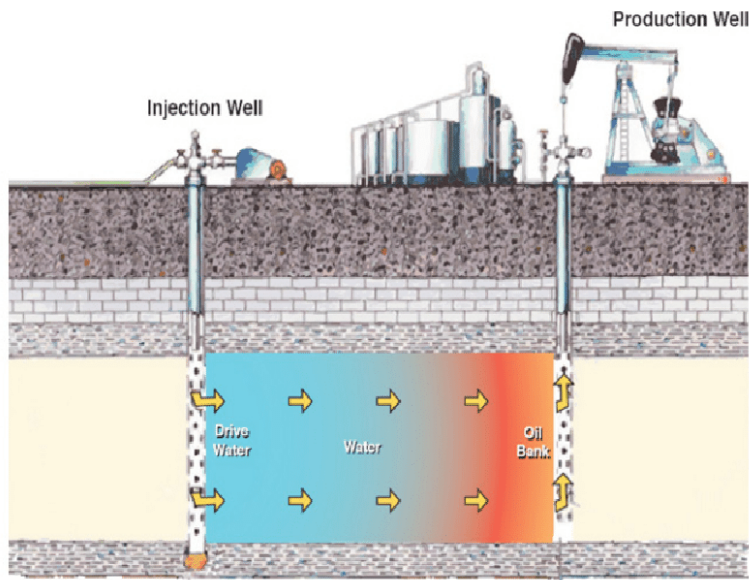


Figure 2 Diagram Illustrating Waterflooding Method of Secondary Recovery [11]

## 2.2. Concept of Fluid Displacement in Waterflooding

The process of fluid displacement in waterflooding is a very important concept in understanding how oil is produced from reservoirs during water injection. The displacement of fluid in reservoirs can generally occur in two main mechanisms, namely piston-like displacement and leak piston-like displacement [12], [13].

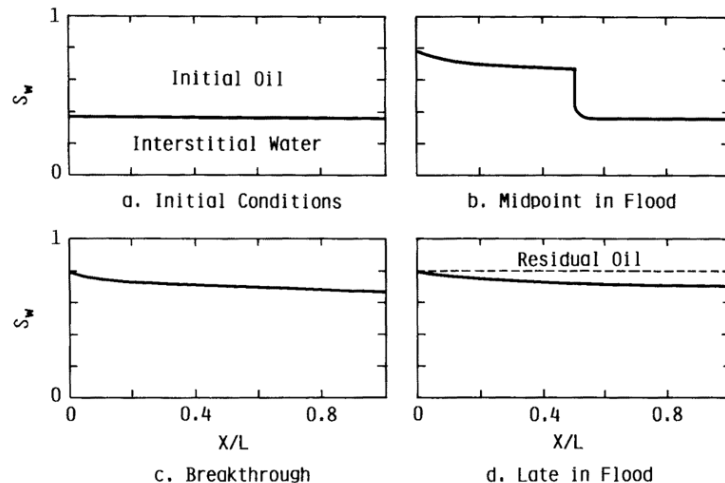


Figure 3 Leak Piston Like Displacement Process [12]

Piston-like displacement is an ideal condition in fluid displacement, where before the front point or water face, only the displacing fluid (water) flows, while behind the front only the oil fluid moves. In this concept, the entire oil zone will be completely displaced by water. However, this ideal condition is very rare in real reservoir conditions, because reservoirs generally have heterogeneity and complex properties[13]. Instead, leak piston-like displacement in Figure 3 is a more realistic displacement mechanism, where before the front point, both the displacing fluid (water) and the displaced fluid (oil) can flow simultaneously, while after the front point only the oil fluid flows. This mechanism creates a transition zone in the form of a saturation distribution that continuously moves forward toward the production well. When this transition zone reaches the production well, a phenomenon known as breakthrough water occurs, where water begins to be produced alongside oil in the production well [13].

### 2.3. Factors Controlling Oil Recovery

The effectiveness of waterflooding is greatly affected by the sweep pattern or injection pattern that is used. The efficiency of this sweep depends on several factors, including the mobility ratio, the areal sweep efficiency, and the injection pattern configuration that is applied in the field [14].

#### 2.3.1. Mobility Ratio in Waterflooding

Mobility Ratio (M) is the ratio between the mobility of the displacing fluid and the displaced fluid [12], defined as follows.

For a waterflood,

$$M = \frac{k_w/\mu_w}{k_o/\mu_o} = \frac{k_w\mu_o}{k_o\mu_w} = \frac{k_{rw}\mu_o}{k_{ro}\mu_w} \quad \text{Equation 1}$$

Where,

- $k_{rw}$  = Relative permeability water,
- $k_{ro}$  = Relative permeability oil,
- $\mu_o$  = Oil viscosity,
- $\mu_w$  = Water viscosity

When  $M < 1$  (favorable mobility ratio), the oil flows more easily than water, resulting in high sweep efficiency and increased oil recovery. Conversely, when  $M > 1$  (unfavorable mobility ratio), water flows more easily than oil, which can cause fingering or early breakthrough, reducing sweep efficiency [14].

#### 2.3.2. Areal Sweep Efficiency in Waterflooding

Areal sweep efficiency ( $E_A$ ) is defined as the fraction of the injection-production pattern area that has been successfully contacted by the displacing fluid (commonly water) during the waterflooding process. This efficiency is an important parameter that indicates how effectively the injected fluid distributes laterally within the reservoir and sweeps oil into the production well [15]. More details on areal sweep efficiency are shown in Figure 4.

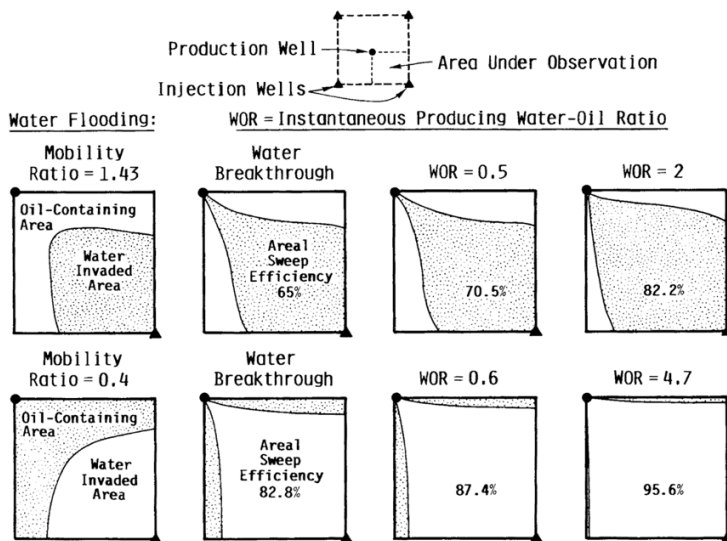


Figure 4 Fluid Mobilities on The Areal Sweep Efficiency [12]

According to Ahmed (2010),  $E_A$  increases over time: it increases from zero at the start of injection until breakthrough, and then increases more slowly onwards. The factors that influence sweep efficiency are as follows [10]: mobility ratio (M), injection and production well sweeping pattern, reservoir heterogeneity, and cumulative volume of water injected ( $W_{inj}$ ).

### 2.3.3. Displacement Efficiency

Displacement Efficiency ( $E_D$ ) is the fraction of oil that can be produced from the swept zone by the injected fluid. This concept represents how effectively the injected water is able to displace oil from the pores of the reservoir rock in the area that has been reached. In other terms, displacement efficiency is a measure of the effectiveness of microscopic sweeping during the waterflooding process. According to Ahmed (2010), displacement efficiency at a given time can be mathematically defined as follows [10]:

$$E_D = \frac{\text{Volume of oil at start of flood} - \text{Remaining oil volume}}{\text{Volume of oil at start of flood}} \quad \text{Equation 2}$$

$$E_D = \frac{(\text{Pore volume}) \left( \frac{S_{oi}}{B_{oi}} \right) - (\text{Pore volume}) \left( \frac{\bar{S}_o}{B_o} \right)}{(\text{Pore volume}) \left( \frac{S_{oi}}{B_{oi}} \right)} \quad \text{Equation 3}$$

Where,

$S_{oi}$  = Initial oil saturation at start of flood

$B_{oi}$  = Oil FVF at start of flood, bbl/STB

$\bar{S}_o$  = Average oil saturation in the flood pattern at a particular point during the flood

### 2.4. Sweeping Patterns in Waterflooding

One of the important initial steps in designing a waterflooding project is the selection of an injection pattern (flooding pattern). The main objective of selecting this pattern is to provide maximum contact between the injected fluid and the oil remaining in the reservoir. Selecting the right sweep pattern will help improve areal sweep efficiency and displacement efficiency. According to Ahmed (2010), several factors that need to be considered in selecting a flooding pattern include [10]:

1. Reservoir heterogeneity and directional permeability
2. Direction of formation fractures
3. Availability of the injection fluid (gas or water)
4. Desired and anticipated flood life
5. Well spacing, productivity, and injectivity

There are four main types of injection patterns used in fluid injection projects, namely Irregular Injection Patterns, Peripheral Injection Patterns, Regular Injection Patterns, and Crestal and Basal Injection Patterns.

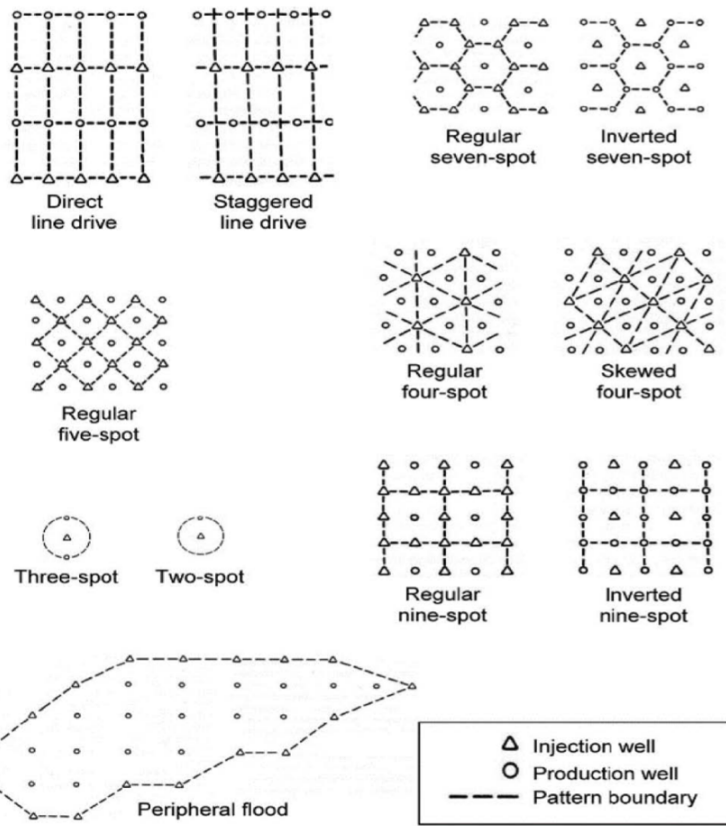


Figure 5 Flood Patterns [16]

### 2.6.1. Irregular Injection Patterns

This pattern is used when production and injection wells are not located regularly due to surface topography or slant-hole drilling design. In this pattern, the area affected by each injection well can vary greatly. It is typically applied to small reservoirs or marginal fields, where some production wells are converted into injection wells in a non-uniform manner. The irregularity of this pattern is often caused by the presence of faults, local variations in porosity or permeability, and economic limitations [10].

### 2.6.2. Peripheral Injection Patterns

This pattern involves placing injection wells at the outer perimeter of the reservoir, while production wells are located in the inner part. The injected water pushes oil from the edge of the reservoir into the center. Warner (2015) states that this pattern has several advantages [1]:

- Provides maximum oil recovery with minimum water production
- Delayed water breakthrough, enabling longer oil production without water contamination
- The number of injection wells is relatively small, resulting in high operational efficiency
- However, reservoir response tends to be slow, as water must travel long distances to reach the production zone in the center of the reservoir

This pattern is suitable for reservoirs with sufficiently high permeability so that water injection can spread effectively over long distances.

### 2.6.3. Regular Injection Patterns

Regular pattern is widely used because most oil field development areas are divided into square grids [16]. Some common patterns include:

- Direct Line Drive

Injection and production wells are arranged in a straight line facing each other. Efficiency depends on the mobility and continuity of the formation.

- Staggered Line Drive  
Production and injection wells are arranged like a line drive but shifted laterally, usually half the distance between wells. This provides a more uniform flow.
- Five-Spot Pattern  
Consists of one production well in the center and four injection wells at the corners forming a square. Very popular because it provides even sweeping and high efficiency.
- Inverted Five-Spot  
The opposite structure of the five-spot, one injector in the center and four producers around it. Often used to slow down water breakthrough.
- Seven-Spot Pattern  
The injection wells are placed at the corners of a hexagon with one producer in the center. This configuration is more compact than the five-spot configuration, making it suitable for heterogeneous reservoirs.
- Nine-Spot Pattern  
Eight injectors surround one producer. This pattern allows sweeping from multiple directions and is suitable for improving flow control.

#### 2.6.4. Crestal dan Basal Injection Patterns

Crestal injection pattern: Injection fluid is injected from the top of the reservoir structure. It is typically used for gas injection, such as gas cap drive. Basal pattern, fluid is injected from the bottom of the reservoir. It is generally used for waterflooding because it utilizes gravitational segregation to flow water upward and sweep oil into the production well [10].

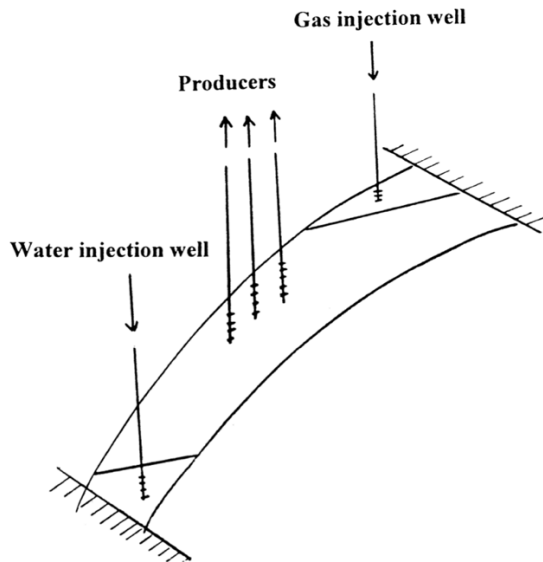


Figure 6 Crestal and Basal Injection Pattern [10]

#### 2.5. Reservoir Simulator

A reservoir simulator is a numerical tool that is used to model fluid behavior in reservoir rock pores during oil and gas production. The objective is to predict reservoir performance based on various operating scenarios, to assist in technical decision making, and to optimize hydrocarbon recovery. The simulator is based on the principles of mass and energy conservation and fluid flow laws such as Darcy's Law [17]. Reservoir modeling and simulation have an important role in integrating geological, petrophysical, and production history data to provide accurate reservoir performance predictions and support data-driven decision making [18].

### 2.5.1. Well Modelling in Reservoir Simulation

In reservoir simulation, wells are treated as sources (injection wells) or sinks (production wells) of fluid mass. In grid-based numerical models, wells are not represented as physical holes, but rather as line sources or sinks placed within grid blocks. One of the main challenges in this approach is that the bottom-hole pressure (BHP) is generally not identical to the numerical pressure in the grid block where the well is located. Therefore, a well model is used to connect the two, bridging the well pressure and grid pressure through a parameter called the well index (WI). The basic relationship between pressure and flow rate in this model is formulated as [19], [20]:

$$q = WI \cdot (p_R - p_{bh}) \quad \text{Equation 4}$$

Well models are used to regulate the relationship between pressure and fluid flow rate, depending on the constraints used in the simulation. In the case of a pressure-constrained well, the base pressure of the well is known and the simulator calculates the flow rate. Conversely, in a rate-constrained well, the injection or production rate is specified, and the simulator calculates the base pressure of the well. The most commonly used well model is the radial steady-state flow model, which is derived from Darcy's law in cylindrical coordinates. In this model, the relationship between the flow rate  $q$  and the pressure difference is given by the equation [20]:

$$q = \frac{2\pi h K}{\mu B \left( \ln \left( \frac{r_e}{r_w} \right) + S \right)} (p_R - p_{bh}) \quad \text{Equation 5}$$

Where,

$p_R$  = Reservoir pressure in the grid cell

$p_{bh}$  = Bottom hole pressure

$K$  = Permeability

$B$  = Formation volume factor,  $B= 0.61738575$  was later derived by Peaceman

$h$  = Reservoir thickness

$r_e$  = Equivalent radius

$r_w$  = Wellbore radius

$S$  = Skin factor

Important research by Peaceman (1978) shows that the numerical pressure in a well block is actually equivalent to the radial flow pressure at an equivalent radius of  $r_e \approx 0.2\Delta x$ , not the pressure at the well radius or the average block pressure [19], [20]. Based on this, the well index is calculated to adjust for this difference in the simulator. In simulators such as MRST, Peaceman's formulation has been explicitly implemented to calculate the well index by considering grid size, well position in the grid, and permeability anisotropy. This approach yields calculation accuracy equivalent to commercial simulators such as CMG, which also adopts Peaceman's formulation with some internal adjustments based on well geometry and type.

### 2.5.2. Mathematical Formulation of Reservoir Flow

Modeling fluid dynamics in reservoirs is a fundamental aspect, as it plays an important role in the process of optimizing production and predicting the performance of subsurface reservoirs. The mathematical representation of fluid flow is based on a combination of Darcy's Law and the Material Balance equation, both of which are then solved using a numerical simulation approach. These models are the basis for modern reservoir simulation processes and enable a quantitative understanding of the interactions between fluids and porous media in complex reservoir conditions.

Darcy's Law [21]:

$$q = -\frac{kA}{\mu} \frac{dP}{dL} \quad \text{Equation 6}$$

Where,

$q$	= Volumetric flow rate, $\text{cm}^3/\text{sec}$
$k$	= Permeability of rock, darcy
$A$	= Cross sectional area, $\text{cm}^2$
$\mu$	= Fluid viscosity, cP
$dP/dL$	= Pressure drop per unit length, atm/cm

Darcy's Law in Field Unit [22]:

$$Q = 1.1271 \frac{kA\Delta P}{\mu L} \quad \text{Equation 7}$$

Where,

$Q$	= Volumetric flow rate, bbl/day
$k$	= Permeability of rock, darcy
$A$	= Cross sectional area, $\text{ft}^2$
$\Delta P$	= Pressure differential, psi
$\mu$	= Fluid viscosity, cP
$L$	= Length of reservoir, ft

Material Balance [18]:

$$N = G_p + W_p - G - W \quad \text{Equation 8}$$

Where,

$N$	= Cumulative oil production
$G_p$	= Cumulative gas production
$W_p$	= Cumulative water production
$G$	= Cumulative gas injection
$W$	= Cumulative water injection

Single-phase and Multi-Phase Flow Models:

In reservoir simulation, fluid flow formulations are categorized into two main approaches: single-phase flow models and multiphase flow models, depending on the number of fluid phases flowing and interacting in the porous medium [18].

Single Phase Flow Model [18]

The single-phase flow model is used to model the flow of a single type of fluid in a porous medium system, where the physical properties of the fluid, such as density and viscosity, are assumed to be homogeneous and constant throughout space and time. The mathematical formulation is based on the continuity equation, which states that the change in fluid mass within a control volume is equal to the difference between the mass entering and exiting [18].

$$\frac{\partial \rho}{\partial t} + \nabla \cdot (\rho v) = 0 \quad \text{Equation 9}$$

Where,

$\rho$	= Fluid density, $\text{kg/m}^3$
$v$	= Fluid velocity, $\text{m/s}$
$t$	= Time, s

Equation 15 expresses that the rate of change of fluid density with the time at a point in the system ( $(\partial\rho/\partial t)$ ) plus the divergence of the mass flux to that point  $\nabla \cdot (pv)$  must be zero. This means that there is no accumulation or loss of mass in the control volume, a fundamental principle of mass conservation. For incompressible fluids,  $\rho$  is constant, which means that the rate of inflow and outflow in the control volume is always balanced.

#### Multi Phase Flow Model:

Multiphase flow models are designed to describe the simultaneous movement of two or more fluid phases (e.g., oil and water) which interact with each other in a porous medium. Each phase has a different density, velocity, and saturation, and is influenced by interfacial forces and spatial distribution [18].

#### Two-Fluid Model:

$$\frac{\partial(\alpha_1\rho_1)}{\partial t} + \nabla \cdot (\alpha_1\rho_1 v_1) = 0 \quad \text{Equation 10}$$

$$\frac{\partial(\alpha_2\rho_2)}{\partial t} + \nabla \cdot (\alpha_2\rho_2 v_2) = 0 \quad \text{Equation 11}$$

Where,

- $\alpha_1, \alpha_2$  = Volume fraction of phase 1 and phase 2
- $\rho_1, \rho_2$  = Fluid density of phase 1 and phase 2, kg/m<sup>3</sup>
- $v_1, v_2$  = Fluid velocity of phase 1 and phase 2, m/s

The equations express that, for each fluid phase, the rate of change of specific mass (the product of volume fraction and density) over time plus the divergence of the mass flux must be zero. This means that each phase individually follows the principle of mass conservation, without assuming that physical properties of the fluid, such as density and velocity, are uniform or identical between phases.

In the context of two-phase flow (e.g., water and oil), the following applies:

$$\alpha_1 + \alpha_2 = 1 \quad \text{Equation 12}$$

Shows that the entire pore volume is filled by two fluid phases. The interaction between phases is also influenced by relative permeability and capillary pressure, which are not directly included in this equation, but are an important part of the complete formulation of the multiphase flow model.

#### 2.5.3. Numerical Simulation Techniques

Considering the limitations of analytical approaches, which are only applicable to simple systems with ideal geometry and homogeneous properties, numerical approaches are used to handle the complexity of actual reservoir systems, such as heterogeneity, irregular geometry, and multiphase flow. In this context, discretization methods are the basis of numerical simulation techniques used in various modern simulators. Discretization methods are numerical techniques used to approximate continuous functions or systems by dividing them into smaller discrete parts. In the context of reservoir simulation, there are three commonly used discretization methods, namely:

##### 1. Finite Difference Method – FDM

This method works by approximating the derivative of a function using the difference in function values at neighboring points. The simulation domain is divided into a grid of points, where the differential equations describing the system are replaced by algebraic equations linking the function values at each grid point. FDM is very useful for solving partial differential equations and is a widely used approach in conventional simulators.

##### 2. Finite Element Method – FEM

In this method, the domain of the simulation is divided into small subdomains called elements. The differential equations governing the system are solved using piecewise functions defined on each element. The solution is obtained by assembling all elements into a global system of equations.

### 3. Finite Volume Method – FVM

This method divides the domain of simulation into a number of control volumes, then approximates the integral form of the differential equation in each volume. The solution is obtained by formulating algebraic equations that represent conservative fluxes between the boundaries of each control volume. FVM is known to be superior in maintaining mass conservation and is very suitable for solving fluid dynamics problems.

Each method has its own advantages and disadvantages depending on the complexity of the problem being simulated and the available computing resources. The selection of a numerical method must be adjusted to the characteristics of the reservoir and the objectives of the simulation study being conducted [18].

#### 2.5.4. Factors Affecting Reservoir Simulation Performance

The performance of reservoir simulation is highly dependent on the physical complexity of the reservoir model, the numerical methods used, and the efficiency of the computational algorithms in solving the fluid flow equation system. Performance aspects in reservoir simulation are not only determined by technical output results such as oil recovery or water cut, but also by runtime efficiency, numerical stability, and the use of computational resources [17], [18]. Several comparative studies have been conducted to evaluate the performance of simulators with similar scenarios and parameters, including the SPE Comparative Solution Project and advanced computational studies using Open Porous Media (OPM) Flow and Computer Modelling Group (CMG).

##### 1. Grid Number and Resolution

The number of grids is directly proportional to the spatial resolution of the simulation. The 9th edition of the SPE Comparative Solution Project study shows that increasing the number of grids from coarse to fine resolution has a significant impact on runtime and result accuracy, especially for cases with high permeability contrast [23]. Similarly, other comparative studies have found that simulators with efficient grid management tend to have more stable numerical performance in waterflood scenarios [24].

##### 2. Solver Types and Numerical Methods

The performance of a solver is determined by the numerical method (FDM, FVM, etc.) and the strategy for solving the system of equations (iterative vs. direct, preconditioning, etc.). A study conducted by Batycky et al. (1997) developed a streamline-based simulator and demonstrated that this approach significantly reduces simulation time in 3D models with high heterogeneity compared to conventional cartesian grid-based simulators [25]. Meanwhile, Van Doren et al. (2006) proposed the Proper Orthogonal Decomposition (POD) method to accelerate simulations, which showed potential efficiency when used for system dimension reduction [26]. Other studies in Odeh (1981) conducted experiments comparing seven 3D black-oil simulators from various companies. The study showed that the fully implicit method is suitable for complex nonlinear conditions, while Implicit Pressure Explicit Saturation (IMPES) is efficient for simple models [27].

##### 3. Time Step Size and Simulation Time Strategy

Adaptive time step settings are very important in maintaining simulation stability. Research conducted by Li (2004) noted that several simulators experienced convergence difficulties when the waterflood front reached areas with low permeability, especially when using time steps that were too large. The use of an adaptive scheme integrated with an appropriate preconditioner can reduce numerical divergence problems [24].

##### 4. Reservoir Complexity and Heterogeneity

Highly heterogeneous reservoirs (e.g., fractured reservoirs or layered geological models) require much longer simulation times. A study by Batycky et al. (1997) showed that streamline-based simulators can provide more efficient solutions under such conditions, but still require accuracy verification against conventional black-oil simulator results [25].

##### 5. Hardware Capacity and Architecture

Computer hardware is super important for large-scale reservoir simulations. A study by Qiu et al. (2023) checked out how well GPU hardware and solver libraries work to speed up the OPM Flow simulator. They found that using GPUs can really cut down on how long it takes without losing accuracy [28], [29].

### 2.5.5. Classification of Reservoir Simulation Based on Fluid Type

Reservoir simulation is classified based on fluid model formulation and the complexity of physical processes represented in the flow equation system. This classification aims to ensure that the simulation approach is suitable for the fluid characteristics, reservoir thermodynamic conditions, and dominant production mechanisms, so that the modeling can represent the dynamic behavior of the reservoir more accurately and relevant to the study objectives [18], [30].

#### 1. Black Oil Model

The black oil model assumes a fluid system consisting of three main components—oil, gas, and water—with fixed compositions in each phase and limited interphase interactions. The relationship between oil and gas is described through pressure-volume-temperature (PVT) parameters such as solution gas-oil ratio ( $R_s$ ), formation volume factor ( $B_o$ ), and bubble point pressure.

#### 2. Compositional Model

The compositional model formulates fluid systems as mixtures of pure hydrocarbon components or pseudo-components, with properties that vary with pressure and temperature. This model uses equations of state (EOS), such as Peng–Robinson or Soave–Redlich–Kwong, to predict phase distribution and thermodynamic properties dynamically.

#### 3. Thermal Model

A thermal model was developed to simulate heat transfer and the effect of temperature on fluid flow and reservoir properties. This model combines mass, energy, and momentum conservation equations and takes into account changes in fluid viscosity, density, and reactivity with temperature. This model is used in thermal-based Enhanced Oil Recovery processes such as steam injection, cyclic steam stimulation, and in-situ combustion, where heat is the primary mechanism for oil mobilization.

### 2.5.6. MATLAB Reservoir Simulation Toolbox (MRST)

MATLAB Reservoir Simulation Toolbox (MRST) is a MATLAB-based reservoir simulation framework developed by SINTEF Digital with the primary objective of supporting research and development of numerical algorithms in the field of fluid flow through porous media. As an open-source simulator, MRST offers high flexibility for modifying and exploring various physical formulations and numerical approaches used in reservoir simulation [2], [31]. MRST uses the finite volume method (FVM) in the discretization of partial differential equations that represent fluid flow in porous media. This approach ensures explicit and accurate mass conservation, as well as flexibility in handling structured and unstructured grids [31].

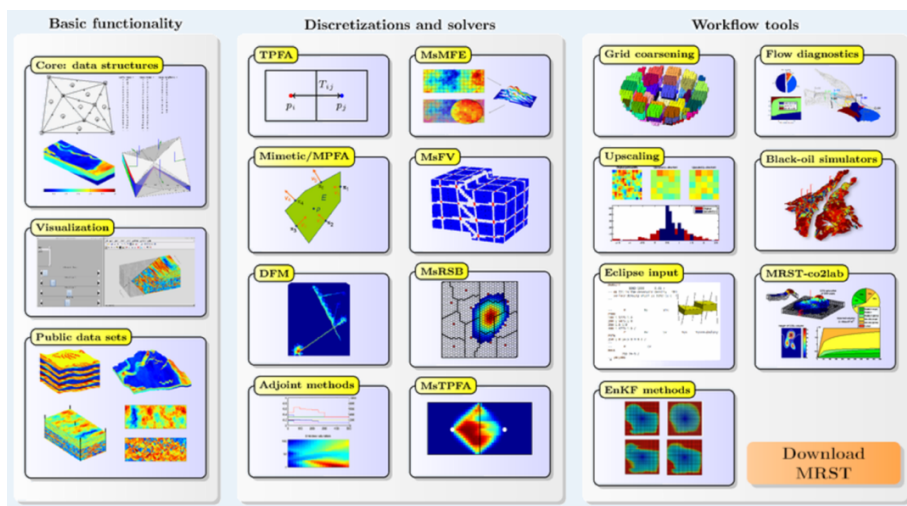


Figure 7 MATLAB Reservoir Simulation Toolbox (MRST) [32]

MRST is built using a modular programming paradigm, where each major feature is organized into independent toolboxes, as shown in Figure 7. This allows users to select and combine only the modules they need, as well as develop custom modules according to their research needs. The MATLAB-based implementation makes MRST easy to access and understand for users with a numerical and engineering background, and is well suited for prototyping new simulation methods [31].

### 3. Methodology

#### 3.1. Workflow

This study uses a systematic workflow to compare the performance of two reservoir simulators, MATLAB Reservoir Simulation Toolbox (MRST) as an open-source simulator and Computer Modelling Group (CMG) as a commercial simulator, in a waterflooding scenario. The process begins with the construction of a synthetic reservoir model using petrophysical parameters, grid geometry, and black-oil fluid properties. The constructed model is then implemented identically in both simulators to ensure input consistency. Initial validation is performed through a zero-balance test to ensure mass conservation is maintained in each simulator before the main simulation is run. Following validation, the study continued with simulations under various sensitivity scenarios, and the simulation results were analyzed using specific evaluation parameters. The overall research workflow is illustrated in Figure 8, which outlines the sequence of activities from model design to result evaluation.

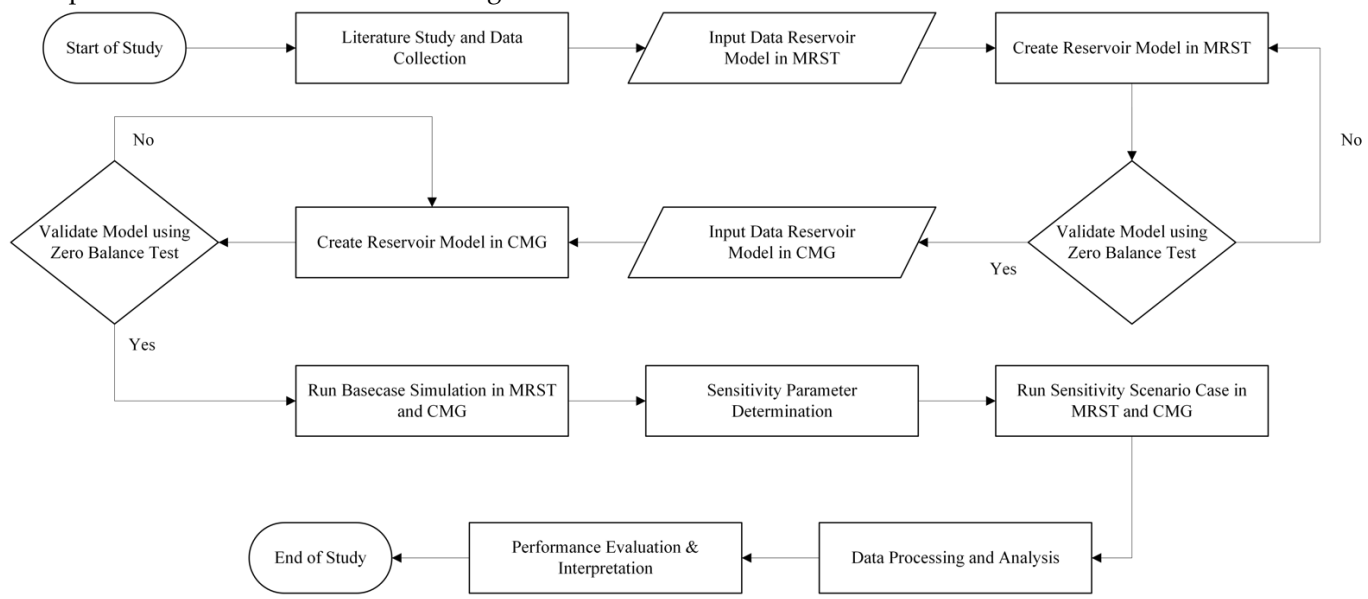


Figure 8 Workflow of Study

#### 3.2. Research Design

This research is designed as a comparative study with an experimental quantitative approach. The main objective is to evaluate the accuracy of results, computational efficiency, and numerical stability between two reservoir simulators, MATLAB Reservoir Simulation Toolbox (MRST) as an open-source platform, and Computer Modelling Group (CMG) as a commercial simulator that has been widely used in the petroleum industry. This design aims to assess the extent to which MRST can produce outputs comparable to commercial simulators that have been widely used in the industry. The initial stages of the research design include the collection of data through literature studies, including reservoir grid size parameters, reservoir rock properties, and black-oil fluid characteristics. The simulation was run by applying variations to several technical parameters that affect performance and accuracy of results, including the number of grid cells, well injection pattern, and bottom hole pressure (BHP). In addition, to measure computational efficiency, the simulation was run on a consumer-grade CPU, namely the 7th generation Intel Core i3, to evaluate the runtime of each simulator. The details of the scenarios are described in subsection 3.3.3. Scenario Design, while the evaluation parameters are explained in subsection 3.5, Evaluated Parameters. The results of each scenario were compared to identify the advantages, significant differences, and potential limitations of both simulators in running waterflooding scenario simulations.

#### 3.3. Data Collection and Synthetic Reservoir Model Setup

The data used to construct the synthetic reservoir model in this study was obtained from the first SPE Comparative Solution Project dataset (SPE-1), as developed and described by Aziz S. Odeh (1981) in a study entitled "Comparison of Solutions to a Three-Dimensional Black-Oil Reservoir Simulation Problem." This dataset was selected due to the completeness of the data provided and the simplicity and relevance of the three-dimensional reservoir model to the

research objectives, particularly in evaluating the performance of reservoir simulators under waterflooding scenarios. In this stage, detailed data preparation and reservoir model configuration were carried out, followed by technical implementation in the MATLAB Reservoir Simulation Toolbox (MRST), and the design of simulation scenarios to evaluate the performance of waterflooding simulations.

### 3.3.1. Reservoir Model Description

In this study, the modeled reservoir is a synthetic reservoir with a three-dimensional configuration (Cartesian Grid), consisting of a total of 300 grid blocks divided in the lateral direction (I and J) and the vertical direction (K). The reservoir has three layers with different thicknesses in each layer. The petrophysical properties used, such as porosity and permeability, are based on the SPE-1 dataset with uniform porosity throughout the layers, while permeability values vary between layers and directions (I, J, K) to realistically reflect reservoir heterogeneity in the simulation.

Table 1 Reservoir Grid Description for MRST and CMG

Direction	Grid	Dimension
I	10 grid	1000 ft
J	10 grid	1000 ft
K	3 grid	-

Table 2 Reservoir Layer Thickness for MRST and CMG

Layer	Thickness
1	20 ft
2	30 ft
3	50 ft

Table 3 Reservoir Properties for MRST and CMG

Layer	Porosity	Permeability I	Permeability J	Permeability K	Water Saturation	Oil Saturation
1	0.3	500 mD	500 mD	300 mD	0.12	0.88
2	0.3	50 mD	50 mD	30 mD	0.12	0.88
3	0.3	200 mD	200 mD	50 mD	0.12	0.88

Table 4 Reservoir Initial Condition Data for MRST and CMG

Parameter	Value
Grid Top	8325 ft
Grid Bottom	8425 ft
Datum Depth	8400 ft
Datum Pressure	4800 ft
Water Oil Contact (WOC)	8500 ft
Gas Oil Contact (GOC)	8200 ft

Table 5 Reservoir Fluid Data for MRST and CMG

Parameter	Value
Oil Density	49.1 lb/ft <sup>3</sup>
Gas Density	0.06054 lb/ft <sup>3</sup>
Water Density	64.79 lb/ft <sup>3</sup>
Formation Volume Factor Water (BWI)	1.029
Compressibility Water (CW)	3.13E-06 1/psi
Reference Pressure for BWI	4014.7 psi
Viscosity Water	0.31 cP

Table 6 Additional Reservoir Fluid Data for CMG

Parameter	Value
Undersaturated Compressibility Oil (CO)	1.37E-5 1/psi
Viscosity Oil Pressure Dependence (VO)	4.60E-05 cP/psi
Viscosity Water Pressure Dependence (CVW)	0 cP/psi

The relative permeability data used in this simulation consists of two fluid systems, Gas-Oil and Water-Oil. The relative permeability value of water ( $K_{rw}$ ) in the Water-Oil system was adjusted from its original value in the SPE-1 dataset, which was initially zero, because the original scenario in the dataset used gas injection. This adjustment of the  $K_{rw}$  value aims to realistically represent water flow in the reservoir in the waterflooding scenario that is the focus of this study. Although the reservoir is oil-wet, the main objective of this study is not to evaluate the effectiveness of waterflooding under specific wettability conditions, but rather to compare the simulation outcomes between MRST and CMG under a consistent injection scenario.

Table 7 Gas-Oil Relative Permeability Data for MRST and CMG

Sg	Krg	Krog
0	0	1
0.001	0	1
0.020	0	0.997
0.050	0.005	0.980
0.120	0.025	0.700
0.200	0.075	0.350
0.250	0.125	0.200
0.300	0.190	0.090
0.400	0.410	0.021
0.450	0.600	0.010
0.500	0.720	0.001
0.600	0.870	0.0001
0.700	0.940	0
0.850	0.980	0
0.880	0.984	0

Table 8 Water-Oil Relative Permeability Data for MRST and CMG

Sw	Krw	Krow
0.120	0	1
0.121	0	1
0.140	0	0.997
0.170	0.010	0.980
0.240	0.050	0.700
0.320	0.150	0.350
0.370	0.250	0.200
0.420	0.400	0.090
0.520	0.600	0.021
0.570	0.700	0.010
0.620	0.800	0.001
0.720	0.900	0
0.820	0.950	0
1	1	0

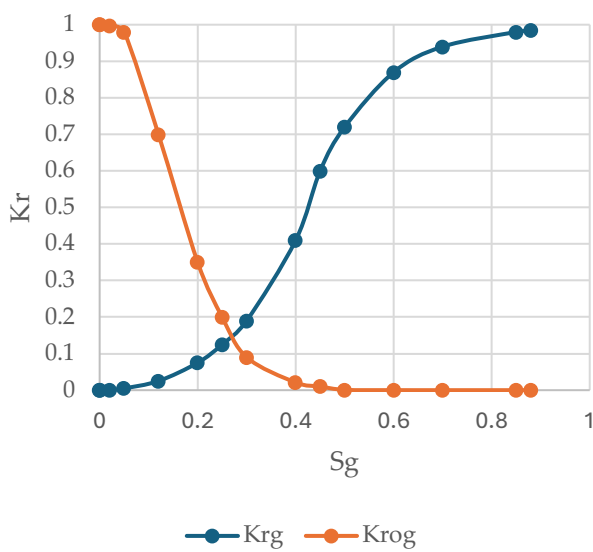
Table 9 Saturated Oil PVT Data for MRST and CMG

Pressure (psi)	FVF Oil	Viscosity Oil (cP)	Rs
14.7	1.062	1.040	1
264.7	1.150	0.975	90.5
514.7	1.207	0.910	180
1014.7	1.295	0.830	371
2014.7	1.435	0.695	636
2514.7	1.500	0.641	775
3014.7	1.565	0.594	930
4014.7	1.695	0.510	1270
5014.7	1.827	0.449	1618
9014.7	2.357	0.203	3006.012

Table 10 Saturated Gas PVT Data for MRST and CMG

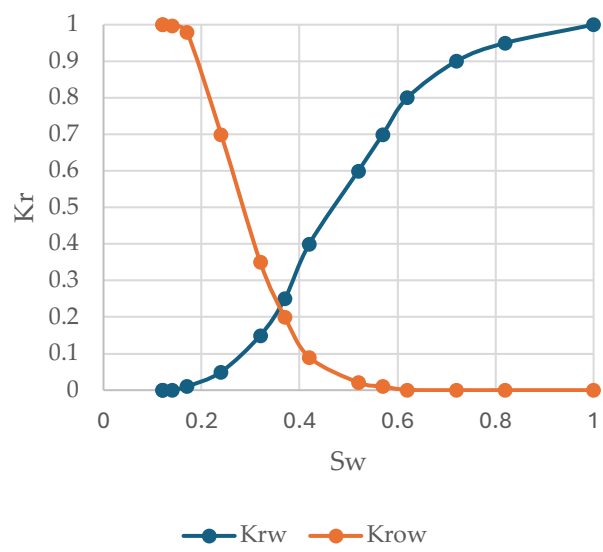
Pressure (psi)	FVF Gas	Viscosity Gas (cP)
14.7	0.166667	0.008000
264.7	0.012092	0.009600
514.7	0.006289	0.011200
1014.7	0.003195	0.014000
2014.7	0.001613	0.018900
2514.7	0.001294	0.020800
3014.7	0.001080	0.022800
4014.7	0.000811	0.026800
5014.7	0.000649	0.030900
9014.7	0.000386	0.047000

Gas-Oil Relative Permeability Curve



(a) Gas Oil Relative Permeability Curve

Water-Oil Relative Permeability Curve



(b) Water Oil Relative Permeability Curve

Figure 9 Relative Permeability Curve

The reservoir model used in this study is based on the SPE-1 dataset, which was originally designed for gas injection scenarios and represents an oil-wet system. While this dataset provides a standardized benchmark model for simulator comparison, its inherent characteristics may not fully represent typical waterflooding conditions, particularly

in terms of wettability and saturation history. Furthermore, the  $K_{rw}$  adjustments made to enable waterflooding simulation may introduce uncertainties in the representation of two-phase flow behavior. It is recommended that future studies incorporate reservoir models with water-wet characteristics and a more comprehensive fluid-rock interaction history to reflect more realistic waterflooding conditions. Additionally, validation with field data or more complex heterogeneous models can improve the generalizability and applicability of the comparative findings between MRST and CMG.

Based on the results of in-place volume calculations from the basic reservoir model, OOIP was calculated to be  $2.61 \times 10^8$  STB, OGIP was calculated to be  $3.32 \times 10^{11}$  SCF, and OWIP was calculated to be  $6.68 \times 10^7$  STB using MRST. Meanwhile, the results of the CMG calculations showed OOIP of  $2.65 \times 10^8$  STB, OGIP of  $4.09 \times 10^{11}$  SCF, and OWIP of  $6.34 \times 10^7$  STB. There was a relative deviation of ~1.5% for OOIP, ~5.1% for OWIP, and ~18.8% for OGIP between the two simulators, table 11 summarizes the initialization results from both simulators. These differences can be explained by the differences in the reservoir initialization methods used by each simulator.

CMG uses an initialization approach based on fluid property tables and depth-dependent initialization, where pressure, saturation, and PVT properties can be precisely calculated at each grid cell based on depth and pressure gradient. In contrast, MRST initializes reservoir properties using functions such as `initResSol`, which applies initial pressure and saturation uniformly across the grid (homogeneous), unless the user manually sets the distribution. Additionally, values such as bubble point pressure ( $P_b$ ), reference pressure for water FVF, and compressibility parameters ( $CVW$ ,  $Co$ ) cannot be explicitly inputted like in CMG but are instead derived through default fluid function approaches such as `initSimpleADIFluid`. Furthermore, differences in gas property representation are a major contributor to higher OGIP deviations compared to OOIP or OWIP. In CMG, although users input the gas formation volume factor ( $B_g$ ), the simulator automatically calculates and incorporates the z-factor (gas compressibility factor) based on pressure and temperature conditions, as well as the PVT correlation used. This z-factor value is a critical component in OGIP estimation, especially under non-ideal gas conditions.

Instead, MRST's default function approach only accepts direct input in the form of  $B_g$  without any calculation mechanism or explicit input for the z-factor. The authors have not yet found a built-in method in MRST to explicitly input or calculate the z-factor in a simple black-oil model. This causes OGIP calculations in MRST to be sensitive to pressure variations and does not involve complex gas compressibility correlations, resulting in greater deviations compared to OGIP calculations in CMG. To overcome these limitations, the author also tried using alternative functions such as `initStateBlackOilAD`, which is technically designed to support black-oil fluid models with a more complex approach. However, the implementation of this function did not run smoothly due to limited documentation, the complexity of the input structure required, and frequent errors during the initialization process. Although there are differences in values, these deviations remain within acceptable tolerance limits and do not compromise the validity of the comparative simulation performance study between scenarios. The prepared model was then technically implemented using MRST as described in the following subsection.

Table 11 Initialization Result

Parameter	MRST	CMG	Difference (%)
Original Oil in Place, stb	2.61E+08	2.65E+08	1.5
Original Water in Place, stb	6.68E+07	6.34E+07	5.1
Original Gas in Place, scf	3.32E+11	4.09E+11	18.8
Original Gas in Place, ft <sup>3</sup> (reservoir condition)	0	0	0

\*Note: OGIP at reservoir condition = 0 due to no free gas at initial condition; gas is entirely in solution phase

However, further investigation is needed regarding the discrepancy observed at the initial timestep. Although the initial reservoir pressure was set to approximately 4800 psi in both simulators, the first timestep outputs show inconsistent values between MRST and CMG. This discrepancy suggests that there may be differences in how each simulator treats the transition from initialization to simulation. As shown in the comparative pressure tables (Figure X), two simulation runs were conducted: one with a total duration of 1 year and another with a shorter duration of 1 day. In both cases, noticeable differences in reservoir pressure were observed even at the earliest timesteps, where MRST

consistently showed slightly lower pressure values compared to CMG. These differences became more significant as the timestep progressed, particularly in the longer simulation. To better understand this, the authors plan to investigate the reservoir pressure data from CMG at the exact same timesteps used in MRST. By analyzing the pressure behavior at a finer temporal resolution during the initial simulation phase, a clearer understanding of the early-time pressure response and the influence of numerical resolution, initialization routines, and timestep handling can be obtained. This effort is expected to clarify the source of deviation and improve the accuracy of cross-simulator comparisons.

Table 12 Pressure Response at Initial Timesteps from MRST and CMG for Different Simulation Durations (Year)

Timestep Year	Reservoir Pressure, psi MRST	Reservoir Pressure, psi CMG	Difference %	Difference psi
0	4791.000	4795.000	-0.1%	4.000
0.005	4772.100	4790.980	-0.4%	18.880
0.010	4759.773	4786.800	-0.6%	27.027
0.021	4735.472	4777.670	-0.9%	42.198
0.041	4688.184	4761.100	-1.5%	72.916
0.082	4605.859	4727.050	-2.6%	121.191
0.164	4454.201	4670.670	-4.6%	216.469
0.329	4206.095	4567.290	-7.9%	361.195
0.493	4021.726	4472.260	-10.1%	450.534
0.657	3918.261	4383.950	-10.6%	465.689
0.821	3863.860	4300.660	-10.2%	436.800
1	3813.785	4212.429	-9.5%	398.644

Table 13 Pressure Response at Initial Timesteps from MRST and CMG for Different Simulation Durations (Day)

Timestep Day	Reservoir Pressure, psi MRST	Reservoir Pressure, psi CMG	Difference %	Difference psi
0	4791.000	4795.000	-0.1%	4.000
0.125	4789.314	4794.710	-0.1%	5.396
0.25	4787.667	4794.280	-0.1%	6.613
0.375	4786.087	4793.850	-0.2%	7.763
0.4375	4785.319	4793.630	-0.2%	8.311
0.5	4784.565	4793.410	-0.2%	8.845
0.5625	4783.823	4793.200	-0.2%	9.377
0.625	4783.093	4792.990	-0.2%	9.897
0.75	4781.665	4792.550	-0.2%	10.885
0.875	4780.276	4792.120	-0.2%	11.844
0.9375	4779.594	4791.910	-0.3%	12.316
1	4778.978	4791.700	-0.3%	12.722

### 3.3.2. Implementation of MRST

The implementation of reservoir modeling was conducted using MATLAB Reservoir Simulation Toolbox (MRST) with a black-oil model. The modeling process followed a structured workflow, starting from the definition of the reservoir grid, rock properties, and fluid characteristics, followed by simulation scheduling and visualization of results. The workflow diagram in Figure 10 summarizes these steps comprehensively. The reservoir grid is formed using the `cartGrid` and `computeGeometry` functions to produce a three-dimensional structure as specified by the model. Petrophysical properties are defined using the `makeRock` function, while fluid properties are set using `initSimpleADIFluid`. Relative permeability and capillary pressure values are compiled based on Corey's correlation and then entered into the fluid object. Furthermore, the reservoir model is constructed using `GenericBlackOilModel`, with initial conditions initialized using `initStateBlackOilAD`. The simulation process is run using `simulateScheduleAD`, and simulation results can be visualized and analyzed further using functions such as `getPlotAfterStep`.

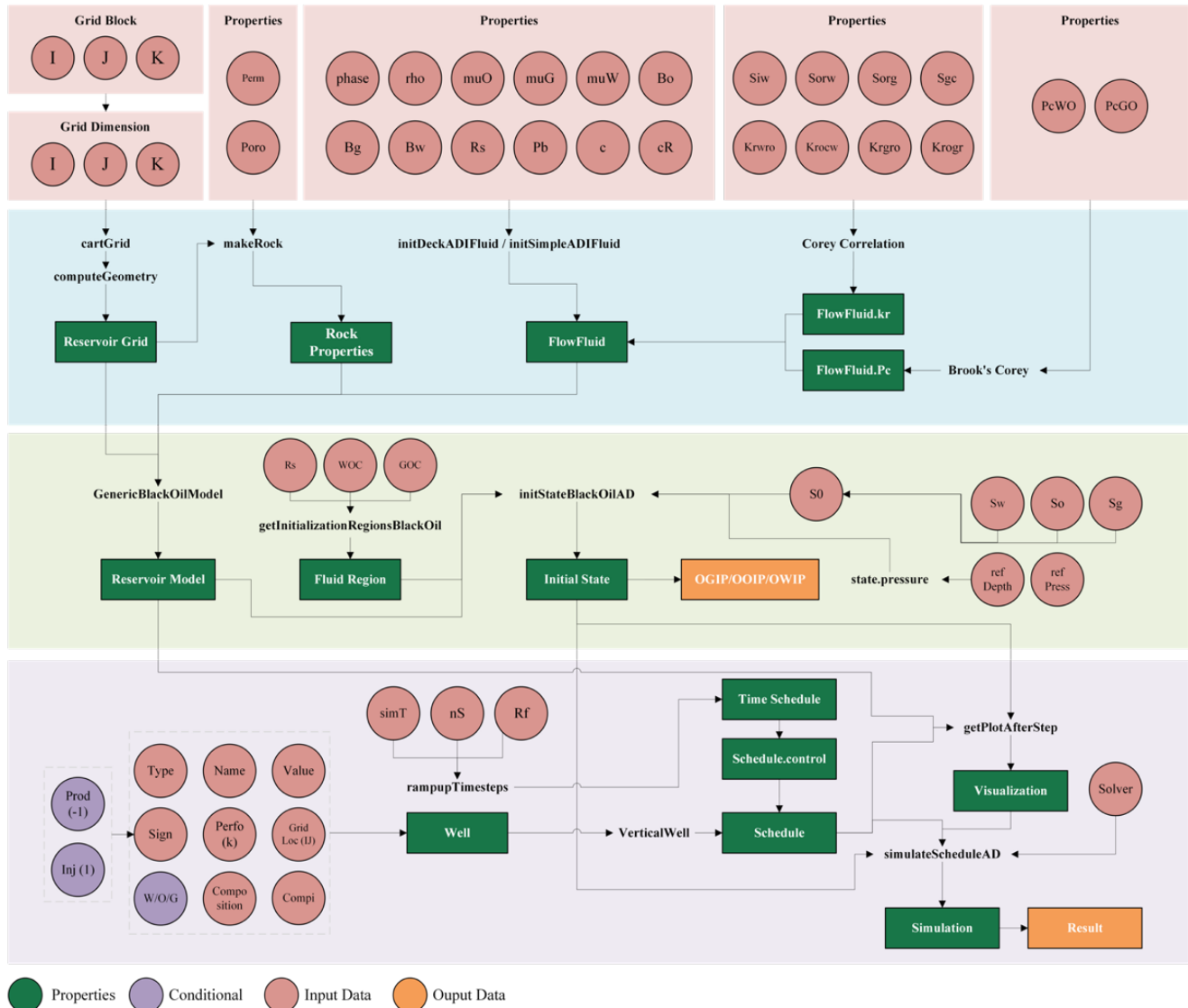


Figure 10 Workflow Reservoir Simulation using MRST

### 3.3.3. Scenario Design for Waterflooding

To evaluate the performance of the reservoir simulator, through this study a series of numerical simulations were conducted based on a combination of four main parameters: well injection pattern, injection well base pressure (BHP), number of grids, and simulator type. Each scenario was designed to test the sensitivity of each parameter to production profile trends and the computation time required to complete the simulation. The sensitivity of the well pattern is shown in the Figure 11.

The entire scenario was developed based on a consistent reservoir baseline (300 grid cells and a production well base pressure of 2000 psi), with one variable varied in each sensitivity group. A total of 42 simulation scenarios were developed, covering the combinations of the above parameters for both MRST and CMG simulations. Detailed information on the grouping of scenarios is presented in Tables 14–17.

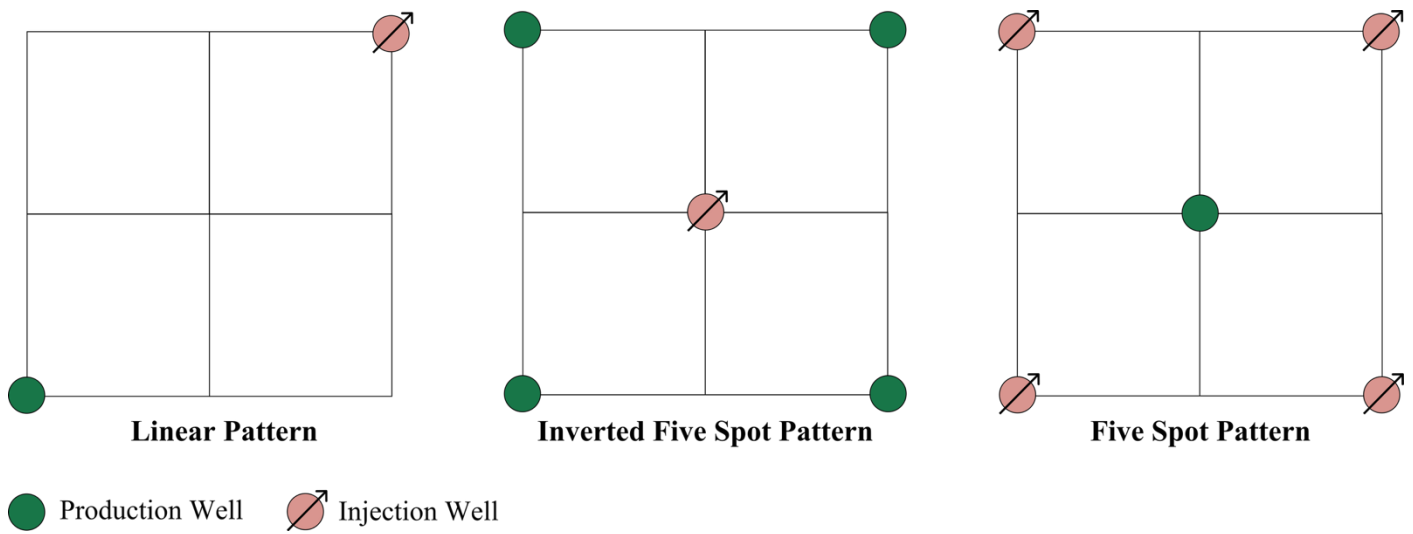


Figure 11 Well Pattern Used for Sensitivity

Table 14 Base Case Scenario for Waterflooding

No	Scenario	Sensitivity	Pattern	Production Well	Injection Well	BHP Production	BHP Injection	Total Grid	Software
1	A1-M	Base Case	Linear	1	1	2000 psi	4500 psi	300	MRST
2	A1-C	Base Case	Linear	1	1	2000 psi	4500 psi	300	CMG

Table 15 Well Pattern Sensitivity for Waterflooding

No	Scenario	Sensitivity	Pattern	Production Well	Injection Well	BHP Production	BHP Injection	Total Grid	Software
1	A2-M	Well Pattern	Five Spot	1	4	2000 psi	4500 psi	300	MRST
2	A3-M	Well Pattern	Inverted Five Spot	4	1	2000 psi	4500 psi	300	MRST
3	A2-C	Well Pattern	Five Spot	1	4	2000 psi	4500 psi	300	CMG
4	A3-C	Well Pattern	Inverted Five Spot	4	1	2000 psi	4500 psi	300	CMG

Table 16 Bottom Hole Pressure Injection Well Sensitivity for Waterflooding

No	Scenario	Sensitivity	Pattern	Production Well	Injection Well	BHP Production	BHP Injection	Total Grid	Software
1	A1-P1-M	BHP Injection	Linear	1	1	2000 psi	2000 psi	300	MRST
2	A1-P2-M	BHP Injection	Linear	1	1	2000 psi	3000 psi	300	MRST
3	A1-P3-M	BHP Injection	Linear	1	1	2000 psi	5000 psi	300	MRST
4	A1-P1-C	BHP Injection	Linear	1	1	2000 psi	2000 psi	300	CMG
5	A1-P2-C	BHP Injection	Linear	1	1	2000 psi	3000 psi	300	CMG
6	A1-P3-C	BHP Injection	Linear	1	1	2000 psi	5000 psi	300	CMG

No	Scenario	Sensitivity	Pattern	Production Well	Injection Well	BHP Production	BHP Injection	Total Grid	Software
7	A2-P1-M	BHP Injection	Five Spot	1	4	2000 psi	2000 psi	300	MRST
8	A2-P2-M		Five Spot	1	4	2000 psi	3000 psi	300	MRST
9	A2-P3-M		Five Spot	1	4	2000 psi	5000 psi	300	MRST
10	A2-P1-C		Five Spot	1	4	2000 psi	2000 psi	300	CMG
11	A2-P2-C		Five Spot	1	4	2000 psi	3000 psi	300	CMG
12	A2-P3-C		Five Spot	1	4	2000 psi	5000 psi	300	CMG
13	A3-P1-M		Inverted Five Spot	4	1	2000 psi	2000 psi	300	MRST
14	A3-P2-M		Inverted Five Spot	4	1	2000 psi	3000 psi	300	MRST
15	A3-P3-M		Inverted Five Spot	4	1	2000 psi	5000 psi	300	MRST
16	A3-P1-C		Inverted Five Spot	4	1	2000 psi	2000 psi	300	CMG
17	A3-P2-C		Inverted Five Spot	4	1	2000 psi	3000 psi	300	CMG
18	A3-P3-C		Inverted Five Spot	4	1	2000 psi	5000 psi	300	CMG

Table 17 Total Reservoir Grid Sensitivity for Waterflooding

No	Scenario	Sensitivity	Pattern	Production Well	Injection Well	BHP Production	BHP Injection	Total Grid	Software
1	A1-G1-M	Total Grid	Linear	1	1	2000 psi	4500 psi	7500	MRST
2	A1-G2-M	Total Grid	Linear	1	1	2000 psi	4500 psi	10800	MRST
3	A1-G3-M	Total Grid	Linear	1	1	2000 psi	4500 psi	14700	MRST
4	A1-G1-C	Total Grid	Linear	1	1	2000 psi	4500 psi	7500	CMG
5	A1-G2-C	Total Grid	Linear	1	1	2000 psi	4500 psi	10800	CMG
6	A1-G3-C	Total Grid	Linear	1	1	2000 psi	4500 psi	14700	CMG
7	A2-G1-M	Total Grid	Five Spot	1	4	2000 psi	4500 psi	7500	MRST
8	A2-G2-M	Total Grid	Five Spot	1	4	2000 psi	4500 psi	10800	MRST
9	A2-G3-M	Total Grid	Five Spot	1	4	2000 psi	4500 psi	14700	MRST
10	A2-G1-C	Total Grid	Five Spot	1	4	2000 psi	4500 psi	7500	CMG
11	A2-G2-C	Total Grid	Five Spot	1	4	2000 psi	4500 psi	10800	CMG
12	A2-G3-C	Total Grid	Five Spot	1	4	2000 psi	4500 psi	14700	CMG
13	A3-G1-M	Total Grid	Inverted Five Spot	4	1	2000 psi	4500 psi	7500	MRST
14	A3-G2-M	Total Grid	Inverted Five Spot	4	1	2000 psi	4500 psi	10800	MRST
15	A3-G3-M	Total Grid	Inverted Five Spot	4	1	2000 psi	4500 psi	14700	MRST
16	A3-G1-C	Total Grid	Inverted Five Spot	4	1	2000 psi	4500 psi	7500	CMG

No	Scenario	Sensitivity	Pattern	Production Well	Injection Well	BHP Production	BHP Injection	Total Grid	Software
17	A3-G2-C	Total Grid	Inverted Five Spot	4	1	2000 psi	4500 psi	10800	CMG
18	A3-G3-C	Total Grid	Inverted Five Spot	4	1	2000 psi	4500 psi	14700	CMG

### 3.4. Zero Balance Test

The zero-balance test is used as an initial validation step to ensure that the reservoir model meets the principles of mass conservation and is numerically stable. In this test, the simulation is set up in the simplest configuration, with one injection well and one production well, both of which are shut-in (not operating), so that there is no fluid flow into or out of the system. This test aimed to observe whether the reservoir system remained in a steady state throughout the simulation. With no injection or production, the pressure, saturation, and other fluid parameters should remain constant and not fluctuate.

The simulation was run on both MRST and CMG simulator software over a short period of time with a fixed timestep, and the results were analyzed for unexpected changes in pressure or saturation values. Good zero balance test results are indicated by the stability of the total fluid mass within the reservoir, with changes approaching zero throughout the simulation time. Results that meet these conditions indicate that the model setup, input parameters, and numerical scheme used are appropriate and do not cause errors or system instability, allowing the model to proceed to waterflooding scenario simulations.

### 3.5. Evaluated Parameter

This study evaluated the performance of waterflooding simulations from various technical and numerical aspects using MRST and CMG simulators. The evaluation was based on key parameters that reflect the effectiveness of water injection, reservoir response, and computational efficiency. The scope of the evaluation was adjusted to the characteristics of each simulation scenario run, both at the macroscopic scale and in terms of local numerical behavior.

#### 1. Recovery Factor (RF)

The recovery factor is calculated as the ratio between the cumulative volume of oil produced and the total original oil in place (OOIP). The RF value is used to assess the effectiveness of water injection scenarios in increasing oil recovery from reservoirs.

#### 2. Breakthrough Time

Breakthrough time is defined as the first time the injected water reaches the production well, indicated by the appearance of significant water saturation or a sharp increase in the water-oil ratio (water cut).

#### 3. Cumulative Oil Production

The cumulative oil volume produced throughout the simulation period provides an overview of the total production of each scenario.

#### 4. Pressure Profile and Production Rate

Reservoir pressure and oil rate trends are evaluated to assess flow stability and depletion patterns. The analysis is performed qualitatively and quantitatively (using slope) in relevant scenarios.

#### 5. Fluid Saturation Distribution

Visualization of water and oil saturation distribution is used to assess the effectiveness of fluid sweeping. Heatmaps are used to show the movement of the waterfront and residual oil at several simulation times.

#### 6. Simulation Runtime (CPU Time)

Runtime is used to measure the computational efficiency of each simulation. This parameter is particularly important when comparing MRST and CMG simulators, as well as when assessing the impact of model complexity (e.g., number of grids) on simulation time.

Parameter evaluation was conducted between scenarios to understand the influence of each variable (well pattern, injection BHP, number of grids, simulator type) on the performance and numerical efficiency of the waterflooding process. This evaluation covered aspects of production results, flow stability, numerical behavior, and computational efficiency, and was used as a basis for comparison between the MRST and CMG simulators.

### 3.6. Data Analysis Method

Simulation results were analyzed quantitatively and comparatively to evaluate the effect of scenario variations on waterflooding process performance. The analysis was conducted by comparing results between scenarios based on key evaluation parameters, such as recovery factor, breakthrough time, cumulative oil production, and simulation runtime. Comparisons between scenarios were presented in the form of production profiles over time, such as oil production rate, water production rate, and recovery factor.

In addition, simulation runtime analysis was used to assess the numerical efficiency of each configuration and to compare the performance between MRST and CMG. Specifically, in the base case, an additional evaluation was performed in the form of fluid saturation distribution in certain reservoir grid cells to support the interpretation of simulation results. It should be noted that this evaluation was only conducted on the base case scenario due to time constraints and technical complexities in extracting visual data from MRST for all scenarios. Nevertheless, the base case was selected as it is considered to represent neutral initial conditions and can serve as a reference for interpreting simulation results in general.

## 4. Result and Discussion

### 4.1. Reservoir Model Setup in MRST

Building fluid models in MRST requires a deep understanding of the code structure and functions used. One of the main challenges is the input process of PVT (Pressure-Volume-Temperature) data. In contrast to CMG which provides a table based input interface to define fluid properties such as solution gas-oil ratio ( $R_s$ ), formation volume factor ( $B_o$ ,  $B_g$ ), or viscosity ( $\mu_o$ ,  $\mu_g$ ) as a function of pressure, MRST requires a manual approach through functions such as `initSimpleADIFluid` or additional modules such as `assignPVTO` where for building complex fluid models MRST only provides the option to use the input file deck.

In CMG, various physical parameters can be input explicitly, including Reference Pressure for Water FVF, Pressure dependence of viscosity ( $C_O$ ,  $C_{VW}$ ), and Oil viscosity ( $V_o$ ) pressure dependence, as well as user-defined bubble point pressure ( $P_b$ ) values directly. In contrast, in MRST, parameters such as  $P_b$  are calculated automatically through internal functions based on gas saturation data or  $R_s$ . The authors did not find a way to explicitly input values such as the reference pressure for water, or the dependency of water viscosity on pressure, which are very common and readily available in CMG.

This makes the fluid model building process in MRST more challenging and limited, especially when compared to CMG which provides better input flexibility and validation support. Although MRST excels in scripting flexibility and open access for modification, in terms of practical implementation, this complexity is one of the main obstacles for general users or beginners in performing realistic and accurate reservoir fluid setup.

### 4.2. Reservoir Model Validation

A preliminary validation test of the reservoir model used, known as a zero-balance test, was conducted prior to the waterflooding scenario analysis. The purpose of this test was to ensure that the numerical model built in the MRST and CMG simulators was accurate, particularly in terms of mass conservation and system stability under no-flow conditions. The zero-balance test was conducted by setting one injection well and one production well in shut-in (non-operational) conditions, so that no fluid entered or exited the system. Assuming a closed reservoir with no external flux, theoretically there should be no change in pressure or fluid saturation throughout the simulation period.

The simulation results are shown in Figures 12-13, which display the distribution of pressure, oil saturation, water saturation, and gas saturation from the initial to the end of the simulation period. Based on the visualization, there were no significant changes in both parameters. The reservoir pressure remained constant, and the initial saturation of water, oil, and gas did not show any changes or fluctuations during the simulation time process. These results confirm that the numerical model built has complied with the principle of mass conservation and does not contain setup errors such as boundary condition errors, initial saturation inconsistencies, or other numerical instabilities.

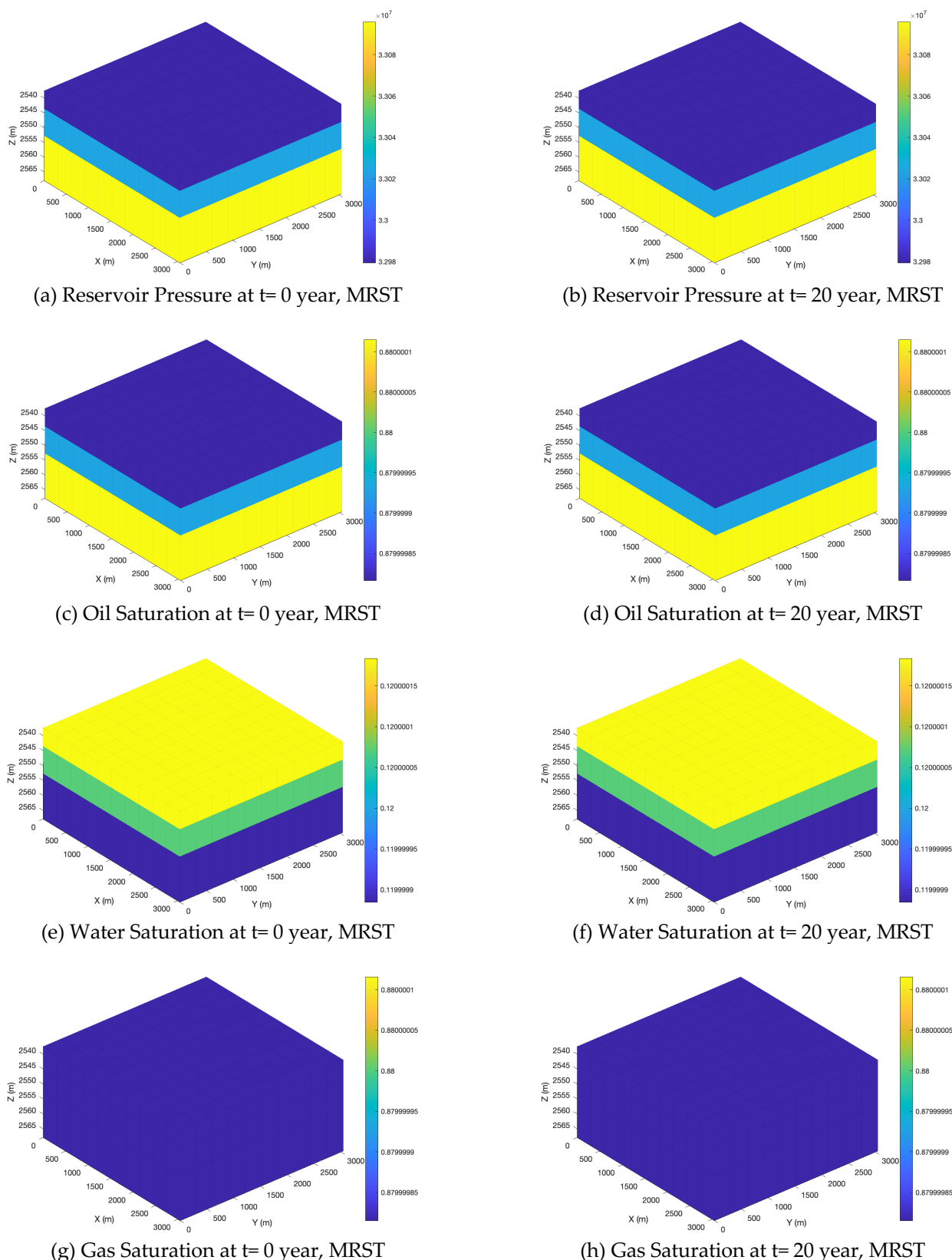


Figure 12 Zero Balance Test Result in MRST

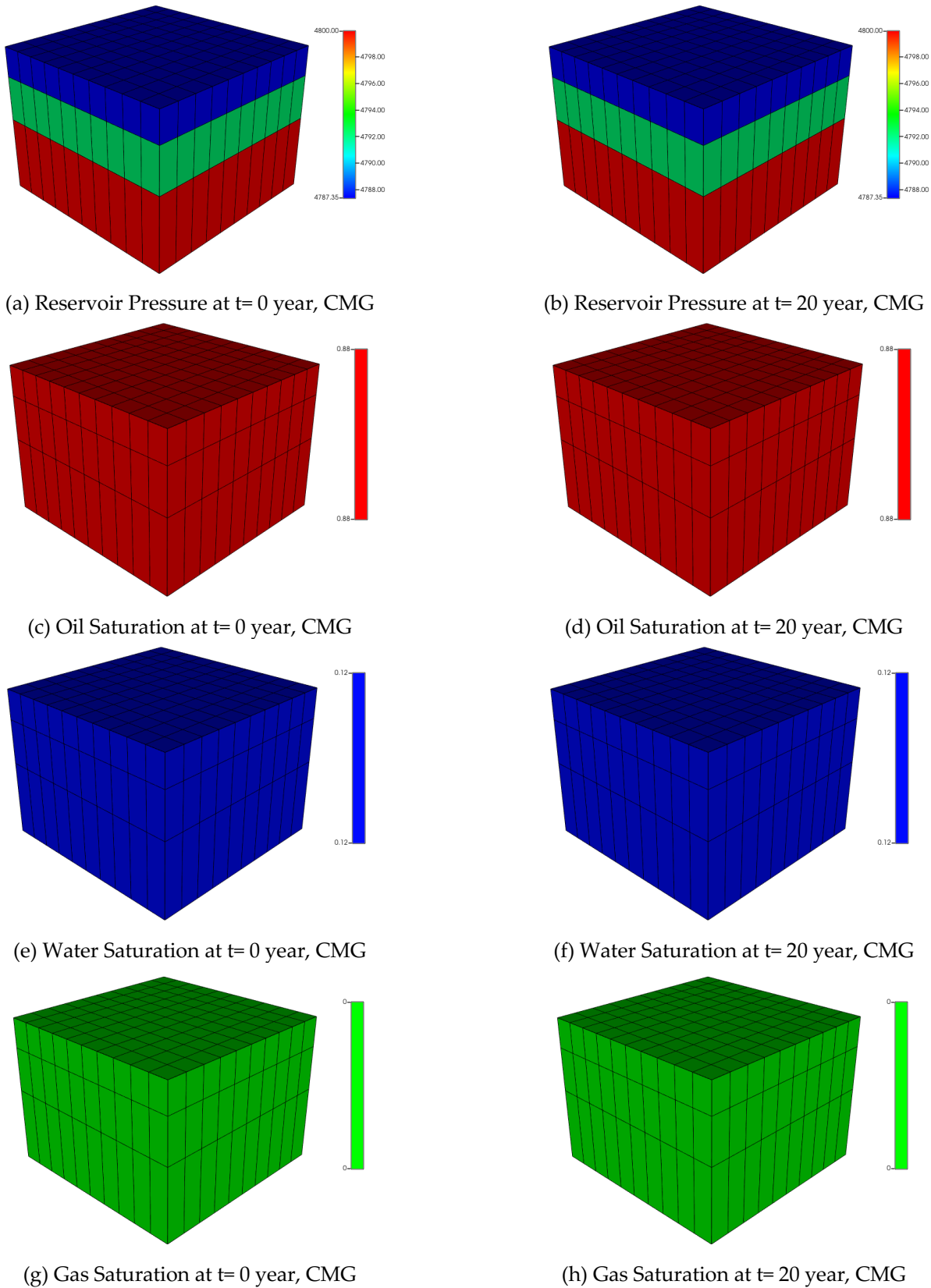


Figure 13 Zero Balance Test Result CMG

#### 4.3. Base Case Simulation

In the initial stage, a base case<sup>1</sup> analysis was conducted to evaluate the reservoir production profile to understand the general response of the simulator to the base waterflooding scenario. The main parameters observed included average reservoir pressure, oil production rate, gas production rate, and gas-oil ratio (GOR). A comparison was made between two simulators, MRST and CMG, to check the consistency of the results and detect any abnormal numerical behavior.

Reservoir pressure profiles from the base case (refer to footnote 1) simulation are shown in Figure 14a, which compares the results between MRST and CMG over the simulation period. During the first year of production, there was a significant difference in initial pressure values between the two simulators. CMG reported a reservoir pressure of around 4200 psi, while MRST showed a lower value of around 3700 psi. However, the pressure decline pattern during the natural depletion phase from year 1–11 shows an almost similar trend in both simulators.

Over the period from year 8–11, the pressure difference between MRST and CMG becomes smaller, confirming that both simulators have similar reservoir depletion responses before the start of water injection. After water injection began in year 11, both simulators showed a consistent increase in reservoir pressure. During year 11–16, the pressure increases trends in MRST and CMG were nearly identical. However, a difference began to appear in year 17, with MRST showing a faster pressure increase, while CMG exhibited a delay, with a significant increase starting in year 18. Although there were slight differences in dynamics during the transition period, at the end of the simulation period (year 20), the reservoir pressure in both simulators converged to the same value, around 3500 psi. These results confirm that the long-term consistency between MRST and CMG was maintained, regardless of differences in pressure response rates during the initial phase of water injection.

Oil production rate profiles from the base case (refer to footnote 1) simulation are shown in Figure 14b. At the beginning of the simulation, both simulators recorded an oil production rate of 16,000 stb/d in the first year. During the natural depletion phase from year 1–11, MRST and CMG showed nearly identical production decline trends, with production rates gradually decreasing in line with reservoir pressure decline. After water injection began in year 11, the oil production rates in both simulators remained stable and similar until year 16, confirming the initial effectiveness of the waterflooding process. However, differences began to appear in year 17, with MRST showing a faster increase in oil production compared to CMG, the oil rate only started to increase around the year 18.

Differences in the timing of production increases indicate the possibility of faster oil bank formation in MRST, or differences in how the two simulators handle the distribution of the water sweep front relative to oil. Further analysis of saturation distribution will be discussed in the next subsection. Although there are differences in the timing of the increase in oil production rates, at the end of the simulation in year 20, the production rates from both simulators once again converge, with oil production values ranging from 14,000 stb/d, confirming that the final oil production results remain comparable between MRST and CMG.

<sup>1</sup> Case A1 as base case scenario applies linear pattern, with a bottom-hole pressure (BHP) constraint of 2000 psi for the production well, 4500 psi for the injection well, and a total of 300 active grid blocks

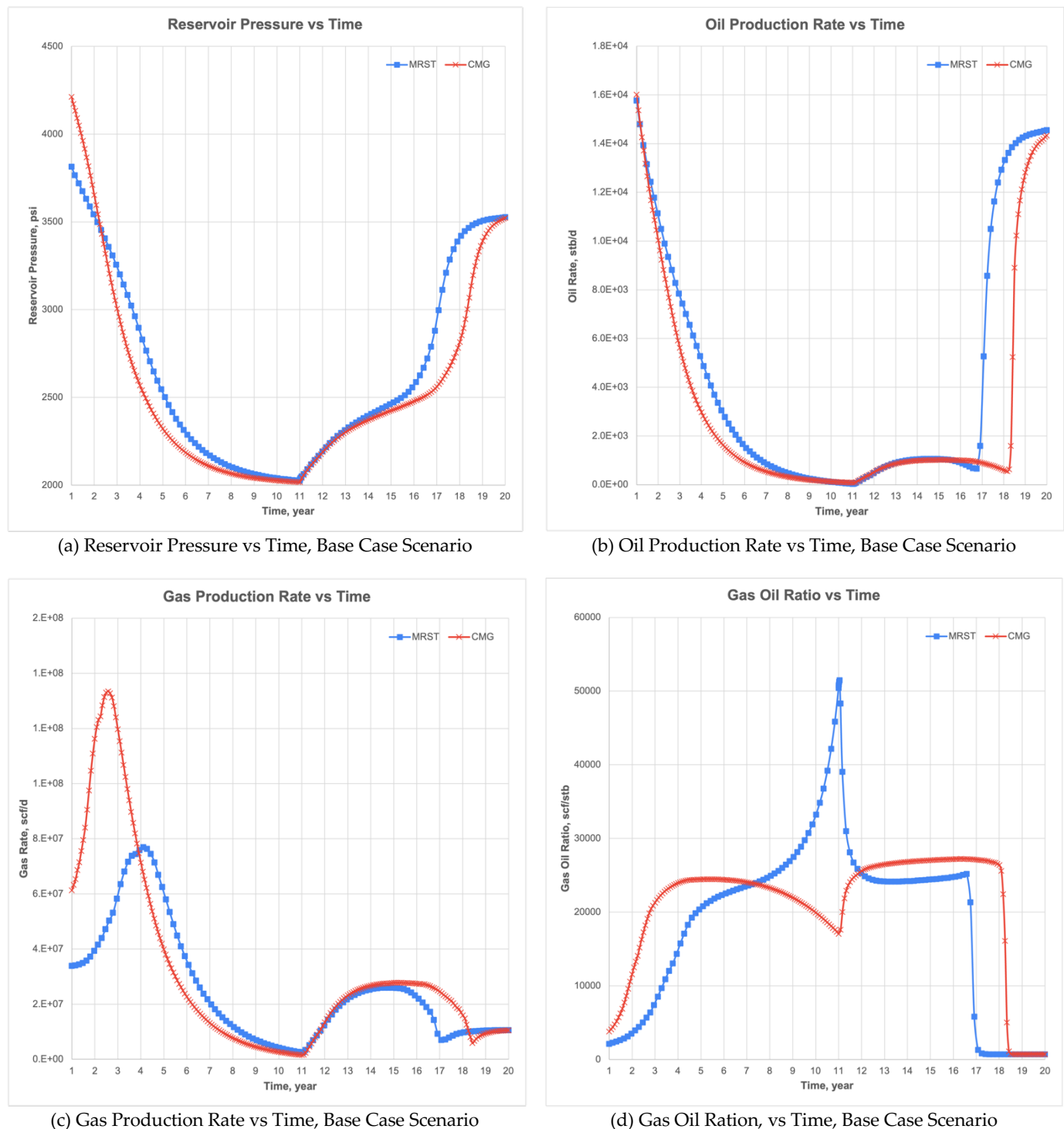


Figure 14 Profile Production, Base Case Scenario

Gas production profiles from the base case (refer to footnote 1) simulation show clearer differences between the two simulators in the first five years of simulation, as shown in Figure 14c. CMG recorded higher gas production rates in the first year, reaching around 60,000,000 scf/d, while MRST only recorded around 34,000,000 scf/d. This difference primarily occurs during the early production phase, reflecting differences in how the gas phase is handled by the two simulators. However, after water injection begins in the year 11, both simulators show nearly identical gas production trends, although CMG maintains a slightly higher gas production rate compared to MRST until the end of the simulation.

period. These results reveal slightly different gas flow characteristics, but overall, gas production trends are similar after water injection.

Gas-oil ratio (GOR) behavior is shown in Figure 14d, which reveals more pronounced differences in trends between MRST and CMG. CMG shows an increase in GOR in the first year, followed by a gradual decline until the year 11, with a slight increase after water injection, before finally declining again in the year 19. In contrast, MRST shows a consistent increase in GOR from the first year until it reaches around 50,000 scf/stb in the year 11, before experiencing a sharp decline after the start of water injection. Differences in GOR behavior indicate that differences in fluid models, especially in handling gas compressibility and multiphase flow, contribute to different numerical responses between the two simulators. It is an important finding in evaluating the accuracy of gas phase predictions in MRST-based simulation models compared to CMG.

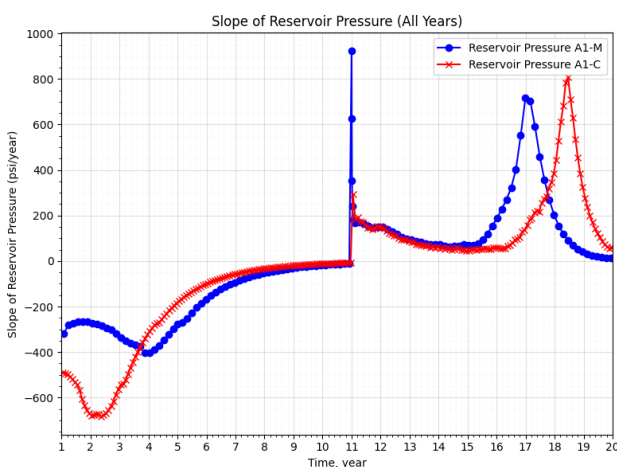
### Decline Trend Analysis

Further analysis was conducted to evaluate changes in reservoir pressure trends and oil production rates throughout the base case (refer to footnote 1) simulation period. Slopes were calculated based on changes in values over time and plotted against time to identify decline dynamics in each simulator. Figure 15a shows the reservoir pressure slope profile over time, while Figure 15b shows the oil production rate slope profile. Up to year 16, MRST and CMG showed similar patterns of pressure and oil production decline, following the natural depletion characteristics of the reservoir. However, more pronounced differences began to emerge in year 17, with MRST showing higher slopes for both reservoir pressure and oil rate compared to CMG. This is consistent with previous observations on the production curve, where MRST showed a faster production increase response after water injection began.

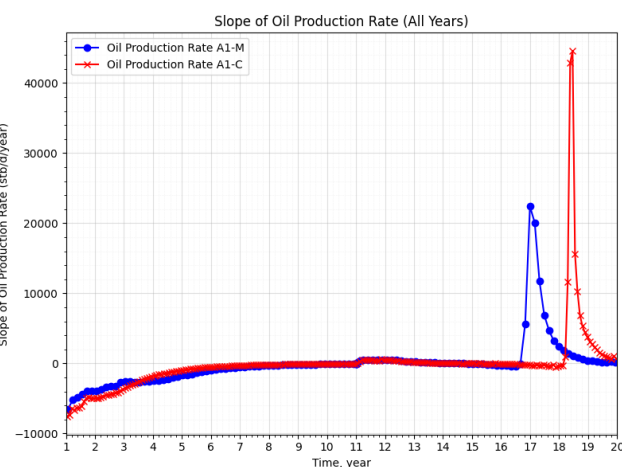
Interestingly, analysis of reservoir pressure slopes also shows that maximum pressure decline occurs earlier in CMG (around year 2.5), which coincides with the highest gas production rate in CMG, while in MRST, maximum pressure decline occurs around year 4, which also coincides with the peak gas production in MRST. This indicates that although gas is not the primary focus in the waterflooding scenario, differences in gas production dynamics at the beginning of the simulation play a significant role in influencing the rate of reservoir pressure decline during the natural depletion phase. To clarify the nature of the decline, linear regression analysis was performed on two important time segments: year 1-11 (natural depletion phase) and year 11- 20 (waterflooding phase). The global slope values for both simulators are summarized in Table 18.

Table 18 Slope Linear Regression Results Value Base Case

Parameter	Slope (Year 1-11)		Slope (Year 11-20)	
	MRST	CMG	MRST	CMG
Reservoir pressure, psi/year	-186.84	-191.71	181.16	147.99
Oil Production Rate, stb/d/year	-1365.65	-1195.27	1764.28	1218.87



(a) Slope vs Time of Reservoir Pressure MRST and CMG



(b) Slope vs Time of Oil Production Rate MRST and CMG

Figure 15 Slope Profile Over Time, Base Case Scenario

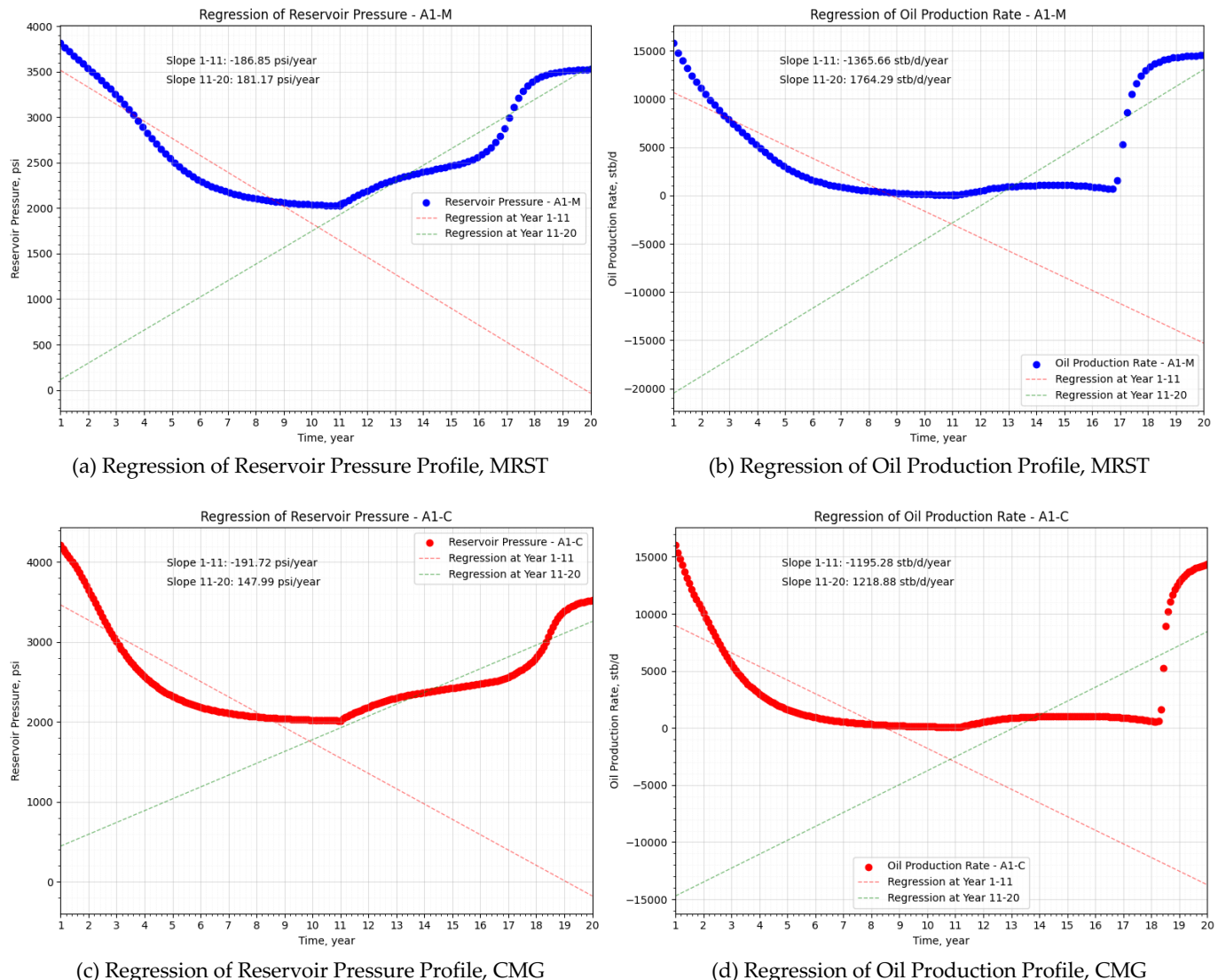


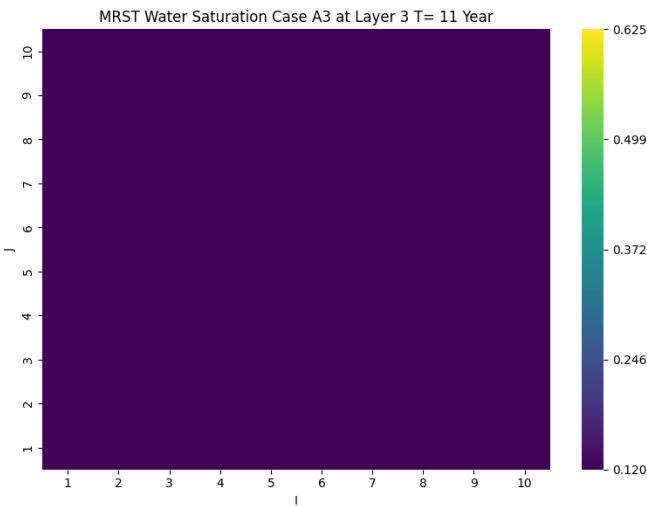
Figure 16 Regression Profile Over Time, Base Case Scenario

During the natural depletion phase (year 1-11), both MRST and CMG showed a negative slope in reservoir pressure and oil production rate, as shown in Figures 16a-b for MRST and Figures 16c-d for CMG, reflecting natural production mechanisms without fluid injection. Both simulators show slope values within a similar range, with MRST exhibiting a slightly steeper decline in oil production rate compared to CMG. During the waterflooding phase (year 11-20), the reservoir pressure and oil production rate slopes reversed to positive values in both simulators, indicating a response to water injection. MRST showed a greater increase in pressure and oil production compared to CMG, which may indicate differences in numerical responses in reservoir pressure or sweep front distribution between the two simulators.

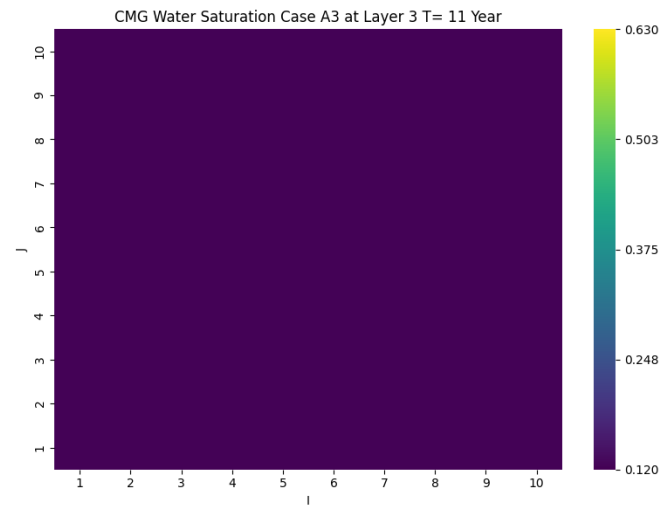
#### Saturation Distribution and Sweep Efficiency Analysis

Water and oil saturation distribution was evaluated in the year 11 and year 17 to observe fluid sweep progress after the initial water injection phase. Saturation heatmaps from both simulators, MRST and CMG, were used to compare water sweep patterns and residual oil in the reservoir. In the year 11, both MRST and CMG still showed very low water saturation in the entire reservoir area. At this point, water injection had begun, but there was no significant spread of the water saturation front around the injection well. Most of the reservoir remained dominated by oil, and the water saturation distribution in both simulators did not show significant differences, as seen in Figures 17a-b for water saturation distribution in the year 11, and Figures 18a-b for oil distribution in the year 11 for MRST and CMG.

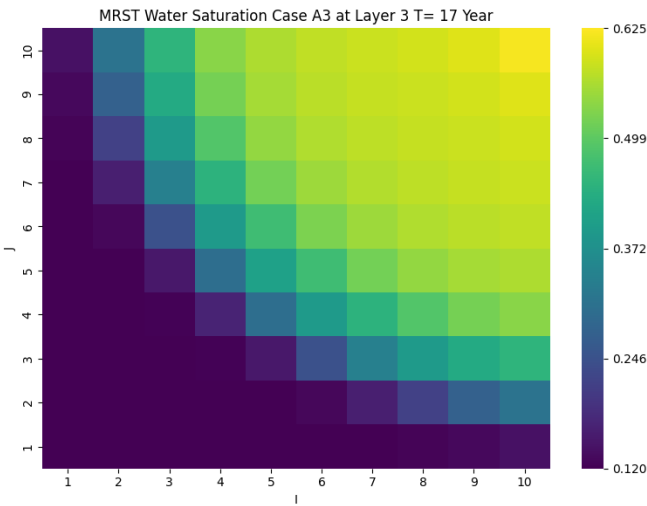
Entering the year 17, fluid sweep progress in the reservoir becomes more clearly visible, with the water saturation front beginning to move further from the injection location. The area with high water saturation starts to expand, while the area with low oil saturation continues to grow. MRST and CMG show very similar saturation distribution patterns, both in terms of the location of the sweep front and the remaining oil area.



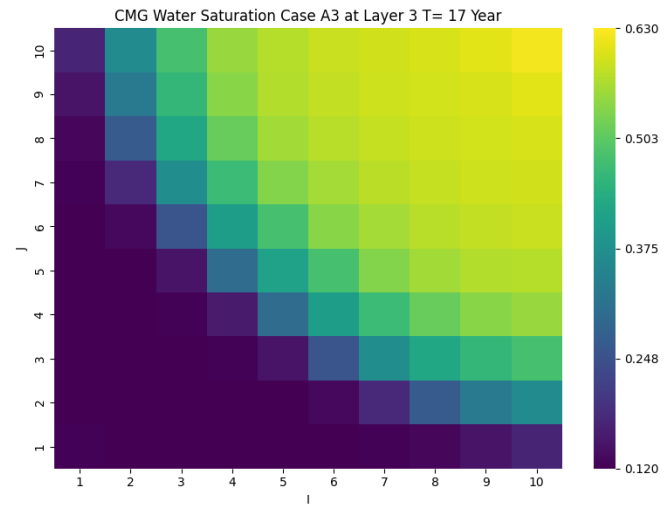
(a) Water Saturation Distribution T=11 Year, MRST



(b) Water Saturation Distribution T=11 Year, CMG



(c) Water Saturation Distribution T=17 Year, MRST



(d) Water Saturation Distribution T=17 Year, CMG

Figure 17 Water Saturation Distribution, Base Case Scenario

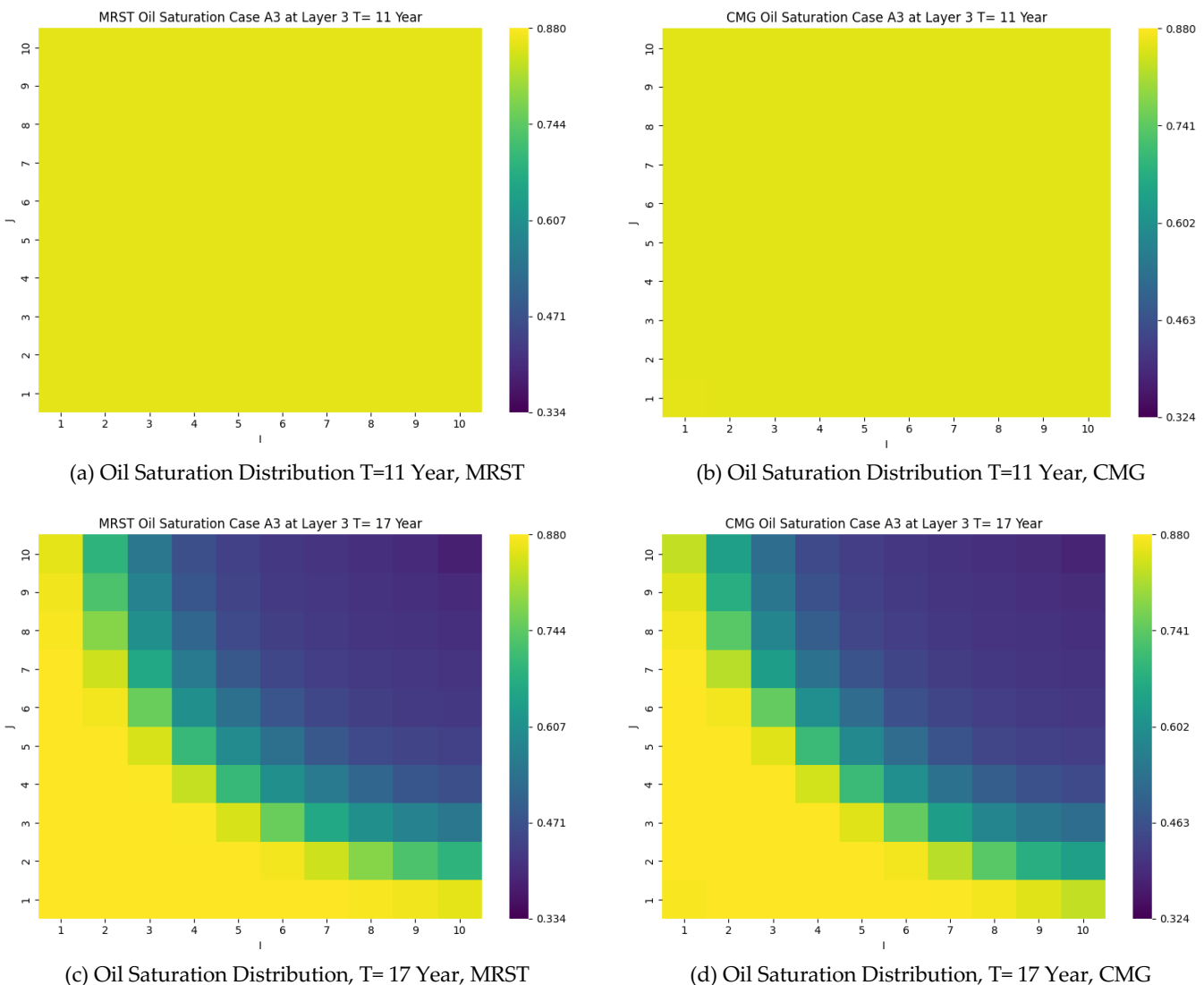


Figure 18 Oil Saturation Distribution, Base Case Scenario

Although the distribution patterns of water and oil saturation in the year 17 appear nearly equivalent between the two simulators, more apparent differences occur in the oil production response, where MRST shows an earlier increase in production rate in the year 17 compared to CMG, which first experiences an increase in the year 18. These differences are likely due to the different numerical approaches and fluid flow solutions adopted by each simulator. For a better understanding of the potential differences in fluid distribution, a relative error analysis of water and oil saturation between MRST and CMG in the year 17 was conducted, as shown in the following section.

#### Relative Error Analysis of Saturation Distribution

To evaluate the accuracy of the simulation results between MRST and CMG, a relative error analysis was conducted on the distribution of oil saturation ( $S_o$ ) and water saturation ( $S_w$ ) at two time points, specifically in year 11 and year 17, particularly in layer 3. Figures 19a-b show the relative error distribution of oil saturation in year 11 and year 17, while Figures 19c-d show the relative error distribution of water saturation at the same time. In year 11, the relative errors of water and oil saturation across the entire reservoir grid were at very low values, with most oil saturation errors ranging around 0.2–0.25%, and water saturation errors were even smaller, approaching 0.00–0.01% across the entire area. These results are in line with previous findings indicating that, in year 11, water injection had just begun, so changes in fluid distribution were still minimal, and the reservoir remained in its initial state.

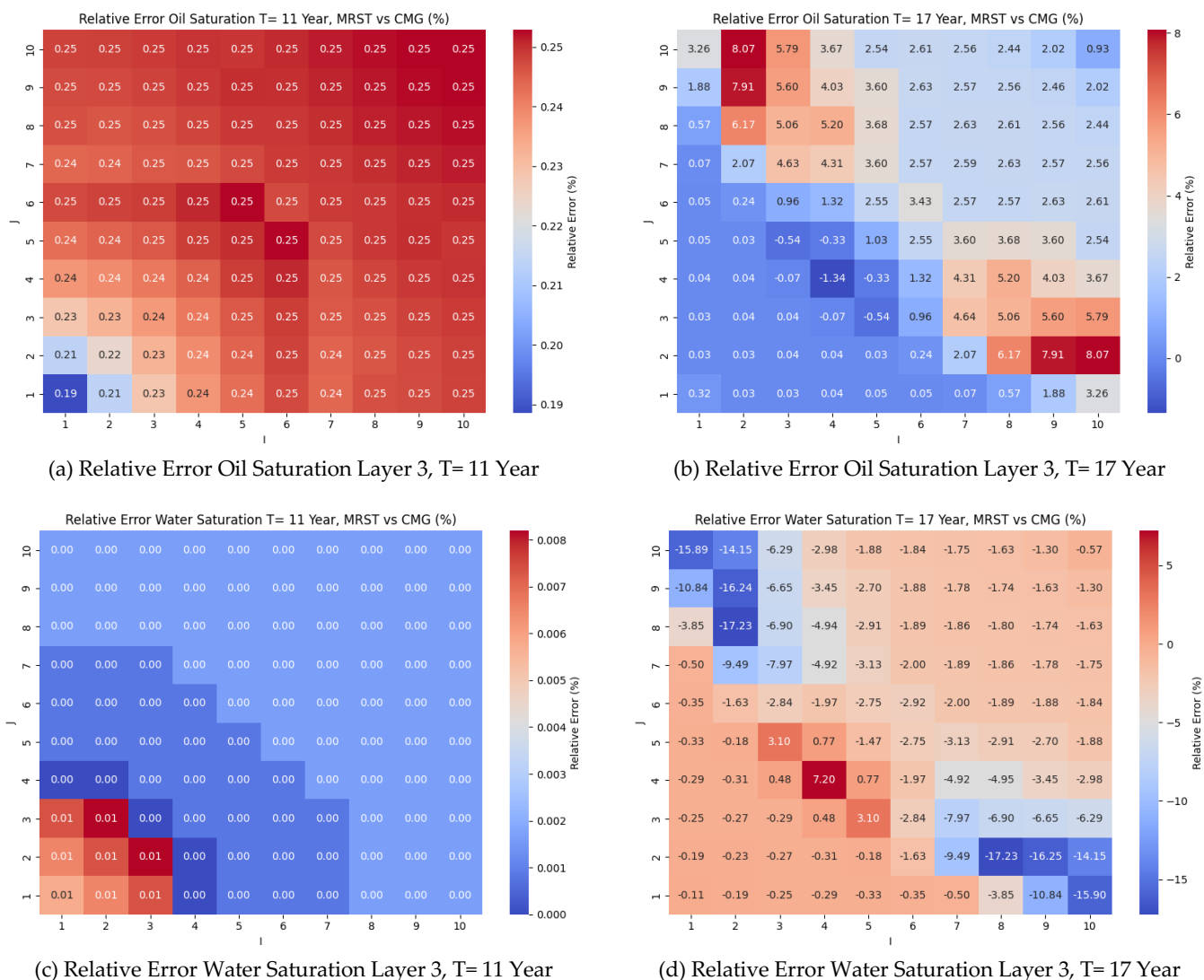


Figure 19 Relative Error Oil and Water Saturation, Base Case Scenario

In year 17, after the waterflooding process had been ongoing for a longer period, the relative error distribution began to show greater variation, particularly in the transition area of the water saturation front, not around the production or injection wells. Oil saturation errors ranged from 0% to a maximum of around 8% in some local areas, while water saturation errors showed more dynamic variation, ranging from -17% to +7%. These differences were primarily concentrated in the areas around the movement of the saturation front, which were numerically sensitive to differences in the timing of the fronts between MRST and CMG, as also indicated by the pressure response in both simulators. Errors in areas that have been swept or not yet swept (in front of and behind the front) are relatively small and uniform, indicating consistency in saturation results outside the front transition zone. This finding implies that the main difference in saturation distribution between MRST and CMG is more related to the arrival time of the front due to differences in numerical approach and solver.

#### Pressure Analysis at Production and Injection Wells

Pressure profiles in the production well grid is shown in Figure 20, which compares the results between MRST and CMG over the simulation period. In general, both simulators show very similar pressure decline patterns during the natural depletion phase (year 1-11), as well as comparable responses to the start of water injection in year 11, with pressures around the production well remaining at low values. Nevertheless, more apparent differences begin to appear in year 17, where MRST shows a faster pressure increase, while CMG shows an increase in pressure starting in year 18.

This phenomenon is in line with the results of observations on the overall reservoir pressure profile and is closely related to the oil production pattern discussed earlier.

Faster pressure increase in MRST may accelerate the push of oil into the production well, leading to an earlier increase in oil production rate compared to CMG. This difference likely originates from the different numerical approaches between the simulators, where MRST may apply more aggressive non-linear or saturation transport solutions, while CMG tends to be more conservative in controlling the saturation front. This reinforces that, even though the macroscopic saturation distribution in the reservoir appears similar, the internal numerical effects of the solver can still influence the production response time.

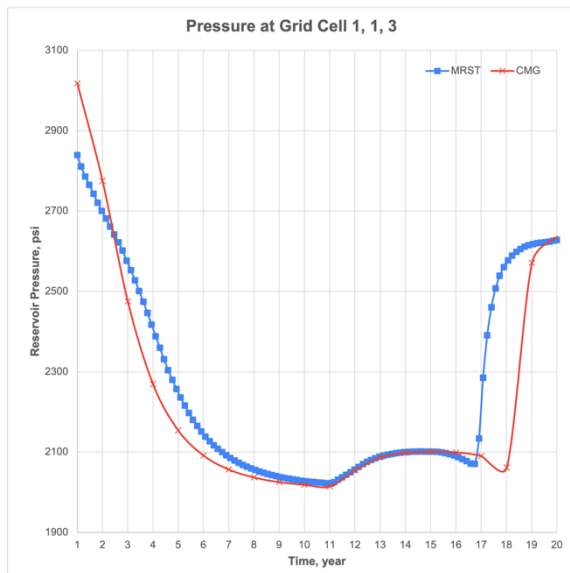


Figure 20 Pressure at Grid Cell Production Well, Base Case Scenario

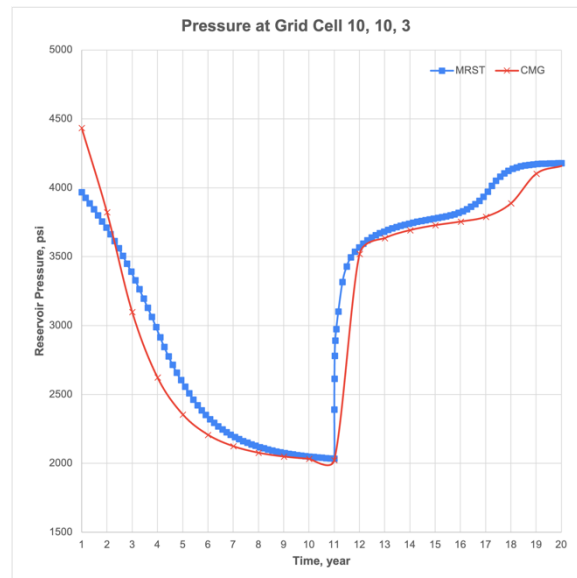


Figure 21 Pressure at Grid Cell Injection Well, Base Case Scenario

Meanwhile, pressure analysis in the injection well grid Figure 21, shows that both simulators provide nearly identical pressure responses throughout the simulation period. After water injection began in year 11, pressure around the injection well increased gradually and stabilized in both MRST and CMG. There were no significant differences in the pressure increase or maximum pressure level between the two simulators. This indicates, from the perspective of injection pressure control, that the stability of waterflooding operations is consistently represented in both MRST and CMG. However, although the injection pressure profiles in both simulators are similar, the behavior of the water injection rate shows differences in behavior, especially in the early phase of injection. This aspect will be discussed further in the following section to gain a deeper understanding of the dynamics of early water injection behavior.

#### Water Injection Rate Behavior Analysis

To complete the analysis of pressure around the injection well, an evaluation of the water injection rate profile over the simulation period was conducted. Figure 22 shows the water injection rate in the injection well for MRST and CMG. In the early year before water injection (year 1-11), there was no fluid flow in the injection well, as expected. However, after water injection began in year 11, there was a significant difference in the water injection rate behavior between MRST and CMG.

In MRST, the water injection rate experienced a very large spike at the beginning of the injection phase, reaching a level much higher than CMG. After the initial spike, the injection rate in MRST decreased and stabilized at a level comparable to CMG until the end of the simulation period. In contrast, in CMG, the water injection rate increased gradually and more smoothly after the start of injection, without experiencing a large surge, and maintained injection stability throughout the period.

This initial spike phenomenon in MRST indicates a difference in numerical control of the injection rate between the two simulators. In MRST, the solver characteristics and non-linear control settings, such as step size adaptivity, well

control stability, or injection phase mobility, may not sufficiently conserve the fluid rate during the initial well opening phase. Conversely, in CMG, the smoother water injection rate stability can be attributed to the solver's adaptive capabilities, particularly in time-stepping size adjustment (adaptive time-stepping). During the initial injection phase, CMG automatically adjusts the timestep size to maintain numerical solution stability and ensure that changes in fluid flow rate remain controlled. This allows CMG to avoid injection rate spikes and produce a more gradual and realistic injection transition compared to MRST.

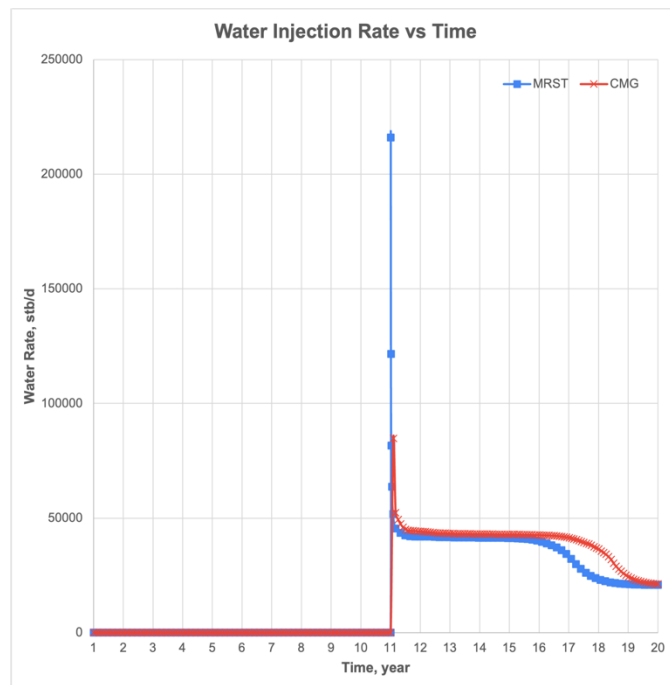


Figure 22 Water Injection Rate Behavior, Base Case Scenario

### Water Breakthrough Time Analysis

To evaluate the breakthrough time in the base case (refer to footnote 1), the simulation was extended to 30 years, with water injection starting in year 11, resulting in a total injection duration of 19 years. The simulation results show that water breakthrough began to be detected in year 11.80 in MRST and year 11.18 in CMG, indicating a breakthrough time difference of approximately 0.62 years between the two simulators. Interestingly, although water breakthrough in MRST was detected slightly later than in CMG, the pressure and oil rate responses in MRST showed a faster increase of about one year compared to CMG. This indicates that MRST predicted the movement of the saturation front approaching the production well faster in terms of pressure and production rate, but the detection of saturation breakthrough in the production well occurred slightly later. This can be seen in Figure 23. In this report, breakthrough times are consistently measured from the onset of water injection, which began in simulation year 11. This approach is applied uniformly across all scenarios to ensure clarity and consistency when comparing the timing of fluid front arrival at the production well.

This difference is consistent with the results of the water saturation error distribution analysis in the 17th year, where the transition zone of the front in MRST showed relatively lower errors compared to CMG, while errors in the swept or not yet swept (in front of and behind the front) areas remained uniform. These results indicate that although the macroscopic distribution of fluid saturation in MRST and CMG is similar, differences in the solver approach still result in differences in the dynamics of the saturation front movement, pressure response, and breakthrough time.

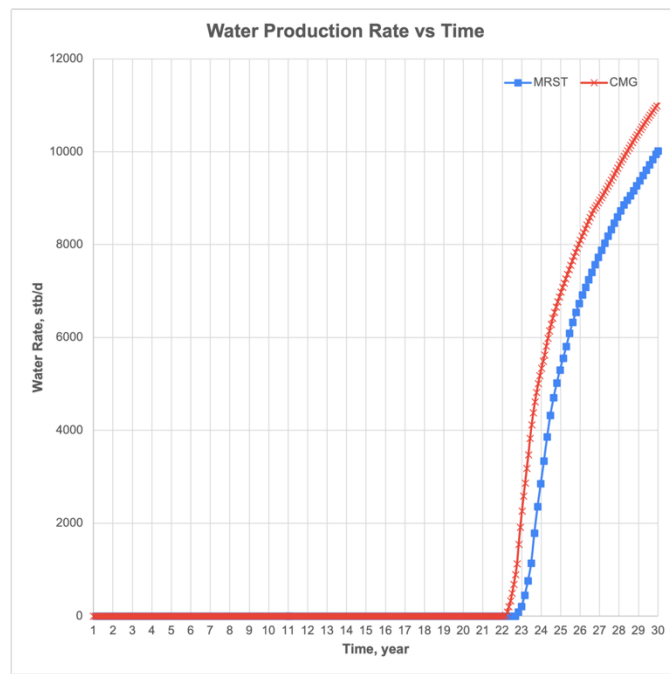


Figure 23 Water Production Rate vs Time, Base Case Scenario

Base case (refer to footnote 1) simulation results show that MRST and CMG provide consistent results in modeling reservoir behavior, in terms of oil production, gas production, and water injection. Although there are some minor differences in response time and production trends, in general, both simulators show similar reservoir behavior characteristics throughout the simulation period. The observed differences reflect variations in numerical methods, multiphase fluid flow solution approaches, and internal computational model handling, particularly in MRST, which shows a slightly faster production response than CMG in several simulation stages.

To provide a clearer overview of the performance of both simulators in this base case, Table 19 presents a comparison of the main results between MRST and CMG, including initial reservoir capacity parameters, cumulative production performance, and indications of waterflooding success. Based on the results of this base case, a sensitivity analysis was conducted on well patterns, injection pressure, and grid resolution in the next section.

Table 19 Base Case (A1) Results between MRST and CMG

Parameter	MRST	CMG	Difference (%)
Recovery Factor (RF), %	14.25	10.62	34.2
Cumulative Oil Production, stb	3.73E+07	2.82E+07	32.2
Cumulative Gas Production, scf	1.88E+11	2.41E+11	22
Cumulative Water Production, stb	1.71E+07	2.11E+07	18.95
Breakthrough Time, year	11.80	11.18	5.54

Note: The detailed configuration for Case A1 refers to a simulation scenario with specific BHP and grid settings, fully described in footnote 1. Breakthrough time is measured relative to the start of injection (year 11)

#### 4.4. Scenario Simulation Result

Following the analysis of the base case simulation results, this section evaluates a variety of scenarios to understand the sensitivity of reservoir performance to several operational parameters and geometric models. The three main parameters varied in these scenarios include well pattern, bottom-hole pressure injection, and grid resolution. Each scenario is designed based on the same reservoir baseline as the base case, with only one parameter changed for each sensitivity group. The purpose of this analysis is to identify how changes in each parameter affect oil production response, water injection performance, reservoir pressure changes, and simulation performance.

#### 4.4.1. Effect of Well Pattern

Variations in well injection patterns significantly affect fluid sweep efficiency and production performance in waterflooding scenarios. In this section, two injection pattern configurations, namely five-spot<sup>2</sup> and inverted five-spot<sup>3</sup>, are analyzed to evaluate the differences in reservoir response generated by each pattern. The observed differences will be examined to understand the implications of injection patterns on overall waterflooding performance.

#### Fluid Sweeping Effectiveness Analysis

The effectiveness of fluid sweeping due to variations in injection patterns was analyzed by comparing the Recovery Factor (RF) values and oil saturation distribution based on heatmap visualization results. Based on the simulation results, the application of the five-spot (refer to footnote 2) and inverted five-spot patterns (refer to footnote 3) showed a significant increase in the Recovery Factor compared to the base case linear pattern, both in MRST and CMG. This indicates that the use of injection patterns with more even distribution successfully improved the fluid displacement mechanism within the reservoir.

To support this analysis, oil saturation heatmaps for the year 20 are presented for each layer (Layer 1, 2, and 3). The visualizations in Figures 24–25 show that in both injection patterns, the areas with low oil saturation (which have been swept by water injection) are more extensive compared to the base case (refer to footnote 1), indicating more effective sweeping.

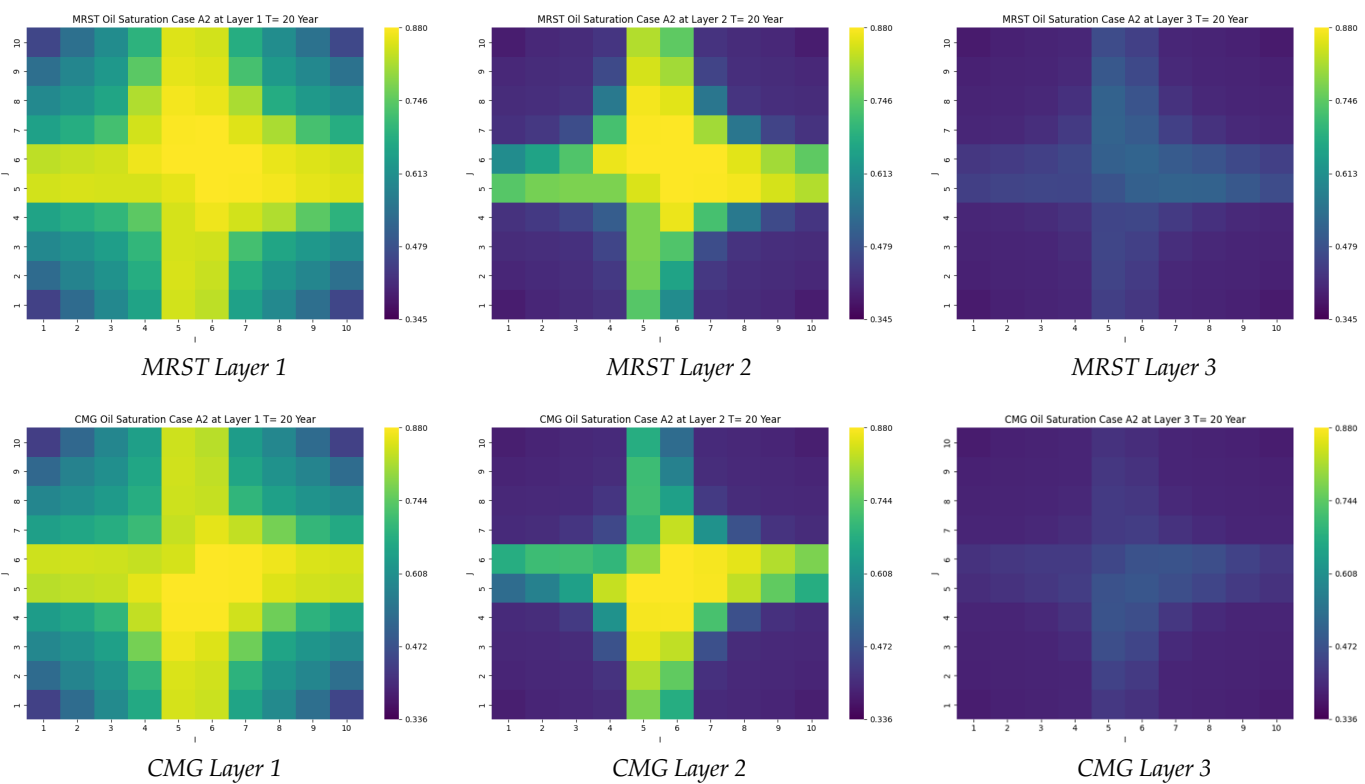


Figure 24 Oil Saturation Distribution at Various Layer, Case A2 (Five Spot)

<sup>2</sup> Case A2 applies five-spot pattern, with a bottom-hole pressure (BHP) constraint of 2000 psi for the production well, 4500 psi for the injection well, and a total of 300 active grid blocks.

<sup>3</sup> Case A3 applies inverted five-spot pattern, with a bottom-hole pressure (BHP) constraint of 2000 psi for the production well, 4500 psi for the injection well, and a total of 300 active grid blocks.

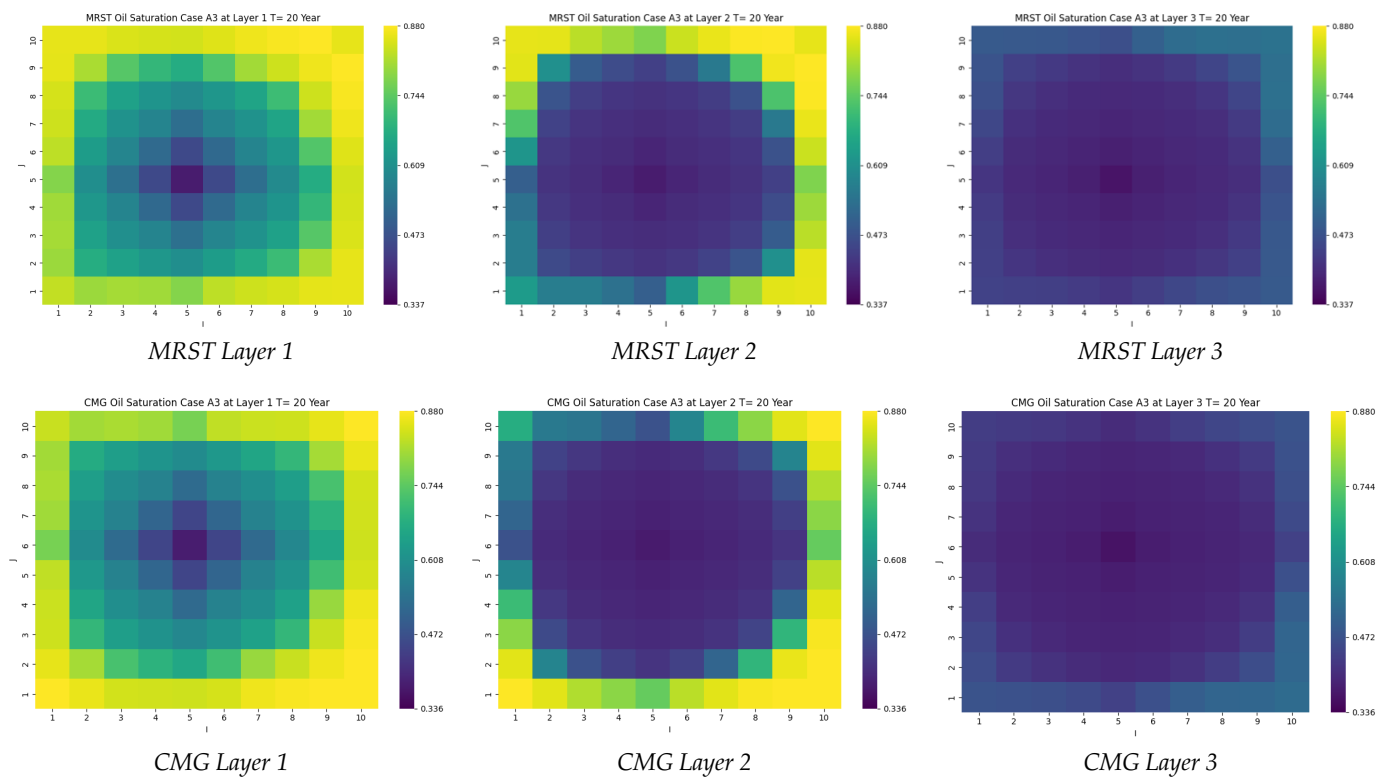


Figure 25 Oil Saturation Distribution at Various Layer, Case A3 (Inverted Five Spot)

Both the MRST and CMG simulators show very similar sweep patterns, with nearly identical oil saturation distributions throughout the reservoir. However, there is a slight difference in the orientation of the saturation front distribution between the two simulators. In the MRST, areas with slightly higher residual oil saturation tend to be oriented toward the upper right of the reservoir, while in the CMG, similar areas are more dominant toward the lower right. This difference reflects minor variations in the internal numerical characteristics of each simulator with respect to the process of fluid front propagation or diffusion.

Furthermore, a comparison between the five-spot (refer to footnote 2) and inverted five-spot patterns (refer to footnote 3) shows that the inverted five-spot pattern provides a broader and more uniform sweep than the five-spot pattern, both in MRST and CMG. The inverted five-spot pattern demonstrates more effective fluid sweeping compared to the five-spot pattern. This is evident from the smaller residual oil area and more uniform distribution of the water saturation front in the reservoir. The inverted five-spot pattern provides more controlled injection flow distribution and reaches production areas more efficiently, thereby improving overall displacement efficiency.

### Water Breakthrough Time Analysis

Breakthrough time (BT) were analyzed to evaluate the initial arrival time of water in the production wells for each injection pattern scenario. This analysis was supported by an evaluation of the water production rate in each production well. In the five-spot pattern scenario (refer to footnote 2), both MRST and CMG show nearly identical breakthrough times, as shown in Figure 26. Water breakthrough in MRST occurs around year 2.63, while in CMG it occurs slightly earlier around year 2.34. The difference in breakthrough time between the two simulators is very small, indicating that in the five-spot configuration, the distribution of sweep and movement of the waterfront are well represented and consistent in both simulators.

Meanwhile, in the inverted five-spot pattern (refer to footnote 3) scenario, the difference in breakthrough time becomes more significant. In MRST, water breakthrough is detected earlier, around year 4.6 before starting the injection period. This detection was obtained from observations of the water production rate in the four production wells, which began to show signs of water production with small fluctuations. However, water production in MRST did not increase steadily, but showed minor fluctuations in the water production rate until around year 14, after which the water production rate began to increase more consistently, as shown in Figures 27a-d. These fluctuations are also reflected in

the oil production rate profile, where during some intervals, the oil rate at MRST even dropped to zero before increasing again. This phenomenon indicates numerical instability in handling the movement of the water saturation front, leading to uncontrolled numerical variations in fluid production. Conversely, in CMG, water breakthrough was detected in the year 4 after injection period, with more stable water and oil production patterns after breakthrough. This indicates that CMG can maintain better control over air front propagation during the inverted five-spot phase.

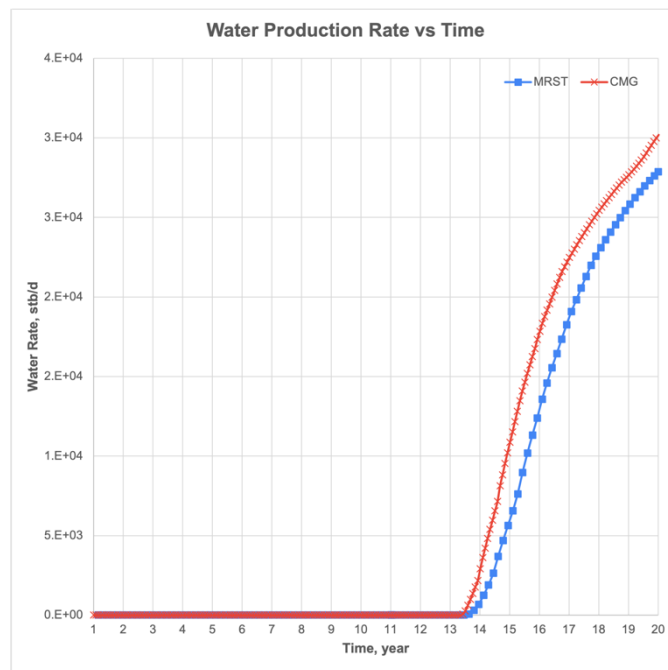
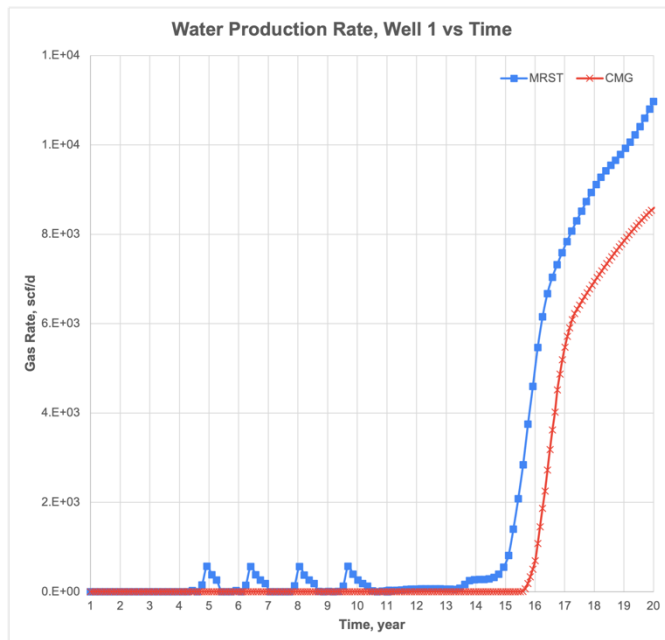
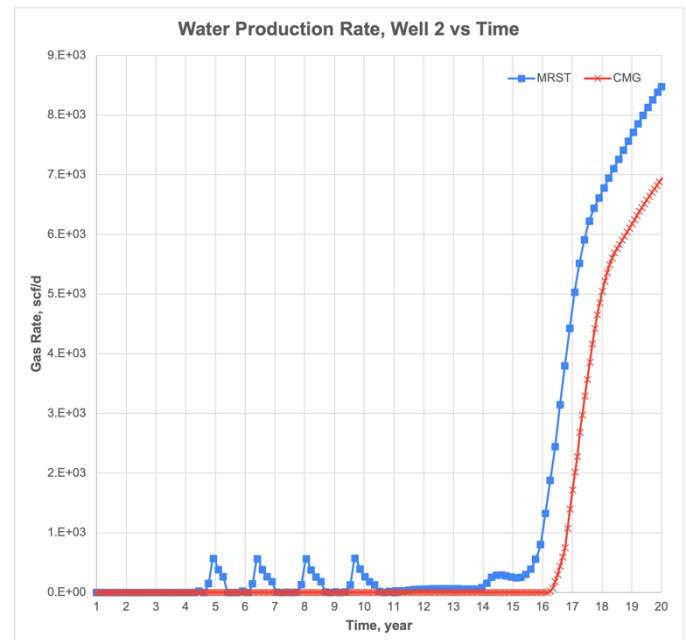


Figure 26 Water Production Rate, Case A2 (Five Spot Pattern)



(a) Water Production Rate of Well 1, Case A3 (Inverted Five Spot Pattern)



(b) Water Production Rate of Well 2, Case A3 (Inverted Five Spot Pattern)

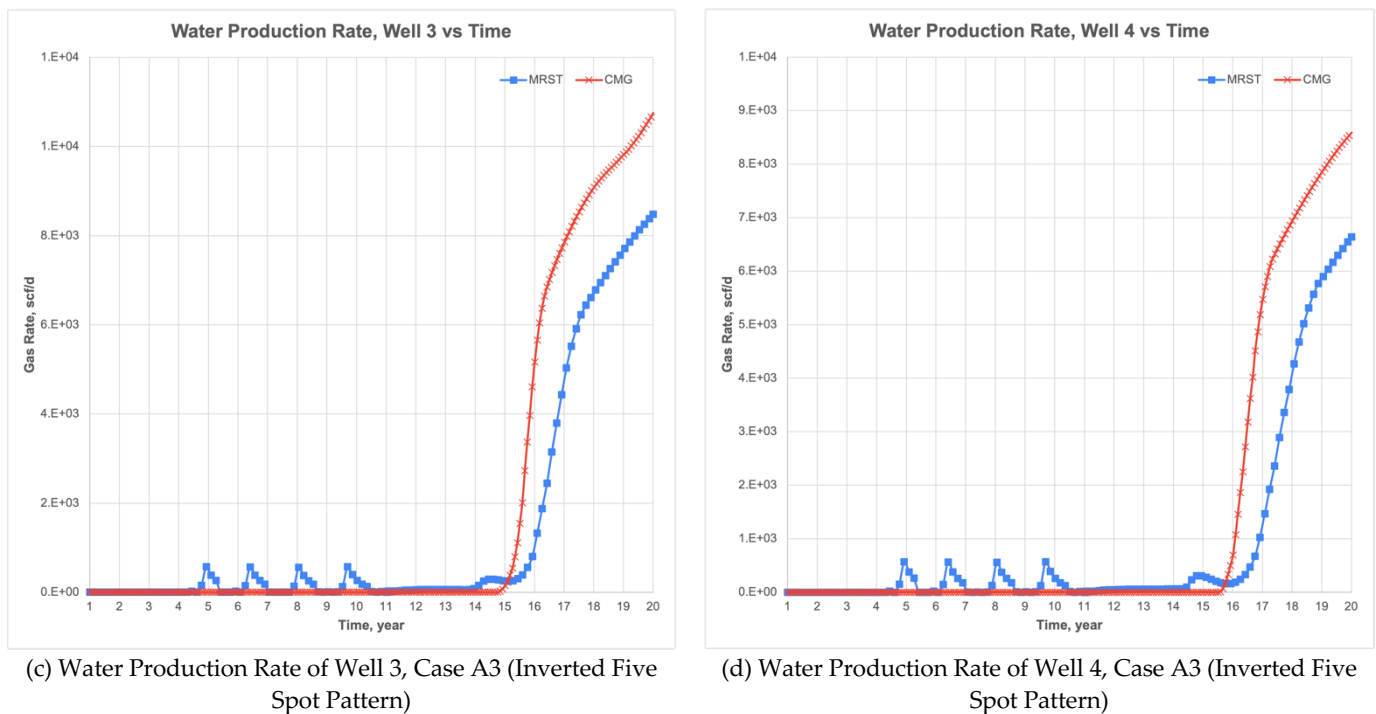


Figure 27 Water Production Rate of Well 1-4, Case A3 (Inverted Five Spot Pattern)

Analysis of injection pattern variations shows that the implementation of five-spot and inverted five-spot patterns can improve fluid sweep efficiency in the reservoir compared to the linear injection pattern in the base case. To support the quantitative analysis of the five-spot (Case A2, refer to footnote 2) and inverted five-spot (Case A3, refer to footnote 3) injection patterns, Table 20 presents a comparison of simulation parameters between MRST and CMG, including recovery factor, cumulative production (oil, gas, and water), and breakthrough time. These results support previous findings that MRST tends to produce higher oil recovery but shows numerical differences in the gas and water phases, especially in the early phase or near breakthrough. These differences can be attributed to the numerical methods, solver schemes, and sensitivity to timestep settings used by each simulator.

Table 20 Summary Well Pattern Sensitivity between MRST and CMG

Parameter	Case	MRST	CMG	Difference (%)
Recovery Factor (RF), %	A2	32.61	28.37	14.93
Cumulative Oil Production, stb		8.52E+07	7.52E+07	13.3
Cumulative Gas Production, scf		2.19E+11	2.70E+11	18.89
Cumulative Water Production, stb		3.76E+07	4.50E+07	16.44
Breakthrough Time, year		2.63	2.34	12.39
Recovery Factor (RF), %	A3	33.69	27.82	21.1
Cumulative Oil Production, stb		8.8E+07	7.4E+07	18.92
Cumulative Gas Production, scf		2.3E+11	2.8E+11	17.86
Cumulative Water Production, stb		3.7E+07	3.9E+07	5.13
Breakthrough Time, year		-4.6	4	-215

Note: Each case (e.g., A2 and A3) refers to simulation scenarios with specific BHP and grid settings, fully described in footnotes 2-3. Breakthrough time is measured relative to the start of injection (year 11). Negative values indicate unphysical behavior, possibly due to numerical issues.

#### 4.4.2. Effect of Injection Pressure

Variations in bottom-hole pressure (BHP) of injection wells have an important role in determining the effectiveness of fluid sweep and the stability of waterflooding operations. In this subsection, the influence of injection pressure

changes on injection well operation stability and water breakthrough time are analyzed for linear, five-spot, and inverted five-spot injection patterns. The analysis focuses on two main aspects: injection rate stability, considering fluctuation behavior, well shut-in, and injection system stability; and water breakthrough behavior, including water arrival time at the production well.

### Water Injection Stability Analysis

In the linear pattern scenario, the differences in injection stability were most apparent in scenario A1-P1<sup>4</sup> (BHP 2000 psi). At this injection pressure, MRST can maintain continuous injection operations throughout the simulation, with the water injection rate increasing steadily from year 13 to year 16 before declining until the end of the simulation period. Meanwhile, CMG shows repeated shut-in and reopening of the well during the injection period, as shown in Figure 28.

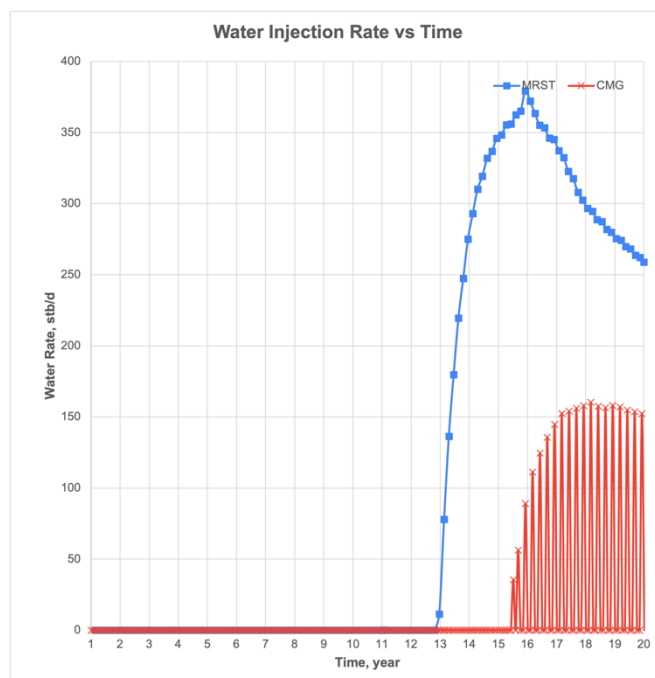


Figure 28 Water Injection Rate, Case A1-P1 (Linear Pattern)

This phenomenon is related to small differences (approximately 5–10 psi) between reservoir pressure and injection BHP, where CMG, through pressure-based flow control, realistically closes the injection well when the pressure difference becomes too small to push fluid into the reservoir. This repeated shut-in behavior reflects that the physical control of the CMG is more conservative in controlling injection stability, while MRST shows tolerance to injection pressure fluctuations. In scenarios A1-P2<sup>5</sup> (BHP 3000 psi) and A1-P3<sup>6</sup> (BHP 5000 psi), both simulators showed good injection stability, with continuous injection well operations and no repeated shut-ins, although a spike in water injection rate was still observed in the first year in the MRST.

In the five-spot pattern with BHP 2000 psi (A2-P1<sup>7</sup>), simultaneous shut-ins were again observed in all four injection wells in the CMG, reinforcing that injection instability at low pressures is a consistent phenomenon in this simulator. On the other hand, in MRST, all four injection wells remained active, but their injection rates showed significant

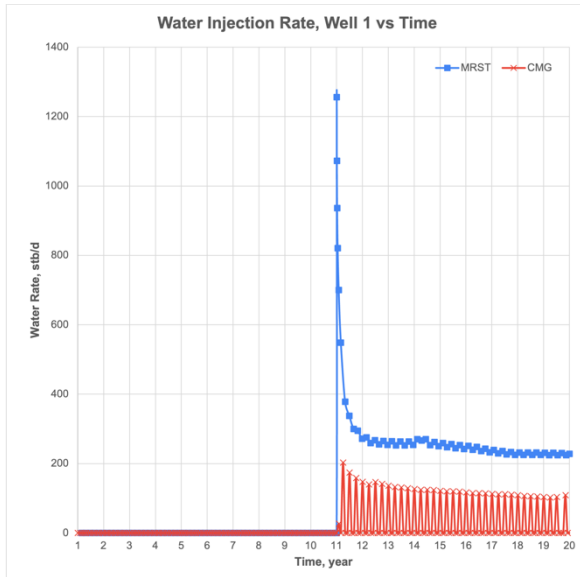
<sup>4</sup> Case A1-P1 applies linear pattern, with a bottom-hole pressure (BHP) constraint of 2000 psi for the production well, 2000 psi for the injection well, and a total of 300 active grid blocks.

<sup>5</sup> Case A1-P2 applies linear pattern, with a bottom-hole pressure (BHP) constraint of 2000 psi for the production well, 3000 psi for the injection well, and a total of 300 active grid blocks.

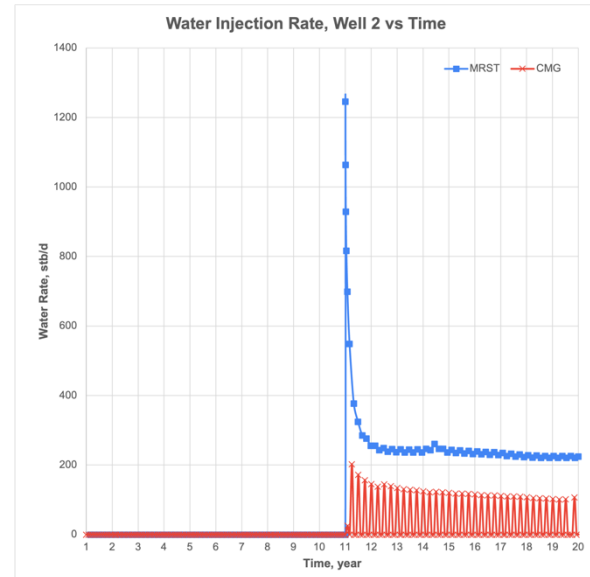
<sup>6</sup> Case A1-P3 applies linear pattern, with a bottom-hole pressure (BHP) constraint of 2000 psi for the production well, 5000 psi for the injection well, and a total of 300 active grid blocks.

<sup>7</sup> Case A2-P1 applies five-spot pattern, with a bottom-hole pressure (BHP) constraint of 2000 psi for the production well, 2000 psi for the injection well, and a total of 300 active grid blocks.

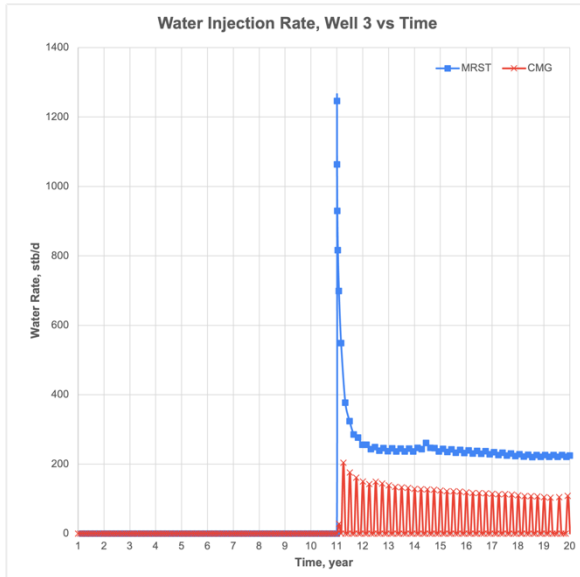
fluctuations, with variations in injection rates over time as shown in Figures 29a-d. This finding indicates that MRST has a slightly different solver handling compared to CMG, where it is more tolerant of small instabilities. Under the BHP 3000 psi and 5000 psi scenarios (A2-P2<sup>8</sup> and A2-P3<sup>9</sup>), both simulators show nearly identical injection operation stability, indicating that increasing injection pressure effectively stabilizes the operation, regardless of the differences in numerical control methods between the simulators.



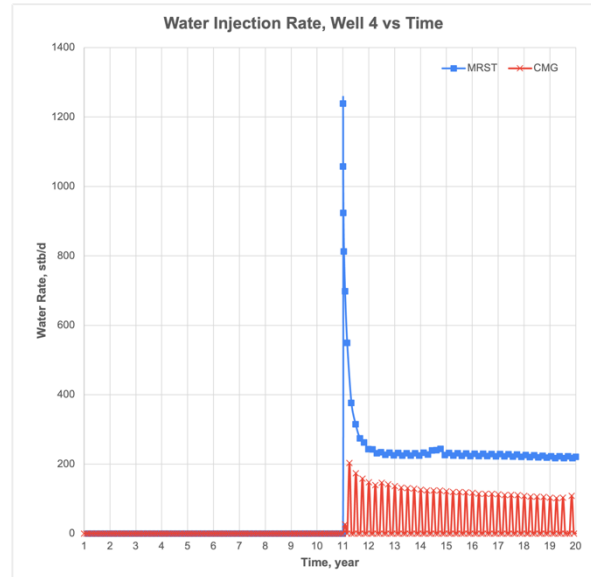
(a) Water Injection Rate Case A2-P1, Five Spot Pattern BHP= 2000 psi, Well 1



(b) Water Injection Rate Case A2-P1, Five Spot Pattern BHP= 2000 psi, Well 2



(c) Water Injection Rate Case A2-P1, Five Spot Pattern BHP= 2000 psi, Well 3



(d) Water Injection Rate Case A2-P1, Five Spot Pattern BHP= 2000 psi, Well 4

Figure 29 Water Injection Rate at Various BHP, Case A2 (Five Spot Pattern)

<sup>8</sup> Case A2-P2 applies five-spot pattern, with a bottom-hole pressure (BHP) constraint of 2000 psi for the production well, 3000 psi for the injection well, and a total of 300 active grid blocks.

<sup>9</sup> Case A2-P3 applies five-spot pattern, with a bottom-hole pressure (BHP) constraint of 2000 psi for the production well, 5000 psi for the injection well, and a total of 300 active grid blocks.

In the inverted five-spot scenario with BHP 2000 psi (A3-P1<sup>10</sup>), a significant difference in the rate of injection was detected. MRST reported an initial injection rate of approximately 1300 stb/d, which gradually decreased to 420 stb/d, while CMG started with a much smaller rate of around 400 stb/d and dropped to 150 stb/d. These differences indicate that MRST exhibits a more aggressive injection response compared to CMG at low pressures, likely due to handling and differences in solver control for small pressure variations, as shown in Figure 30. At higher injection pressures (BHP 3000 psi<sup>11</sup> and 5000 psi<sup>12</sup>), injection system stability improves, allowing both simulators to produce more consistent injection rates despite differences in their numerical approaches.

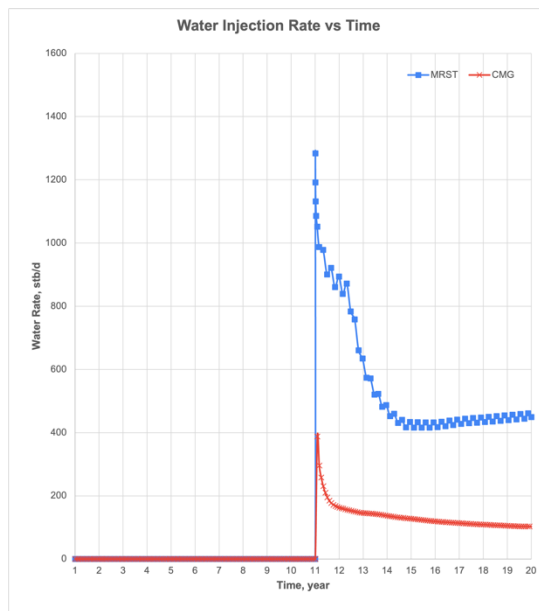


Figure 30 Water Injection Rate, Case A3-P1 (Inverted Five Spot Pattern)

#### Water Breakthrough Time Analysis

Water breakthrough analysis was conducted to evaluate the effect of injection pressure variations on the arrival time of water in the production well. In the linear pattern (A1-P1, A1-P2, and A1-P3), both MRST and CMG did not show any water breakthrough until the end of the simulation period for all injection pressures tested, which were 2000 psi, 3000 psi, and 5000 psi (refer to footnote 4-6). This indicates that the linear injection pattern is still insufficiently effective to drive the water saturation front to reach the production well within a 20-year period. Therefore, this shows that both simulators exhibit the same behavior.

<sup>10</sup> Case A3-P1 applies inverted five-spot pattern, with a bottom-hole pressure (BHP) constraint of 2000 psi for the production well, 2000 psi for the injection well, and a total of 300 active grid blocks.

<sup>11</sup> Case A3-P2 applies inverted five-spot pattern, with a bottom-hole pressure (BHP) constraint of 2000 psi for the production well, 3000 psi for the injection well, and a total of 300 active grid blocks.

<sup>12</sup> Case A3-P3 applies inverted five-spot pattern, with a bottom-hole pressure (BHP) constraint of 2000 psi for the production well, 5000 psi for the injection well, and a total of 300 active grid blocks.

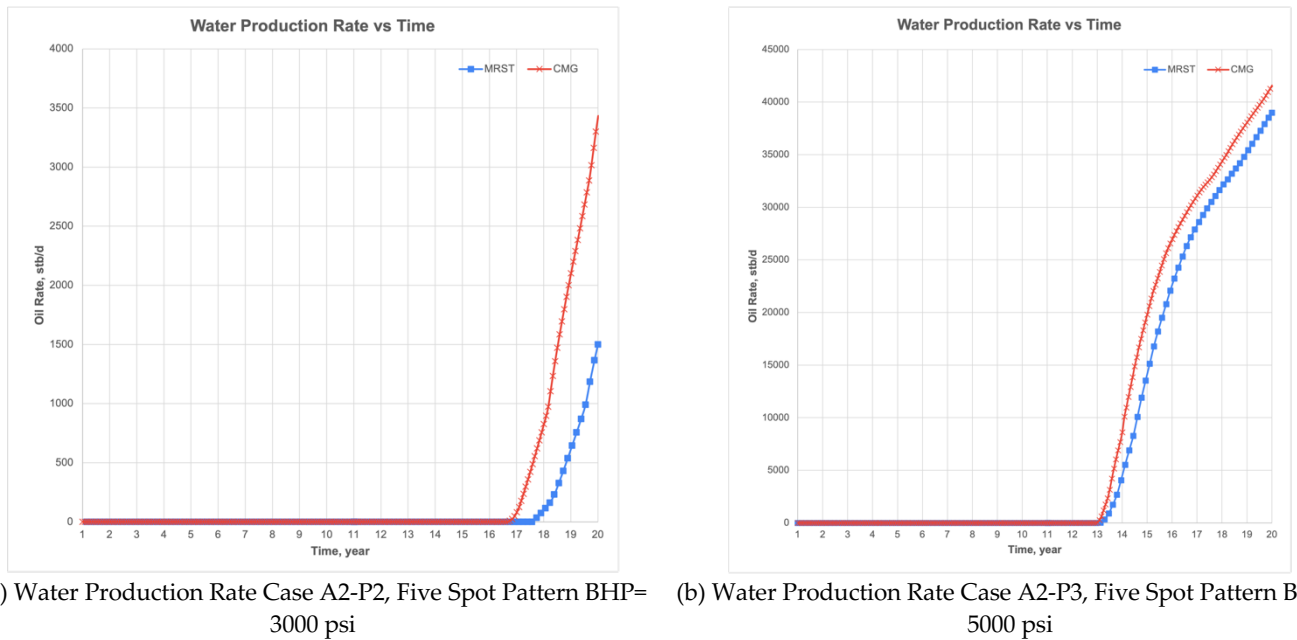


Figure 31 Water Production Rate, Case A2 (Five Spot)

In the five-spot pattern, different behaviors became apparent when the injection pressure was increased. At BHP 2000 psi (refer to footnote 7), neither MRST nor CMG experienced water breakthrough, indicating that this injection pressure was not yet capable of providing maximum sweeping effect so that water did not reach the production well. However, at BHP 3000 psi (refer to footnote 8), water breakthrough is detected, with CMG experiencing breakthrough earlier at year 5.68, while MRST experiences breakthrough at year 6.74. This indicates that at medium pressure, CMG tends to show slightly faster propagation of the water saturation front compared to MRST, as seen in Figure 31a. At BHP 5000 psi (refer to footnote 9), breakthrough occurs almost simultaneously in both simulators, at year 2.01 for CMG and year 2.34 for MRST, as shown in Figure 31b, indicating that at high pressure, sweeping dynamics become more uniform between the two simulators.

The most significant difference is observed in the inverted five-spot pattern. At BHP 2000 psi (refer to footnote 10), MRST shows very early water breakthrough, detected around the year 4 before injection period, with unstable water production and fluctuations throughout the simulation period, and this is detected in all four production wells, as shown in Figure 32a. This phenomenon not only affects water production but also reflects in the oil production profile, resulting in zero production values during certain intervals. On the other hand, CMG at the same pressure did not show any water production until the end of the simulation period, indicating that the propagation of the waterfront in CMG is significantly more restrained and stable.

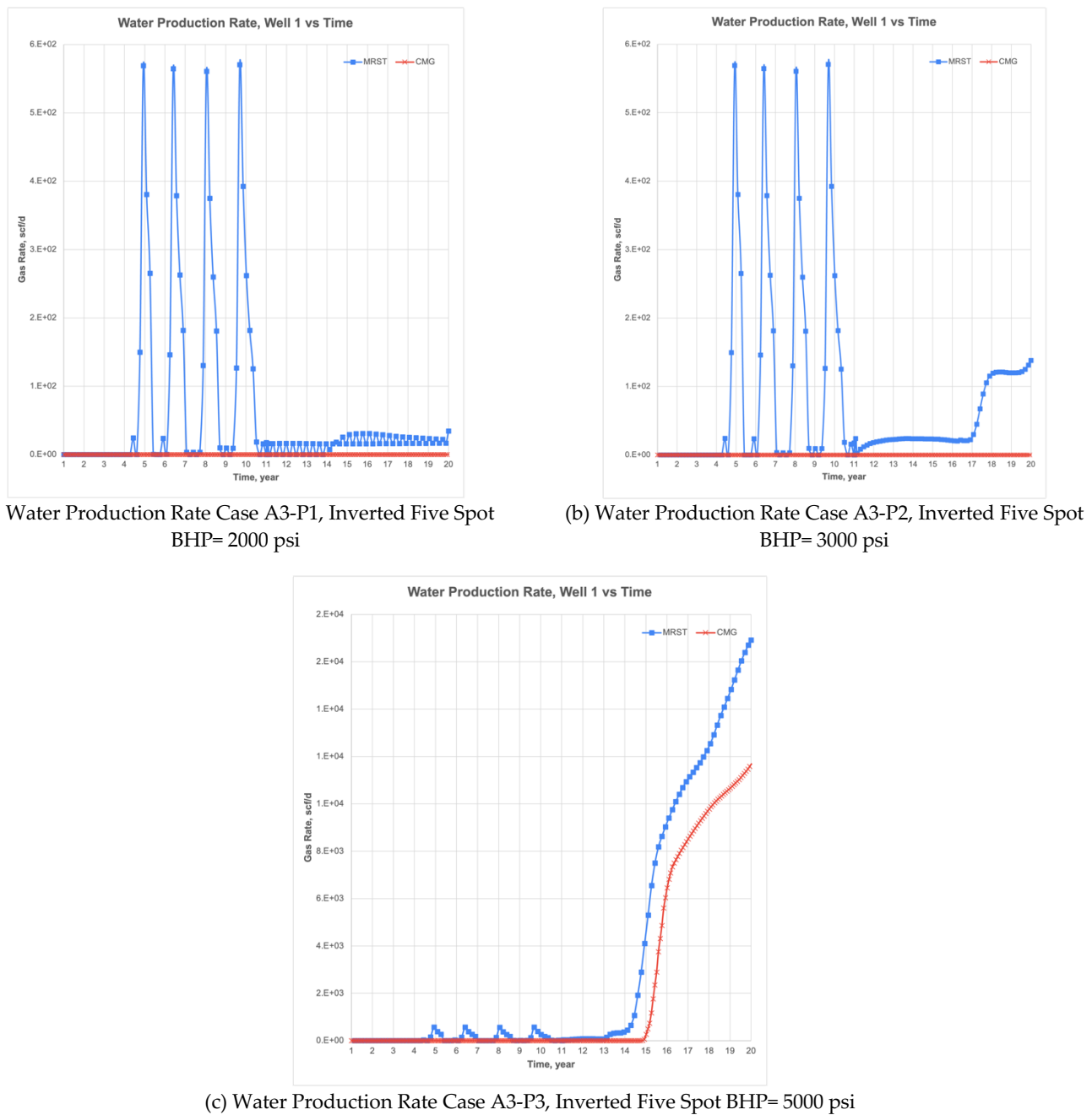


Figure 32 Water Production Rate, Case A3 (Inverted Five Spot)

At BHP 3000 psi (refer to footnote 11), Figure 32b shows that a similar phenomenon continues to occur, with MRST experiencing water breakthrough in the year 4 before injection period with an unstable water production pattern, while CMG only experienced a very slow breakthrough in the year 8.93, with small water production limited to only one production well. At BHP 5000 psi (refer to footnote 12), the difference between MRST and CMG slightly decreases, with MRST still showing an early breakthrough in the year 4 before injection period with fluctuating water production, while CMG experiences a breakthrough in the year 4 with more stable and controlled water production, as shown in Figure 32c.

The analysis results indicate that MRST exhibits a tendency toward early breakthrough and water production instability, particularly in the inverted five-spot pattern and at low to medium injection pressures. In contrast, CMG consistently shows more stable waterfront movement and a slower breakthrough, reflecting more conservative numerical control over the propagation of the water saturation front. The difference in injection characteristics between

the two simulators can be explained through the concept of well models, particularly the Peaceman model, which links well pressure and grid pressure. When the pressure difference is very small, the injection rate approaches zero or even becomes negative. In this case, CMG automatically shuts down the well to avoid flow instability, while MRST maintains injection at a fluctuating rate. This indicates that numerical approaches and well pressure control handling are key factors influencing injection stability at low pressures. The overall results of the injection pressure sensitivity can be seen in Table 21.

Table 21 Summary Injection Pressure Sensitivity between MRST and CMG

Parameter	Case	MRST	CMG	Difference (%)
Recovery Factor (RF), %		8.06	6.96	15.8
Cumulative Oil Production, stb		2.11E+07	1.85E+07	14.05
Cumulative Gas Production, scf	A1-P1	1.36E+11	1.79E+11	24.02
Cumulative Water Production, stb		0	0	0
Breakthrough Time, year		-	-	-
Recovery Factor (RF), %		8.44	7.37	14.52
Cumulative Oil Production, stb		2.21E+07	1.96E+07	12.75
Cumulative Gas Production, scf	A1-P2	1.65E+11	2.10E+11	21.43
Cumulative Water Production, stb		0	0	0
Breakthrough Time, year		-	-	-
Recovery Factor (RF), %		17.67	14	26.21
Cumulative Oil Production, stb		4.62E+07	3.72E+07	24.19
Cumulative Gas Production, scf	A1-P3	1.93E+11	2.46E+11	21.54
Cumulative Water Production, stb		0	0	0
Breakthrough Time, year		-	-	-
Recovery Factor (RF), %		8.74	7.64	14.39
Cumulative Oil Production, stb		2.29E+07	2.03E+07	12.81
Cumulative Gas Production, scf	A2-P1	1.38E+11	1.79E+11	22.91
Cumulative Water Production, stb		0	0	0
Breakthrough Time, year		-	-	-
Recovery Factor (RF), %		18.13	14.97	21.11
Cumulative Oil Production, stb		4.74E+07	3.97E+07	19.39
Cumulative Gas Production, scf	A2-P2	1.97E+11	2.50E+11	21.20
Cumulative Water Production, stb		5.34E+05	3.97E+07	98.65
Breakthrough Time, year		6.74	5.68	18.66
Recovery Factor (RF), %		36.17	31.78	13.81
Cumulative Oil Production, stb		9.46E+07	8.43E+07	12.21
Cumulative Gas Production, scf	A2-P3	2.25E+11	2.76E+11	18.48
Cumulative Water Production, stb		5.80E+07	6.64E+07	12.65
Breakthrough Time, year		2.34	2.01	16.42
Recovery Factor (RF), %		9.35	8.4	11.31
Cumulative Oil Production, stb		2.44E+07	2.23E+07	9.42
Cumulative Gas Production, scf	A3-P1	1.38E+11	1.79E+11	22.90
Cumulative Water Production, stb		1.52E+06	0	100
Breakthrough Time, year		-4.44	-	-
Recovery Factor (RF), %		11.96	9.50	25.89
Cumulative Oil Production, stb		3.13E+07	2.52E+07	24.20
Cumulative Gas Production, scf	A3-P2	1.91E+11	2.40E+11	20.41
Cumulative Water Production, stb		9.40E+05	9.38E+00	100
Breakthrough Time, year		-4.44	8.93	-149.72
Recovery Factor (RF), %	A3-P3	38.22	32.26	18.47

Parameter	Case	MRST	CMG	Difference (%)
Cumulative Oil Production, stb		9.99E+07	8.56E+07	16.71
Cumulative Gas Production, scf		2.36E+11	2.85E+11	17.19
Cumulative Water Production, stb		6.24E+07	6.36E+07	1.89
Breakthrough Time, year		-4.44	4	-211

Note: Each case (e.g., A1-P1 to A3-P3) refers to simulation scenarios with specific BHP and grid settings, fully described in footnotes 4-12. Breakthrough time is measured relative to the start of injection (year 11). Negative values indicate unphysical behavior, possibly due to numerical issues.

#### 4.4.3. Effect of Grid Resolution

Evaluation of the effect on grid resolution in reservoir simulation was conducted by comparing the slope of reservoir pressure decline and oil production rate during the natural depletion phase (years 1 to 11) for three well patterns: linear pattern, five-spot pattern, and inverted five-spot pattern. In this study, the author did not use a specific approach or method in varying the number of grids. The variation in the number of grid cells was done directly by increasing the number of blocks (from 300 to 7,500, 10,800, and 14,700 blocks) without changing the physical boundaries and total reservoir volume. This means that an increase in the number of grids represents finer spatial discretization, with smaller block sizes, while the reservoir model dimensions and total properties such as OOIP, OWIP, and OGIP remain constant and the same as the base case.

To represent the grid refinement across each well pattern, specific cases were assigned: A1-G1<sup>13</sup>, A1-G2<sup>14</sup>, and A1-G3<sup>15</sup> for the linear pattern; A2-G1<sup>16</sup>, A2-G2<sup>17</sup>, and A2-G3<sup>18</sup> for the five-spot pattern; and A3-G1<sup>19</sup>, A3-G2<sup>20</sup>, and A3-G3<sup>21</sup> for the inverted five-spot pattern. All these cases correspond to 7,500, 10,800, and 14,700 grid blocks, respectively.

The primary objective of varying the grid resolution is to evaluate the sensitivity of simulation performance to the spatial accuracy of the model. Simulation results show that in the linear pattern, increasing grid resolution results in higher reservoir pressure values in the first year compared to the base grid, both in MRST and CMG, indicating that the fine grid can capture the initial reservoir pressure distribution more accurately and closer to the actual conditions. The initial oil production rate on the fine grid is slightly lower than the base grid, with a more gradual and gentle decline throughout the natural depletion period, reflecting the effects of spatial accuracy and more realistic pressure gradient distribution in the fine grid model.

In the five-spot pattern, variations in grid resolution did not show significant differences in reservoir pressure values and oil production rates, both in MRST and CMG, indicating that the influence of the fine grid on fluid flow is relatively small in this injection pattern. Meanwhile, in the inverted five-spot pattern, the behavior is like the linear

<sup>13</sup> Case A1-G1 applies linear pattern, with a bottom-hole pressure (BHP) constraint of 2000 psi for the production well, 4500 psi for the injection well, and a total of 7,500 active grid blocks.

<sup>14</sup> Case A1-G2 applies linear pattern, with a bottom-hole pressure (BHP) constraint of 2000 psi for the production well, 4500 psi for the injection well, and a total of 10,800 active grid blocks.

<sup>15</sup> Case A1-G3 applies linear pattern, with a bottom-hole pressure (BHP) constraint of 2000 psi for the production well, 4500 psi for the injection well, and a total of 14,700 active grid blocks.

<sup>16</sup> Case A2-G1 applies five-spot pattern, with a bottom-hole pressure (BHP) constraint of 2000 psi for the production well, 4500 psi for the injection well, and a total of 7,500 active grid blocks.

<sup>17</sup> Case A2-G2 applies five-spot pattern, with a bottom-hole pressure (BHP) constraint of 2000 psi for the production well, 4500 psi for the injection well, and a total of 10,800 active grid blocks.

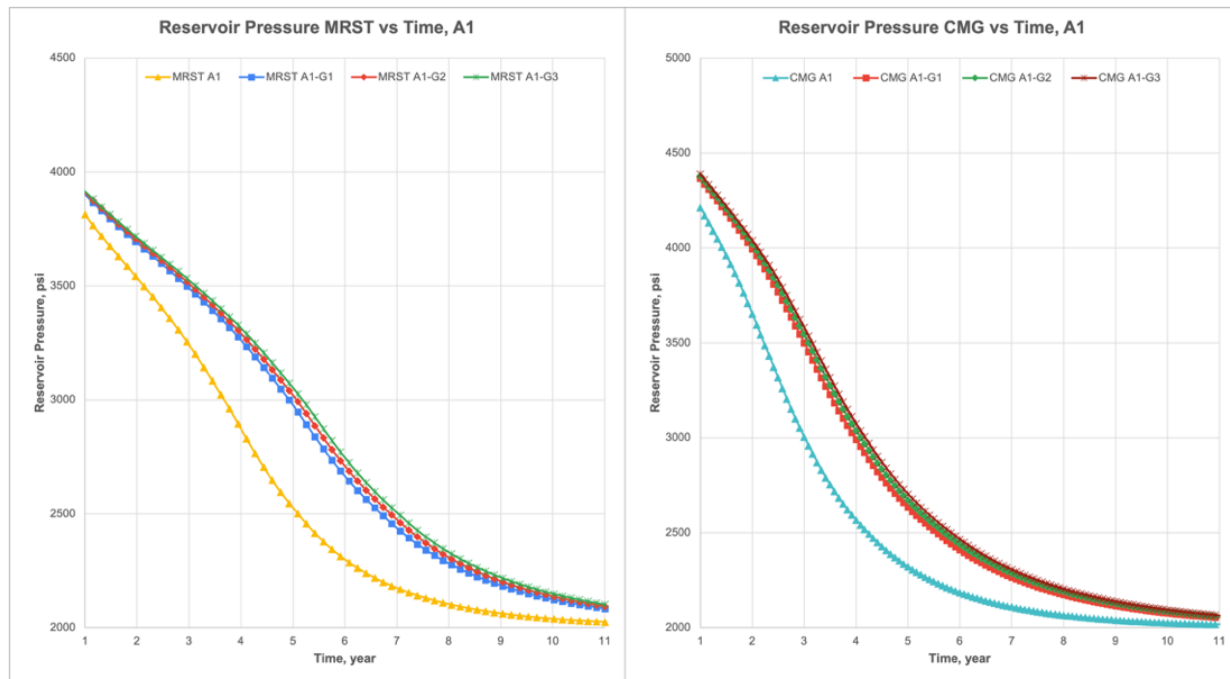
<sup>18</sup> Case A2-G3 applies five-spot pattern, with a bottom-hole pressure (BHP) constraint of 2000 psi for the production well, 4500 psi for the injection well, and a total of 14,700 active grid blocks.

<sup>19</sup> Case A3-G3 applies inverted five-spot pattern, with a bottom-hole pressure (BHP) constraint of 2000 psi for the production well, 4500 psi for the injection well, and a total of 7,500 active grid blocks.

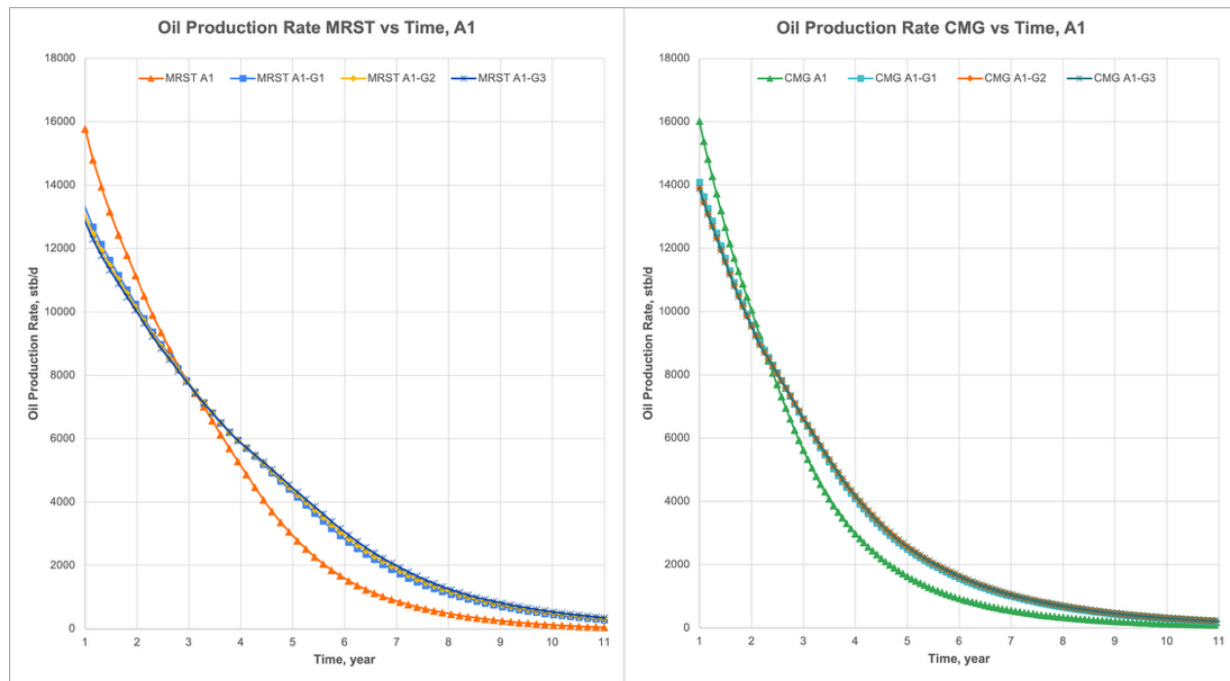
<sup>20</sup> Case A3-G2 applies inverted five-spot pattern, with a bottom-hole pressure (BHP) constraint of 2000 psi for the production well, 4500 psi for the injection well, and a total of 10,800 active grid blocks.

<sup>21</sup> Case A3-G1 applies inverted five-spot pattern, with a bottom-hole pressure (BHP) constraint of 2000 psi for the production well, 4500 psi for the injection well, and a total of 14,700 active grid blocks.

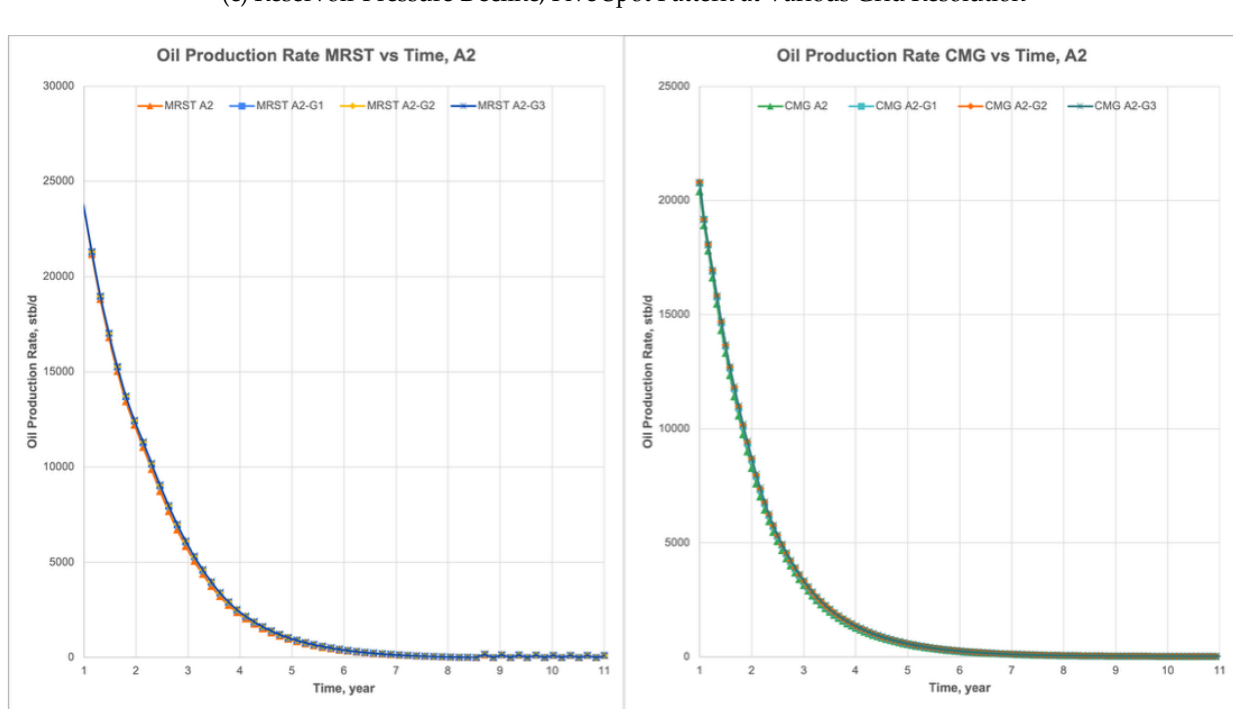
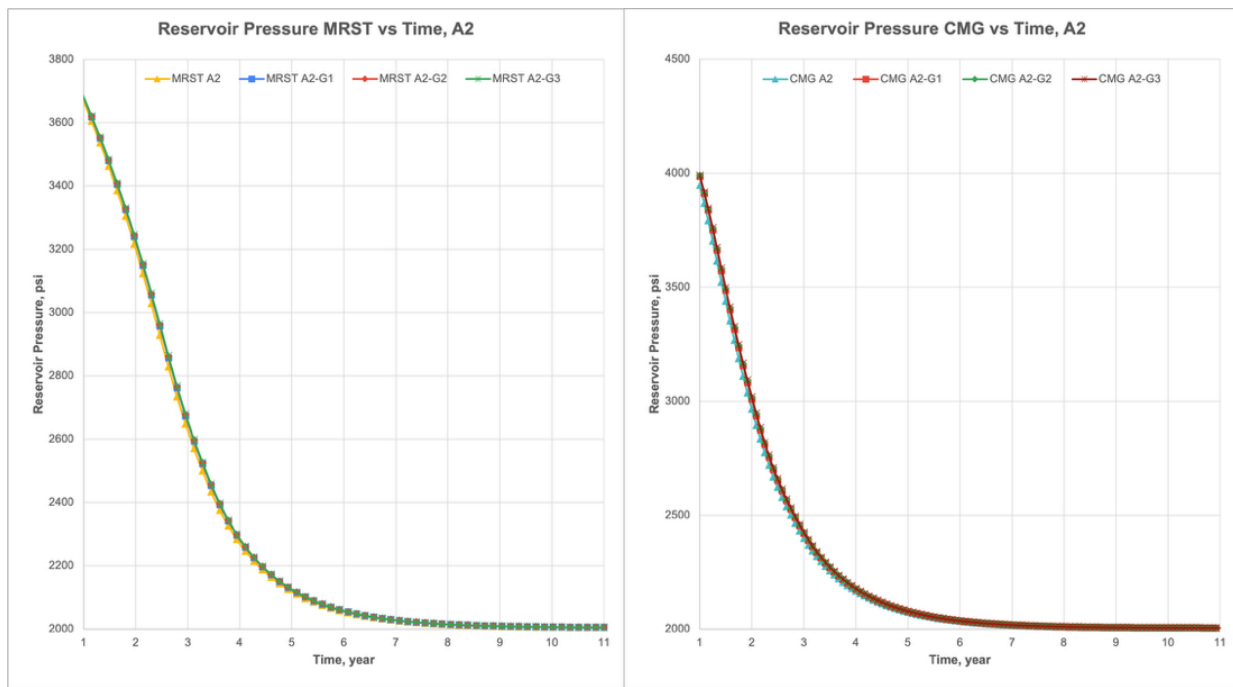
pattern, where an increase in grid resolution results in higher initial reservoir pressure values and slightly lower initial oil production rates compared to the base grid, with a more gradual and controlled decline slope in pressure and oil production. This indicates that a fine grid has a greater effect on injection patterns with linear or oriented flow distributions than on more dispersed injection patterns such as the five-spot pattern. Additionally, finer grid resolution allows for more accurate calculations of pressure distribution and initial fluid mobilization, resulting in higher initial response around the production wells. This effect may be related to improved accuracy in calculating near-wellbore pressure gradients due to the influence of the well model on small cells in the fine grid. Table 22 summarizes the slope values for each scenario, and the production profile results for each scenario are shown in Figures 33a-f.



(a) Reservoir Pressure Decline, Linear Pattern at Various Grid Resolution



(b) Oil Production Rate Decline, Linear Pattern at Various Grid Resolution



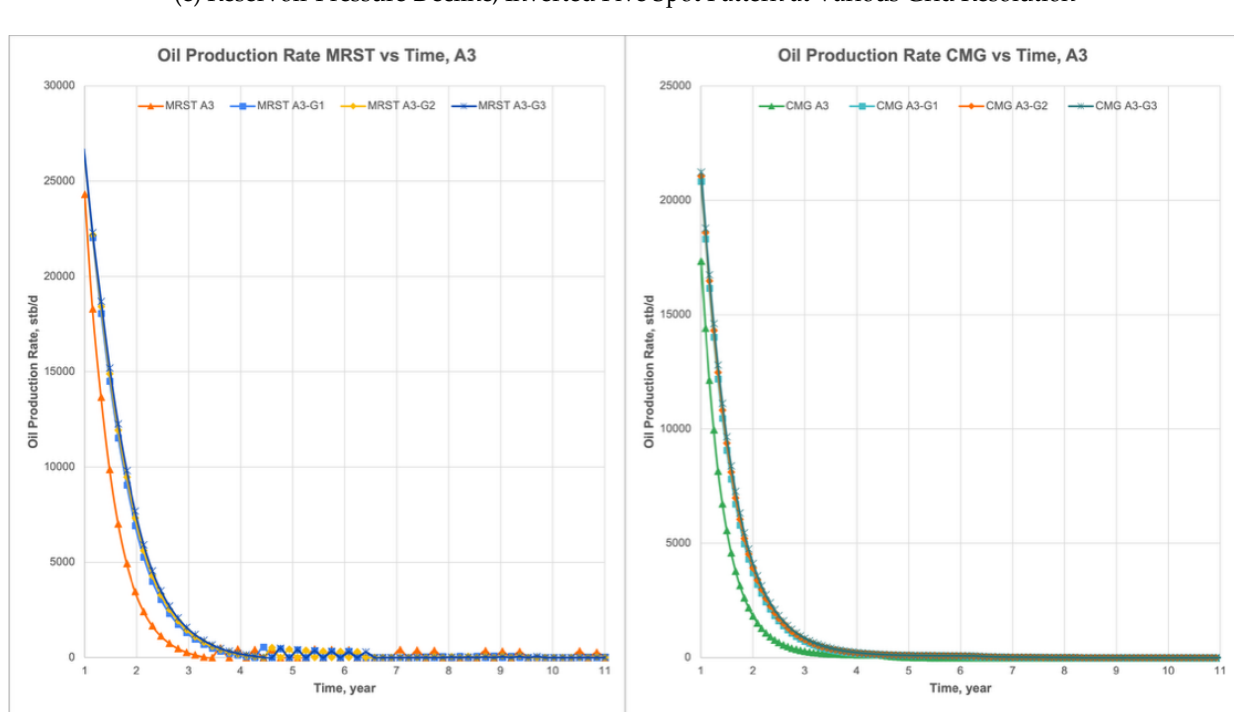
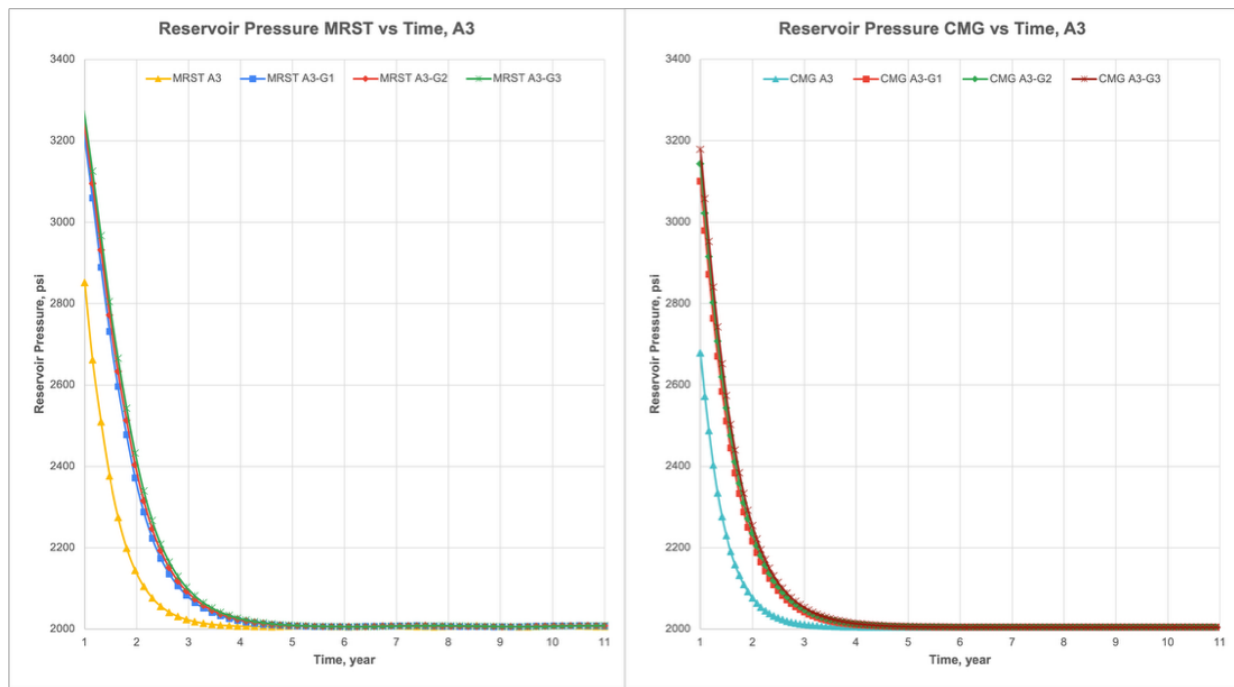


Figure 33 Effect of Grid Resolution in Reservoir Pressure and Oil Production Rate Decline

Table 22 Summary of Slope Linear Regression Value Grid Resolution Sensitivity

Parameter	Case	Slope (Year 1-11)	
		MRST	CMG
Reservoir Pressure, psi/year	A1	-186.84	-191.71
Oil Production Rate, stb/d/year		-1365.65	-1195.27
Reservoir Pressure, psi/year	A1-G1	-202.42	-233.33
Oil Production Rate, stb/d/year		-1225.73	-1165.81

Reservoir Pressure, psi/year	A1-G2	-202.48	-236.46
Oil Production Rate, stb/d/year		-1206.48	-1157.35
Reservoir Pressure, psi/year	A1-G3	-202.32	-238.86
Oil Production Rate, stb/d/year		-1190.04	-1149.76
Reservoir Pressure, psi/year	A2	-134.96	-119.59
Oil Production Rate, stb/d/year		-1486.81	-1089.67
Reservoir Pressure, psi/year	A2-G1	-137.67	-123.90
Oil Production Rate, stb/d/year		-1512.45	-1121.36
Reservoir Pressure, psi/year	A2-G2	-137.99	-124.62
Oil Production Rate, stb/d/year		-1514.46	-1126.74
Reservoir Pressure, psi/year	A2-G3	-138.26	-124.62
Oil Production Rate, stb/d/year		-1516.01	-1127.86
Reservoir Pressure, psi/year	A3	-28.07	-18.27
Oil Production Rate, stb/d/year		-755.44	-468.96
Reservoir Pressure, psi/year	A3-G1	-53.33	-38.35
Oil Production Rate, stb/d/year		-1076.35	-705.50
Reservoir Pressure, psi/year	A3-G2	-56.33	-40.76
Oil Production Rate, stb/d/year		-1106.36	-727.00
Reservoir Pressure, psi/year	A3-G3	-58.93	-43.03
Oil Production Rate, stb/d/year		-1131.72	-747.92

Note: Each case (e.g., A1-G1 to A3-G3) refers to simulation scenarios with specific BHP and grid settings, fully described in footnotes 13-21.

Furthermore, to evaluate the effect of spatial resolution on breakthrough time, a representative example was taken from five-spot pattern scenarios with different grid resolutions, namely A2 (refer to footnote 2) and A2-G3 (refer to footnote 18). The simulation results show that increasing the grid resolution results in a slower breakthrough time in both simulators, as shown on Figure 34. In the case A2 with total 300 active grid blocks, the breakthrough is detected at year 13.63 in MRST and year 13.34 in CMG, while in A2-G3 with total 14,700 active grid blocks, the breakthrough time retreats to year 15.11 in MRST and year 15.01 in CMG. This finding indicates that increased spatial resolution smoothens the propagation of the water saturation front, enabling more accurate sweep predictions and slowing the arrival of injection fluid to the production well. The slower breakthrough time difference in the fine grid model is due to the reduction of numerical effects such as dispersion and numerical overprediction of front movement in coarse grid.

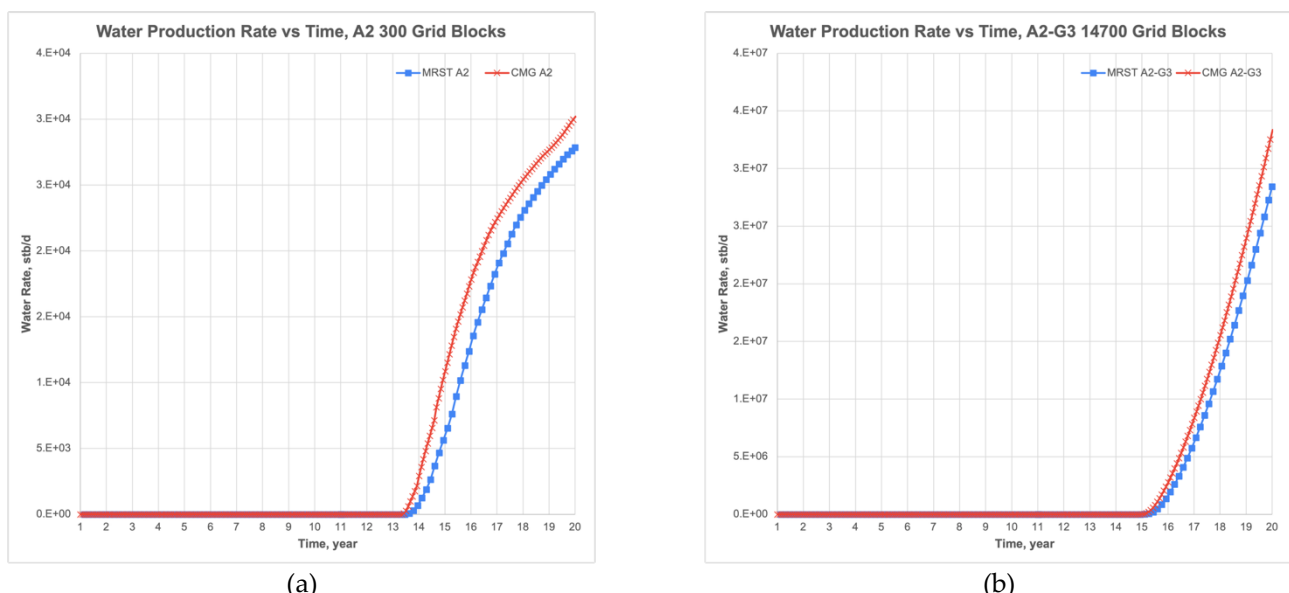


Figure 34 Effect Grid Resolution on Breakthrough Time

This finding confirms that increasing grid resolution does not always smooth the global slope decline trend but has the potential to influence the initial dynamics of pressure distribution and fluid flow, especially in more complex injection patterns such as inverted five-spot. Interestingly, the simulation results also show that increasing grid resolution causes a slight decrease in recovery factor compared to the base grid, both in MRST and CMG, especially in linear patterns. For example, in linear patterns, the recovery factor decreases as the grid is refined, both in MRST (14.25% to 11.28%) and CMG (10.62% to 7.92%). This downward trend is also consistently observed in five-spot and inverted five-spot patterns, although the magnitude varies between patterns and simulators.

This phenomenon is expected to be related to the increased accuracy of pressure and saturation distribution in the fine grid model, which captures flow resistance near the well in greater detail due to the decrease in the well index in the Peaceman well model as the grid block size decreases. This numerical effect causes the initial oil production rate to be more controlled, and the cumulative oil production to be more conservative compared to the estimates on the coarse grid. The experimental results indicate that increasing grid resolution improves simulation prediction quality by producing more linear pressure profiles and oil production rates, numerically more stable, and closer to the expected reservoir behavior. The overall summary of grid sensitivity results is presented in Table 23.

Table 23 Summary Grid Resolution Sensitivity between MRST and CMG

Parameter	Case	MRST	CMG	Difference (%)
Recovery Factor (RF), %		11.72	8.26	41.89
Cumulative Oil Production, stb		3.06E+07	2.19E+07	39.73
Cumulative Gas Production, scf	A1-G1	1.81E+11	2.37E+11	23.63
Cumulative Water Production, stb		0	0	0
Breakthrough Time, year		-	-	-
Recovery Factor (RF), %		11.48	8.06	42.43
Cumulative Oil Production, stb		3.00E+07	2.14E+07	40.19
Cumulative Gas Production, scf	A1-G2	1.80E+11	2.36E+11	23.73
Cumulative Water Production, stb		0	0	0
Breakthrough Time, year		-	-	-
Recovery Factor (RF), %		11.28	7.92	42.42
Cumulative Oil Production, stb		2.95E+07	2.10E+07	40.48
Cumulative Gas Production, scf	A1-G3	1.80E+11	2.36E+11	23.73
Cumulative Water Production, stb		0	0	0
Breakthrough Time, year		-	-	-
Recovery Factor (RF), %		32.67	28.43	14.91
Cumulative Oil Production, stb		8.54E+07	7.54E+07	13.26
Cumulative Gas Production, scf	A2-G1	2.20E+11	2.73E+11	19.41
Cumulative Water Production, stb		2.97E+07	3.50E+07	15.14
Breakthrough Time, year		3.94	3.84	2.60
Recovery Factor (RF), %		32.56	28.34	14.89
Cumulative Oil Production, stb		8.51E+07	7.52E+07	13.16
Cumulative Gas Production, scf	A2-G2	2.20E+11	2.73E+11	19.41
Cumulative Water Production, stb		2.90E+07	3.41E+07	14.96
Breakthrough Time, year		4.11	3.92	4.84
Recovery Factor (RF), %		32.45	28.24	14.91
Cumulative Oil Production, stb		8.48E+07	7.49E+07	13.22
Cumulative Gas Production, scf	A2-G3	2.20E+11	2.73E+11	19.41
Cumulative Water Production, stb		2.84E+07	3.34E+07	14.97
Breakthrough Time, year		4.11	4.01	2.49
Recovery Factor (RF), %		34.47	28.70	20.10
Cumulative Oil Production, stb	A3-G1	9.01E+07	7.61E+07	18.40
Cumulative Gas Production, scf		2.29E+11	2.80E+11	18.21

Parameter	Case	MRST	CMG	Difference (%)
Cumulative Water Production, stb		3.30E+07	3.35E+07	1.49
Breakthrough Time, year		-5.91	4.93	-
Recovery Factor (RF), %		34.33	28.61	19.99
Cumulative Oil Production, stb		8.98E+07	7.59E+07	18.31
Cumulative Gas Production, scf	A3-G2	2.28E+11	2.79E+11	18.28
Cumulative Water Production, stb		3.23E+07	3.28E+07	1.22
Breakthrough Time, year		-6.08	5.01	-
Recovery Factor (RF), %		34.21	28.52	19.95
Cumulative Oil Production, stb		8.94E+07	7.57E+07	18.10
Cumulative Gas Production, scf	A3-G3	2.28E+11	2.79E+11	18.28
Cumulative Water Production, stb		3.17E+07	3.22E+07	1.55
Breakthrough Time, year		-6.24	5.01	-

Note: Each case (e.g., A1-G1 to A3-G3) refers to simulation scenarios with specific BHP and grid settings, fully described in footnotes 13-21. Breakthrough time is measured relative to the start of injection (year 11). Negative values indicate unphysical behavior, possibly due to numerical issues.

#### 4.5. Simulator Comparison

Apart from comparing the technical results of fluid production and distribution, a comparison between MRST and CMG was also conducted in terms of computational performance (CPU runtime). Computational time efficiency is an important aspect in reservoir simulation applications, especially for complex scenarios that require a large number of grids, wells, and long simulation periods. In this subsection, an analysis was conducted on the simulation time (CPU runtime) required by each simulator to complete all baseline and sensitivity scenarios that were run. This comparison aims to identify the relationship between scenario complexity (injection pattern, injection pressure, grid resolution) and computational time requirements.

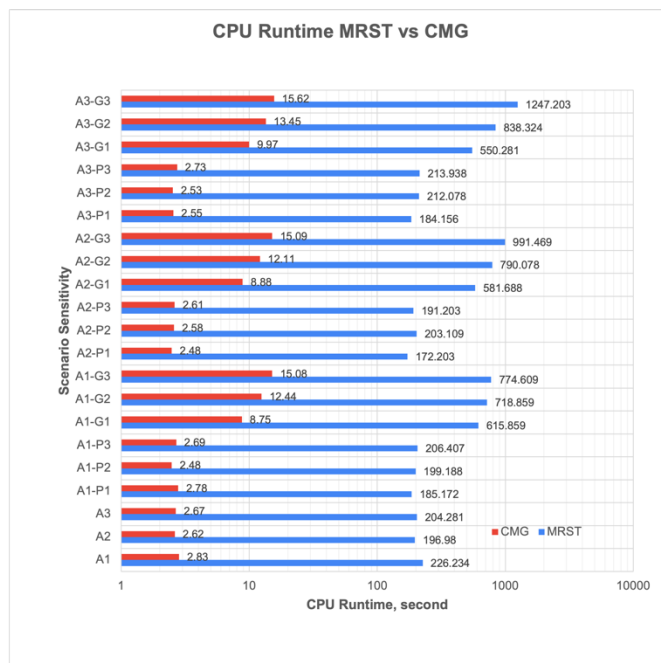


Figure 35 CPU Runtime MRST vs CMG

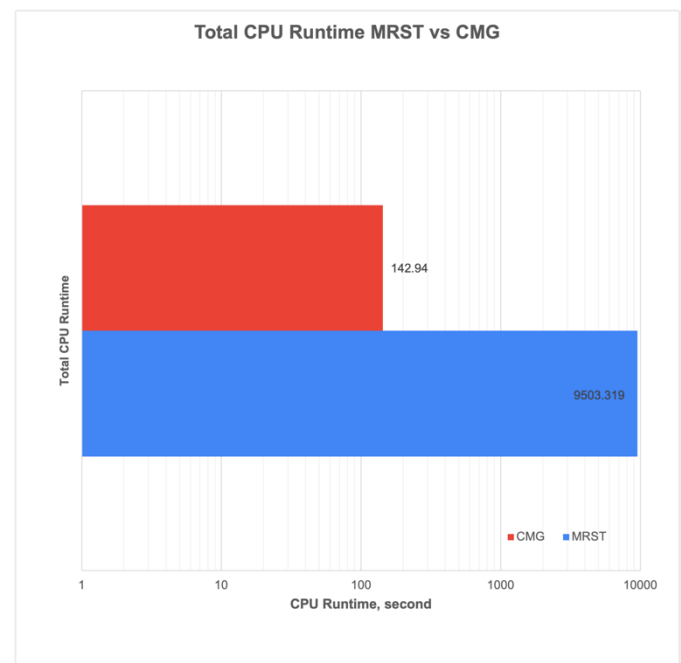


Figure 36 Total CPU Runtime MRST vs CMG

The comparison of CPU runtime between MRST and CMG for all simulation scenarios shows a significant difference in computational time efficiency. In general, CMG shows a shorter computational time than MRST for all types of scenarios, both in the base case, injection pattern variations, injection pressure, and grid resolution. All simulation tests were conducted on the same device to ensure consistency of results, using a laptop with an Intel®

Core™ i3-7100U CPU @2.40 GHz processor. This relatively simple device specification also provides a realistic representation of the simulator's computational performance under resource-constrained conditions.

The results show that the total CPU runtime to complete all 21 scenarios reached approximately 9503 seconds ( $\approx 2.64$  hours) on MRST, while CMG only required approximately 143 seconds ( $\approx 2.4$  minutes). This means that CMG is more than 77 times faster than MRST in running the same simulation. The comparison of CPU runtime is visualized in a graph to clarify trends and highlight differences across each scenario, as shown in Figures 35–36.

In the base case scenarios (A1, A2, A3) and sensitivity scenarios for injection patterns and injection pressure (A1-P, A2-P, A3-P), CMG completed each simulation in less than 15 seconds. Meanwhile, MRST requires between 180 and 800 seconds for simple scenarios, even exceeding 1,200 seconds for fine grid scenarios (such as A3-G3). The effect of increasing grid resolution becomes increasingly evident on CPU runtime. In CMG, increasing the number of grids from the base case to fine grids (G1, G2, G3) only increases runtime by approximately 3 to 5 times, while in MRST, increasing resolution causes runtime to surge dramatically, exceeding 5–7 times compared to the base case. Nevertheless, MRST still offers advantages in terms of model transparency, algorithm development flexibility, and ease of numerical scenario experimentation, making it highly suitable for research and development of new concepts in reservoir simulation.

## 5. Conclusion and Suggestion

### 5.1. Conclusion

This study provides a comprehensive approach to evaluating the performance of waterflooding-based reservoir simulators by comparing MATLAB Reservoir Simulation Toolbox (MRST) and CMG in various scenarios involving grid variations, well injection patterns, injection base pressure, and computational efficiency analysis.

1. This study successfully evaluated the performance of MRST and CMG simulators in various simulation scenarios. At varying grid numbers, the simulation results showed that increasing the grid resolution from 300 to 14,700 blocks did not universally smooth the slope of reservoir pressure decline and global oil production rate but affected the initial dynamics of pressure distribution and fluid flow in varying ways depending on the injection pattern. In the linear pattern and inverted five-spot pattern, a finer grid showed higher initial reservoir pressure and slightly lower initial oil production rates compared to the base grid, with a more gradual decline trend, whereas in the five-spot pattern, grid variations yielded relatively similar results. In terms of well pattern variations, the five-spot and inverted five-spot patterns showed significant increases in recovery factor compared to the linear pattern, with the inverted five-spot pattern resulting in more effective fluid sweeping.
2. The comparison of simulation results between MRST and CMG shows similar trends in terms of oil production, breakthrough time, and saturation distribution, although some numerical differences were found. MRST exhibits instability in the water injection rate at low injection pressures, minor fluctuations in the water production profile, oscillations in the GOR, and unstable early water breakthrough, particularly in the inverted five-spot pattern. This indicates limitations in the numerical solver's control and sensitivity to adaptive timestep settings. Additionally, difficulties in fluid model setup particularly limitations in PVT inputs such as the z-factor and handling pressure-dependent properties in MRST could potentially cause variations in behavior compared to CMG.
3. CMG generally demonstrates superiority in numerical stability, solver control, and runtime efficiency, with computation times up to 77 times faster than MRST for scenarios with a large number of grids. Meanwhile, MRST offers flexibility in model development, algorithm transparency, and potential for code modification for the development of new methods. Based on the results of this study, CMG is recommended for large-scale industrial or commercial applications requiring speed and operational stability, while MRST is more suitable for academic research, algorithm development experiments, and exploratory studies that require flexibility and access to the simulator's programming logic.

### 5.2. Suggestion

Based on the results of research and practical experience during the simulation process, several recommendations can be made for the development and use of MRST in reservoir waterflooding simulations.

1. A deeper understanding of each module and function available in MRST is required to build a good and coherent reservoir model. Basic programming skills, especially MATLAB coding, are very important considering the many stages of model creation that must be done manually through scripts. Additionally, the process of extracting simulation results from MRST is still relatively challenging and requires a solid understanding of the program's logic, so new users will need to dedicate more time to mastering this workflow.
2. MRST is more recommended for use in academic research aimed at exploring new methods in reservoir simulation. The flexibility of MRST in combining various modules and solver options makes it highly suitable for methodological experiments, the development of new physical models, and conceptual studies. However, for large-scale field simulation applications requiring time efficiency, MRST is less suitable due to the time-consuming trial-and-error process in coding, which can significantly slow down overall project progress.
3. During the development of comprehensive reservoir models, particularly in the creation of fluid models and model initialization, the presence of mentors or experts experienced in MRST is essential. The authors' experience shows that relying solely on online forums is often ineffective, given the slow response times and limited answers available.

4. The use of the SPE-1 dataset, although useful as a standardized benchmark model for simulator comparison, comes with certain limitations. This dataset was originally designed for gas injection and represents an oil-wet reservoir system, which is not ideal for evaluating waterflooding performance. Therefore, the results obtained may not fully capture the complexity of waterflooding behavior in more realistic field conditions. For future work, it is recommended to consider alternative models with water-wet characteristics, more heterogeneous rock properties, or even real field data to improve the relevance and representativeness of the simulation outcomes.

## Reference

- [1] H. R. "Hal" Warner, *The Reservoir Engineering Aspects of Waterflooding*. Society of Petroleum Engineers, 2015. doi: 10.2118/9781613994214.
- [2] S. Krogstad, K.-A. Lie, O. Møyner, H. Nilsen, X. Raynaud, and B. Skaflestad, *MRST-AD – an Open-Source Framework for Rapid Prototyping and Evaluation of Reservoir Simulation Problems*, vol. 3. 2015. doi: 10.2118/173317-MS.
- [3] K.-A. Lie, *An Introduction to Reservoir Simulation Using MATLAB/GNU Octave*. Cambridge University Press, 2019. doi: 10.1017/9781108591416.
- [4] J. E. Killough, "Ninth SPE Comparative Solution Project: A Reexamination of Black-Oil Simulation," in *SPE Reservoir Simulation Symposium*, SPE, Feb. 1995. doi: 10.2118/29110-MS.
- [5] A. S. Odeh, "Comparison of Solutions to a Three-Dimensional Black-Oil Reservoir Simulation Problem (includes associated paper 9741 )," *Journal of Petroleum Technology*, vol. 33, no. 01, pp. 13–25, Jan. 1981, doi: 10.2118/9723-PA.
- [6] F. Huang, W. GD, and L. G, "Study on Validation of the OPM Reservoir Simulator by Comparative Solution Project," *Petroleum & Petrochemical Engineering Journal*, vol. 4, no. 4, pp. 1–8, 2020, doi: 10.23880/ppej-16000241.
- [7] T. D. Qiu, A. Thune, M. Blatt, A. B. Rustad, and R. Nane, "An Evaluation and Comparison of GPU Hardware and Solver Libraries for Accelerating the OPM Flow Reservoir Simulator," Sep. 2023.
- [8] T. Ahmed and D. N. Meehan, "Chapter 6 - Introduction to Enhanced Oil Recovery," in *Advanced Reservoir Management and Engineering (Second Edition)*, T. Ahmed and D. N. Meehan, Eds., Boston: Gulf Professional Publishing, 2012, pp. 541–585. doi: <https://doi.org/10.1016/B978-0-12-385548-0.00006-3>.
- [9] A. H. Alagorni, Z. Bin Yaacob, and A. H. Nour, "An Overview of Oil Production Stages: Enhanced Oil Recovery Techniques and Nitrogen Injection," *International Journal of Environmental Science and Development*, vol. 6, no. 9, pp. 693–701, 2015, doi: 10.7763/IJESD.2015.V6.682.
- [10] T. Ahmed, "Chapter 14 - Principles of Waterflooding," in *Reservoir Engineering Handbook (Fourth Edition)*, T. Ahmed, Ed., Boston: Gulf Professional Publishing, 2010, pp. 909–1095. doi: <https://doi.org/10.1016/B978-1-85617-803-7.50022-5>.
- [11] V. Kulynycz and P. Janowski, "Comparison of the oil recovery between waterflooding and CO<sub>2</sub>-EOR method for the JSt oil reservoir," *AGH Drilling, Oil, Gas*, vol. 34, no. 3, p. 796, 2017, doi: 10.7494/drill.2017.34.3.787.
- [12] G. P. Willhite, *Waterflooding*. Society of Petroleum EngineersRichardson, Texas, USA, 1986. doi: 10.2118/9781555630058.
- [13] D. Rini, Latuan, F. Klea, and I. G. O. S. Prajanji, "Waterflooding Management: Challenges and Solutions During the Injection Process to Obtain Effectively and Environmentally Based Oil Recovery in Oil and Gas Industry," *IOP Conf Ser Earth Environ Sci*, vol. 690, no. 1, p. 012037, Mar. 2021, doi: 10.1088/1755-1315/690/1/012037.
- [14] J. T. Smith, W. M. Cobb, and P. T. T. C. (U. S. ). M. Office, *Waterflooding*. Midwest Office of the Petroleum Technology Transfer COuncil, 1997. [Online]. Available: <https://books.google.co.id/books?id=cqx5HAAACAAJ>
- [15] H. R. "Hal" Warner, *The Reservoir Engineering Aspects of Waterflooding*. Society of Petroleum Engineers, 2015. doi: 10.2118/9781613994214.
- [16] C. Temizel *et al.*, "Data-Driven Optimization of Injection/Production in Waterflood Operations," in *SPE Intelligent Oil and Gas Symposium*, SPE, May 2017. doi: 10.2118/187468-MS.
- [17] H. Yang, S. Sun, Y. Li, and C. Yang, "A fully implicit constraint-preserving simulator for the black oil model of petroleum reservoirs," *J Comput Phys*, vol. 396, pp. 347–363, Nov. 2019, doi: 10.1016/j.jcp.2019.05.038.
- [18] Y. Khalili and M. Ahmadi, "Reservoir Modeling & Simulation: Advancements, Challenges, and Future Perspectives," *Journal of Chemical and Petroleum Engineering*, vol. 57, no. 2, pp. 343–364, 2023, doi: 10.22059/jchpe.2023.363392.1447.
- [19] D. W. Peaceman, "Interpretation of Well-Block Pressures in Numerical Reservoir Simulation(includes associated paper 6988 )," *Society of Petroleum Engineers Journal*, vol. 18, no. 03, pp. 183–194, Jun. 1978, doi: 10.2118/6893-PA.
- [20] M. Carlson, *Practical reservoir simulation: using, assessing, and developing results*. 2003.
- [21] T. Ahmed, "Fundamentals of Rock Properties," in *Reservoir Engineering Handbook*, Elsevier, 2010, pp. 189–287. doi: 10.1016/B978-1-85617-803-7.50012-2.

- [22] H. B. Bradley and F. Gipson, "Petroleum engineering handbook," 1987. [Online]. Available: <https://api.semanticscholar.org/CorpusID:106461764>
- [23] J. E. Killough, "Ninth SPE Comparative Solution Project: A Reexamination of Black-Oil Simulation," in *SPE Reservoir Simulation Symposium*, SPE, Feb. 1995. doi: 10.2118/29110-MS.
- [24] D. Li, "Comparative Simulation Study of Water Flood," in *SPE Asia Pacific Oil and Gas Conference and Exhibition*, SPE, Oct. 2004. doi: 10.2118/88459-MS.
- [25] R. P. Batycky, M. J. Blunt, and M. R. Thiele, "A 3D Field-Scale Streamline-Based Reservoir Simulator," *SPE Reservoir Engineering*, vol. 12, no. 04, pp. 246–254, Nov. 1997, doi: 10.2118/36726-PA.
- [26] J. F. M. van Doren, R. Marković, and J.-D. Jansen, "Reduced-order optimal control of water flooding using proper orthogonal decomposition," *Comput Geosci*, vol. 10, no. 1, pp. 137–158, Mar. 2006, doi: 10.1007/s10596-005-9014-2.
- [27] A. S. Odeh, "Comparison of Solutions to a Three-Dimensional Black-Oil Reservoir Simulation Problem (includes associated paper 9741 )," *Journal of Petroleum Technology*, vol. 33, no. 01, pp. 13–25, Jan. 1981, doi: 10.2118/9723-PA.
- [28] F. H., "Study on Validation of the OPM Reservoir Simulator by Comparative Solution Project," *Petroleum & Petrochemical Engineering Journal*, vol. 4, no. 4, pp. 1–8, 2020, doi: 10.23880/ppej-16000241.
- [29] T. D. Qiu, A. Thune, M. Blatt, A. B. Rustad, and R. Nane, "An Evaluation and Comparison of GPU Hardware and Solver Libraries for Accelerating the OPM Flow Reservoir Simulator," Sep. 2023.
- [30] T. Ahmed, "Fundamentals of Reservoir Fluid Behavior," in *Reservoir Engineering Handbook*, Elsevier, 2010, pp. 1–28. doi: 10.1016/B978-1-85617-803-7.50009-2.
- [31] K.-A. Lie, *An Introduction to Reservoir Simulation Using MATLAB/GNU Octave*. Cambridge University Press, 2019. doi: 10.1017/9781108591416.
- [32] SINTEF, "MATLAB Reservoir Simulation Toolbox (MRST)," SINTEF. Accessed: Mar. 27, 2025. [Online]. Available: <https://www.sintef.no/projectweb/mrst/>